UNIVERSITY OF CALIFORNIA
RIVERSIDE

Advancing Performance of a Photocatalytic Water Purification Microreactor With Enhanced Surface Area for NASA's Water Recovery System Through Application of Novel Titanium Micromachining Techniques

A Dissertation submitted in partial satisfaction
of the requirements for the degree of

Doctor of Philosophy

in

Mechanical Engineering

by

Kairui Xia

September 2022

Dissertation Committee:
Dr. Masaru Rao, Chairperson
Dr. Haizhou Liu
Dr. P. Alex Greaney

The Dissertation of Kairui Xia is approved:

_____

_____

_____

Committee Chairperson

University of California, Riverside

ACKNOWLEDGMENTS

I would first like to thank my PI Prof. Rao who gave me a precious opportunity to become a research member under his advisement. I joined this lab at the end of my first year of graduate school as a Master student, I was not sure what kind of project I should work on. What made me make up my mind to join the Biomedical Microdevices Lab was Prof. Rao's MEMS course. From then on, I have been lucky to learn about various MEMS techniques and fabricate my own microdevice, it makes me realize that I really like this field and want to work in this field even after graduation. I want to also thank my PI for teaching me how to be a good researcher. When I first joined the lab, I did not know what a researcher should do and made some mistakes. I am glad that after years of doing research in this lab, I finally have a decent understanding of what a good researcher should be like and how to keep learning the new knowledge. I believe what I have learned from these years of research will benefit me for my whole life in many aspects.

I would also like to thank all the colleagues in the Biomedical Microdevices Laboratory, Duncan Ashby, Dr. Bryan Woo, Dr. Harish Dixit, Dr. Samantha Corber, Dr. Benjamin Sommerkorn, Dr. Ryan Peck, Edver Bahena, Sanika Nishandar, Morgan Dundon, Pranee Pairs,, and Walter Su for helping and supporting me whenever I got lost while doing research, I have built great friendships with them and it is an amazing experience for me as an international student. And I would like to give especial thank to Dr. Duncan Ashby, I am grateful for all the guidance he gave me at the beginning of my PhD career, and it is my pleasure to work with him.

I would like to express my gratitude to all my collaborators. I want to thank Prof. Alex Greaney and Pegah Mirabedini for developing the computation model to give us a better understanding of light interactions with our device. I want to thank Prof. Haizhou Liu, Liang Wu, and Tan Cheng for helping me with the concentration measurements of different chemicals. As a student from Mechanical Engineering background, I do not have sufficient understanding about some contents in the Chemical Engineering field, you gave me lots of good advises and help whenever I ran into a problem with my study. I am really looking forward to the future publication for which we work together. My thanks will also go to assistant provost Jun Wang, he gave me lots of good advice about studying in UC Riverside, and also looked after us international students well. And I also want to thank all the professors who I worked as a TA for, I learnt a lot about teaching and responsibility from this experience, it will benefit me a lot in my future life.

Thank you to all the staff working at Center for Nanoscale Science and Engineering center at UC Riverside. Without all hard work from Mark Heiden, Frank Lee, and Dr. Dong Yan, I would not have a good fabrication environment for me to work in. The CNSE center really witnessed lots of my effort and dedication, I gained countless precious knowledge and experience from this facility which I wish I could use in my future career. I also want to express my special thanks to Dr. Dong Yan, he gave me a good training on almost every instrument I needed to use, and his dedication of work made sure that all instruments could run at their best conditions even when there was short of hands, he always picked up the phone without any delay when I called him to report issues in instruments. Thank you for your hard work, students like me can successfully complete work and strive for more goals.

Finally, I would like to thank my friends and family. I met a lot of great people in UC Riverside, and also in this beautiful California state. Thank you Alvin Huang, John Huang, Huawei Li, Carson Chiu, Claire Li, Terry Wei, Zoey, Zhe An, Catherine, Ginger Jiang etc. All my lovely friends have accompanied me through all these years, and our friendships always drive away any loneliness I have for living abroad alone. I believe our precious friendships will last forever no matter where we are. In the end, I would like to thank all my families especially my parents Dr. Jiangjing Xia and Min Zhang, they are the biggest supporter for me in my life. No matter highs or lows, they are always there to support me. Living and studying abroad for seven years is not easy, it is their love that keeps me working hard not fearing any difficulties. I am really lucky to be your child and I would really like to say thank you to both of you.

ABSTRACT OF THE DISSERTATION

Advancing Performance of a Photocatalytic Water Purification Microreactor With Enhanced Surface Area for NASA's Water Recovery System Through Application of Novel Titanium Micromachining Techniques

by

Kairui Xia

Doctor of Philosophy, Graduate Program in Mechanical Engineering
University of California, Riverside, September 2022
Dr. Masaru Rao, Chairperson

Exploring the vast space has always been one of the greatest dream for all human beings. The International Space Station (ISS) is currently working as a test platform for experimenting various essential equipment for further deep-space exploration and colonization. Because of limited space for storing water on ISS, Water Recovery System (WRS) is heavily depended to produce recycled drinkable water from collected wastewater. As one important component of WRS, the thermal catalytic reactor is designated to remove all Volatile Organic Compounds (VOCs) which is difficult to be dissolved by other treatments. However, the high temperature and pressure working environment makes some of its fragile parts need continuous replacements leading to increased cost and potential risks.

Herein, we propose a photocatalytic microfluidic reactor (PMFR) which can be operated at normal temperature and pressure to replace the thermal catalytic reactor. For this titanium (Ti) PMFR, micropillar arrays covered with nanoporous titania (NPT) are

designed to attain increased surface area to volume ratios, reduced diffusion lengths, and greater uniformity of irradiation. For the first time, the microelectromechanical systems (MEMS) techniques are used to fabricate a Ti-based microfluidic reactor. For the first degradation study with organic dye Methylene Blue, the micropillar reactor (MP) was found to dramatically outperform its planar counterpart and the 50 μm deep MP (MP50) presented at least two times higher degradation activity than other reported PMFRs. The second study introduced a VOC half-life estimation model designed based on the steady-state concentration of hydroxyl radicals (·OH). This radical was considered as the main reactant of the photocatalytic degradation of VOCs, and its concentration was measured by using nitrobenzene as probe. Half-lives for all VOCs existed in the Ersatz wastewater proposed by NASA were estimated, and results indicated that the MP50 was capable of dissolving most of these VOCs at or under around 100 seconds. The third and last study looked into the MP50 degradation performance with two common stubborn VOCs – ethanol and 1,4-dioxane. Results showed that MP50 eventually fully mineralized about 11.78% of ethanol. As for 1,4-dioxane, MP50 successfully degraded around 78.83% of it with a reaction rate constant two to three orders of magnitude higher than that of other bulk reactors reported in literatures. These findings demonstrate a great potential for the micropillar PMFR to replace thermal catalytic reactor on ISS and even be used for more varieties of water purifications.

TABLE OF CONTENTS

LIST OF FIGURES

LIST OF TABLES

1. Introduction

1.1. Water Situation on the Aerospace

Water, as one of the most important elements for the living of human beings, is always facing the problem of pollution. On earth, around 11% of population does not have easy access to purified water according to the United Nations.[1] This situation is mainly caused by the continuous contamination to water resources through numerous different approaches, such as landfills, improper disposal of hazardous waste and releases, and spills from stored chemicals and petroleum products.[2] Building large-scale water decontamination facilities is a difficult task for a lot of developing countries considering the technology limitations and the high cost. As an extension of human territory, the International Space Station (ISS) in space is also suffering from this problem.

As the technology keeps developing, more attention has been paid to the manned deep-space exploration. NASA has been the one organization who pays the most effort to running the crewed deep-space explorations and has attained many outstanding outcomes. According to the results from many preliminary explorations, Mars is very likely to be the next destination for astronauts to explore.[3] Discoveries made by the Mars exploration program will help pave the way for future human missions into the deep space planet.[4] Based on research, it takes about seven month to travel from earth to Mars, which means the transportation of important supplies from earth is expensive but considerable.[5] As for exploring into a deeper-space, sending supplies from earth will no longer be a viable choice because of the further distance leading to a higher delivery cost. Hence, it is important for

crews to be equipped with sufficient resources to survive independently during the trip to the deeper-space and build a planet base after arrival. To achieve this goal, having a reliable life-support system comes up as one of the most important priorities. The ISS is currently being used as an experimental platform to examine the feasibility of all kinds of space exploration equipment in preparation for the future deeper-space exploration project.

To maintain an appropriate living environment for the crew members, the Environmental Control and Life Support System (ECLSS) is the currently being operated on the ISS. This system is consisted of three main components – the Water Recovery System, the Air Revitalization System and the Oxygen Generation System.[6] Among all the functions, producing enough drinkable water is one of the most essential tasks that the ECLSS needs to perform considering the difficulties of storing and obtaining water on ISS. Storing a large volume of water on ISS is not viable due to the limited space onboard, and continuously ferrying water from earth will result in a huge transportation cost.[7] According to the Environmental Protection Agency (EPA), the cost for launching water are about $10000/lb and the water necessary to support six crew members on ISS is approximately 25 lbs per day.[8] To avoid the high cost of transporting water from earth, the Water Recovery System (WRS) has been heavily relied on to produce recycled water on ISS, and it has been able to produce enough water for crew consumption up to now.[9] The successful function of WRS offers an opportunity to kill two birds with one stone, crews are able to collect drinkable water and the storage space for wastewater is reduced in the meantime.

1.2. Problem Within WRS

The WRS has two key components – the Urine Processor Assembly (UPA) and the Water Processor Assembly (WPA). The UPA is designed to recover water from pretreated urine and flush water while the WPA mainly focuses on recovering wastewater consists of condensate from the ISS system and UPA distillate.[10] After putting the WRS into use for several years, some reliability problems occur within the WPA which need some attentions. A schematic of the WPA is presented in **Figure 1**.

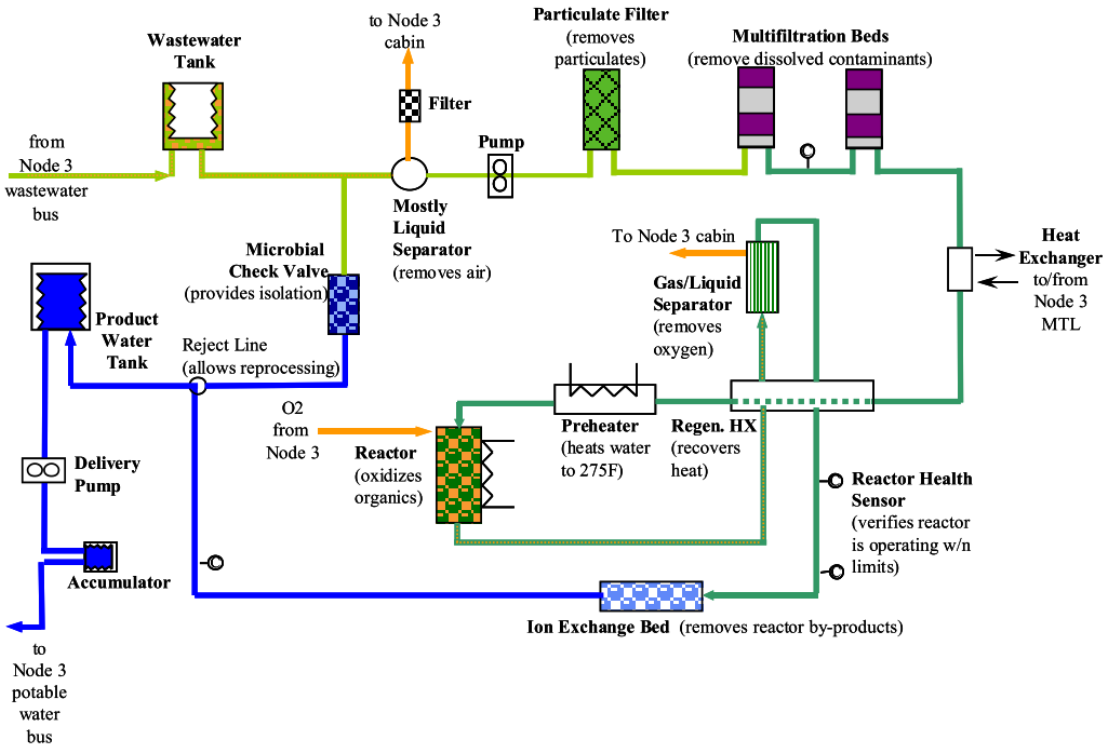

Figure 1. A brief schematic of the WPA system.[11] Air in wastewater is first separated by liquid separator. Particulate filter removes contaminant particles with large sizes through physical filtration. Multifiltration Beds employ ion exchange and adsorption to remove non-volatile organic and inorganic compounds. The volatile organic compounds are treated by the thermal catalytic reactor.

When wastewater flows into WPA, the Liquid Separator firstly removes all the air existed in the liquid. Then the Particular Filter filters out medium and large scale particulates. Right after the pre-treatments, only small scale dissolved contaminants are left in the wastewater. The two Multifiltration Beds remove non-volatile organic and inorganic contaminants via adsorption and ion exchange. Then the highly soluble, low molecular weight organic contaminants enter the Thermal Catalytic Reactor for the next-step treatment. This reactor oxidizes the organic contaminants into CO_2, organic acids and water in the presence of elevated temperature, high pressure and a catalyst.[12] However, the extreme working environment has caused some challenges for the parts which operate within the WPA. Up to 2018, there has been six instances of increasing Total Organic Carbon (TOC) in the post-treatment water produced by WPA, which resulted in a higher TOC level than the NASA drinkable water safety requirement of 3 ppm.[13] After investigation, the main cause of this TOC level increase was found to be the o-ring failure inside the hot zone of the Thermal Catalytic Reactor. Leakage happened as the o-ring could not bear the high temperature and pressure working environment, and several replacements of some vulnerable parts have been conducted which resulted in some excessive costs and health concerns for the crews.[14]

1.3. Project Motivation

For solving the current existing problem within the WPA caused by the Thermal Catalytic Reactor, we propose a novel design of a photocatalytic microfluidic reactor

(PMFR) with titanium dioxide (TiO_2) as the photocatalyst. This PMFR is aiming to reach the identical volatile organic compounds (VOCs) degradation goal as the current Thermal Catalytic Reactor by using the photocatalysis reaction, and has a great potential to replace the reactor within the WPA. The PMFR is able to be operated under room temperature and normal pressure which avoids the frequent vulnerable parts exchange caused by the elevated temperature and high pressure while using Thermal Catalytic Reactor. Meanwhile, the UV-rich environment on ISS benefits the photocatalysis reaction which has a potential to largely reduce the size of the device and the power required. The small scale of the PMFR can reduce the mass diffusion length, which makes more contaminant particles get in contact with the photocatalysts. The penetration of photons is also easier when they reach the surface of PMFR because of the micro-scale of the vertical device length. Another point which makes this design more novel is the use of microelectromechanical systems (MEMS) microfabrication techniques for fabricating the PMFR. MEMS has been an important technology which started developing about 80 years ago, and has become one of the most crucial technology in today's world. This technology has been used in many fields such as automobile systems, electronic devices and medical devices.[15] MEMS device can provide some advantages such as very small size, mass and volume, very low power consumption, easy integration to modify, small thermal constant, batch fabricated in large arrays et al.[16] By applying the MEMS technology, the PMFR can be benefited from all the advantages mentioned above. For proposed device, tens of thousands of titanium micropillars are produced and formed into arrays by applying MEMS microfabrication techniques, these pillars work as the scaffolding for the photocatalyst TiO_2. And a layer of

TiO_2 is created with the porous structure by using some chemical methods established by the former researchers. The micropillar arrays deposited with nanoporous titania (NPT) further increase the photocatalyst surface area to volume ratio (SA:V) and shorten the mass diffusion length, thus increase the VOCs degradation efficiency. This project is aiming at obtaining the PMFR concept through microfabrication techniques, comparing the micropillar design with conventional planar design, and proving the practical VOCs degradation viability with experiments.

1.4. Dissertation Outline

This dissertation mainly introduces the design and fabrication of a novel PMFR which is used for water purification, and the validation of this device's photocatalytic degradation performance with different organic contaminants. Chapter 2 introduces some basic background information about this proposed Ti PMFR, it provides a good understanding about why the design and the Ti material are selected. Chapter 3 presents a detailed design of the PMFR followed by an illustration of the fabrication process. Chapter 4 is about the first degradation study with an organic dye of Methylene Blue, the influence of different pillar heights are examined and the PMFR with best performance is found. Comparison of the PMFR with other reported microfluidic reactors is also made to indicate the superior performance of PMFR. Chapter 5 covers the second study which focuses on quantifying hydroxyl radicals, the main reactant that contributes to the contaminants degradation. A half-life estimation model is also created based on the radical concentration

to predict the degradation effect of PMFR on certain organic compounds. Chapter 6 demonstrates the last study where two common problematic organic compounds – ethanol and 1,4-dioxane are used as the target contaminants. Results for degradation experiments of both contaminants are presented separately, and an extensive comparison between PMFR's degradation performance on 1,4-dioxane and that by other reported bulk reactors is conducted to examine the advantage brought by the novel PMFR design. In the end, chapter 7 shows a summarization of this dissertation, and it also presents some future work that can be done to further optimize the device.

2. Background

2.1. Principles of Photocatalysis

Photocatalysis is a light induced reaction for which the presence of catalyst accelerates the reaction. When photons with energy higher or equal to the bandgap (ΔE) of a semiconductor such as TiO_2 hit the semiconductor, the electrons on the valence band become excited and jump to the conduction band leaving a positively charged hole in the valence band.[17,18] This movement can be described by

$$TiO_2 + hv \rightarrow h_{VB}^{+} + e_{CB}^{-} \quad (1)$$

where hv is the photon, h_{VB}^{+} is the positive charged hole on the valence band, e_{CB}^{-} stands for the electron which excites on the conduction band. After electron-hole separation, recombination may happen where the excited electron loses the energy, goes back to the

valence band and recombine the hole. For the holes and electrons which do not recombine, the photon energy is converted into chemical energy, this process can be described by

$$h_{VB}^{+} + H_2O \rightarrow H^{+} + \cdot OH \quad (2)$$

$$e_{CB}^{-} + O_2 \rightarrow \cdot O_2^{-} \quad (3)$$

From this process, the hyper-reactive hydroxyl radicals ($\cdot OH$) and the oxygen radicals ($\cdot O_2^{-}$) are formed.[17,18] A simple illustration of the photocatalysis process is shown in **Figure 2**.

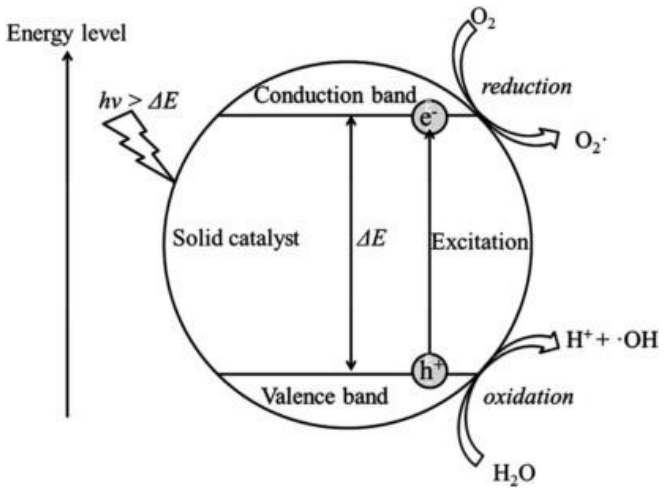

Figure 2. A schematic to show the mechanism of photocatalytic reaction in aqueous solution.[19] Highly reactive free radicals and electron holes generated through the reaction mainly account for the degradation of pollutants in water.

Researches about using photocatalysis with TiO_2 to treat organic contaminants in the aqueous solution began about three decades ago.[20] The hydroxyl radicals have been proved many researches to be the main reactant to dissolve microorganisms or pollutants.[21,22] Apart from the water purification, TiO_2 photocatalysis has also been used

in many different fields including self-cleaning surfaces, sterilization, hydrogen evolution and photoelectrochemical conversion.[23] For the proposed PMFR in this project, the hyper reactive free radicals mainly the ·OH generated by the photocatalysis is put into work to degrade organic contaminants in aqueous solutions.

2.2. Titanium Dioxide Material

TiO_2, as the naturally occurring oxide of titanium, has a long history of being applied to various fields in industry. TiO_2 was discovered in 1821, and it had been widely used as a replacement of the toxic lead oxides in pigments for white paint in the beginning of 20th century.[24] After many years of developing, the usage of TiO_2 in pigments has been applied to many areas such as paints, plastic, paper, and leather. The European Union legislation on safety of food additives also approved the use of TiO_2 as food coloring many years ago which made TiO_2 even more popular in industry as pigments. Based on the high refractive index of TiO_2, many industries tend to put TiO_2 into the production of anti-reflection coatings for critical devices and automobiles, and numerous sunscreen creams also include TiO_2 nanoparticles to strengthen the anti-UV ability.[25]

As for being used as a photocatalyst, TiO_2 owns a number of advantages compared to other conventional catalysts such as ZnO, CeO2, ZrO2, etc. The fact that TiO_2 is considered as a chemical inert semiconducting material with highly stable mechanical characteristics makes it a perfect choice as the catalyst.[26] The great photoactivity allows TiO_2 to perform efficiently while photocatalysis takes place.[27] Researches also discovered

the low toxic property of TiO_2 which makes TiO_2 a biologically inert material, this good biocompatibility makes it a popular material selection for biomedical devices such as in-body sensors and medical chips.[28–30] Meanwhile, the relatively low price of TiO_2 can effectively lower the processing and manufacturing cost making TiO_2 a great material choice financially.[31] Ever since the finding of hydrogen production through TiO_2 photocatalysis in the early 1970s, the applications have been extended to numerous fields such as hydrogen production, air cleaning, metal anti-corrosion, hydrophilic and self-purification.[27,32] Water purification is one of the biggest field to that the TiO_2 photocatalysis is applied, all merits mentioned previously make TiO_2 one of the most widely used photocatalysts for this field. The research interests have been continuously growing in both the industrial and academic fields.[33–36] These successful applications of TiO_2 on photocatalysis water treatment encourages the use of TiO_2 as the catalyst for this project.

TiO_2 possesses three crystalline structures naturally – rutile (a = b= 4.593 Å, c = 2.959 Å), anatase (tetragonal, a = b = 3.785 Å, c = 9.54 Å) and brookite (orthorhombic, a = 5.143 Å, b = 5.456 Å, c = 9.182 Å).[37] According to research, the irreversible transition of the two thermaldynamically phases - anatase and brookite, are able to transform into the stable rutile phase at a high temperature.[38] Among the three phases, anatase has the most active photocatalysis ability due to the fact that it owns a larger band gap over the other phases.[39] What is more, anatase possesses an indirect band gap while the rutile owns either a direct band gap or an indirect band gap which is very similar to a direct band gap. A longer electron-hope pair life will be obtained with an indirect band gap according to the

study, thus making the anatase have more charge carriers to join the surface reactions.[40] TiO_2 has different physical structures with different dimension such as spheres, fibers, channels and nanosheets.[41] A higher surface-to-volume ratio is likely to be acquired by a higher dimension of structure. This increasing SA:V can lead to a reduction in the electrons and holes recombination rate and an increase in the interfacial charge carrier transfer rate, which then benefits the photocatalysis process. Degussa P25 is the most widely studied and used TiO_2 photocatalyst, and it usually exists in the powder form. It provides two remarkable merits, a relatively large accessible surface area and a relatively high mass transfer rate for reactants. There is a combination of ~80% anatase and ~20% rutile in the P25, and it has been proved that this intimate contact between two phases enhances the separation of electrons and holes, thus reduces the chance of recombination.[42] However, the powder form brings some shortcomings. Concerning the catalysts becoming the secondary pollutant in the purified water, filtration is always needed to remove the P25 nanoparticles from the post-treatment water to ensure its purity, which makes this process more time-consuming. In order to overcome this drawback, lots of interests are put into coating different substrates with TiO_2 films.[43,44] Researchers have tried many different methods to achieve the goal, some popular methods are sol-gel[45,46], electrochemical[47], hydrothermal[48] and chemical deposition[49]. Although the thin-film helps eliminate the filtration needed for powders, the relatively low catalyst surface area limits the contact between UV photons and catalysts thus reduce the photoefficiency.[50] Herein, a nanoporous structure of TiO_2 is adopted for the PMFR to help increase the total surface area for catalyst.

2.3. Nanoporous Titania

Many studies have been done to seek a way to enhance the photocatalysis efficiency, what have been found is that one of the most effective methods is through increasing the SA:V for catalyst. To achieve this goal, many researches tried the preparations of titania nanotubes, nanowires and nanorods to create more surface area.[51–53] A common way to produce the nano-shaped titania is through hydrolysis and condensation of titanium alkoxides. However, a thermal treatment is always required following this process for inducing crystallization as well as removing the residual alkoxide groups. The specific area of catalyst decreases caused by the particle agglomeration and grain growth as the sequence of thermal treatment.[54] Although the hydrolysis of titanium inorganic salts such as $TiCl_4$ under ambient temperature can produce well-crystallized titania, the counter anions generated from inorganic salts is most likely to remain in the products thus contaminate the titania product.[55]

To overcome these drawbacks, Wu et al. reported growing titania nanorods directly from the titanium substrate by using hydrogen peroxide (H_2O_2) as the oxidizing agent.[56] The adhesion between the titanium substrate and nanorods was very strong because of direct interaction between titanium and H_2O_2. And the use of the oxidant eliminated the possibility of bringing contaminants into the titania product thus guaranteed the product's purity. Since then, more interests have been put into the production of nanostructured titania through direct oxidation on titanium substrate. Two years later, DeRosa et al. reported that they successfully produced crack-free nanoporous titania (NPT) with anatase crystal structure on thin layer titanium substrates through oxidation with aqueous H_2O_2.[57]

Compared to conventional titania, NPT possesses several advantages. The three dimensional porous structure dramatically increases the SA:V of the catalysts hence increases the amount of free radicals generated by photocatalysis. In addition, this structure enhances the fluid accessibility which increases the amount of contaminant particles which can have contact with the catalyst. NPT also eliminates the concern about the product purity because it grows directly from titanium substrate though reaction with oxidants. Last but not the least, the fabrication method guarantees a complete coverage over complex geometries, which makes NPT suitable to be used for most of the applications. A SEM micrograph of the NPT used for the proposed PMFR is shown in **Figure 3**.

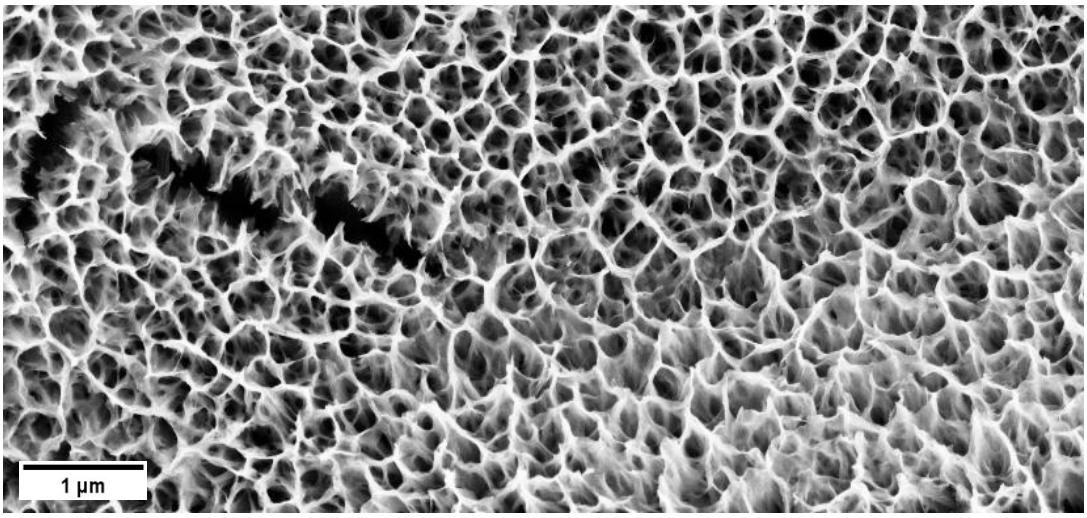

Figure 3. The SEM micrograph of NPT used in the proposed PMFR. The highly porous structure enlarges the surface area of catalysts, and it also enhances the fluid accessibility. Photocatalysis benefits a lot from the 3-D structure.

NPT has already been used for several applications such as medical implants, gene therapy, energy conversion, and catalysis.[58–61] In 2006, Zuruzi et al. successfully applied NPT to production of a highly sensitive gas sensor, and they found that NPT helped the

device to have faster response time, lower operation temperatures and superior sensitivity compared to the conventional gas sensor. As for water purification, Song et al. performed groups of photocatalytic degradation experiments on selected dyes using different types of nanostructured NPT. For the results, they reported that the titanium thin films with nanorods or nanotubes possessed higher degradation efficiency than the commercial P25 titania and sol-gel derived titania. On the basis of these experiments and applications, we propose the use of NPT for our PMFR. NPT can be easily grown on the surface of titanium in the reaction chamber regardless of the complex geometry, and all the benefits brought by NPT is hypothesized to increase the photocatalytic efficiency for the PFMR.

2.4. Conventional Reactors

The process of classical photocatalytic contaminants degradation can be divided into five independent steps: 1) transfer of reactants to the catalysts surface; 2) adsorption of the reactants; 3) reaction in the adsorbed phase; 4) desorption of the products; 5) removal of the products from the interface region, where photocatalysis reaction happens in the step 3.[62] In order to find out the photocatalytic degradation performance on organic contaminants, numerous types of reactors have been designed and tested.[63] What researchers have discovered from experiments is that the reactor design plays an important part in the reaction since a good reactor design is able to help overcome some limitations that photocatalytic water purification is currently experiencing. According to Wang et al., the three major limitations for conventional reactors are low mass transfer efficiency, low

photon transfer efficiency, and deficiency of dissolved oxygen.[64] The mass transfer efficiency determines how easily the contaminants are able to travel to the catalyst surfaces where photocatalysis reaction takes place, and how fast the redox products can be removed. The photon transfer efficiency affects the amount of photons that can reach the catalysts surfaces, more photons lead to a higher reaction rate, and a uniform UV irradiation is usually required for a better production of free radicals. For the third limitation, it occurs because of the limited concentration of oxygen naturally dissolved in water, photocatalysis in liquid phase requires the participation of dissolved oxygen where the limited oxygen concentration tends to affect the reaction efficiency.

For the numerous reactor designs, most of them can be defined as conventional bulk reactors according to the relatively large volume of reaction space. The bulk reactors have been proved to be effective by many studies with different reactor designs such as P25 particles with mechanical stirrer, TiO_2 thin-film on fixed bed reactors, fluidized bed reactors, and many others.[65–67] Conventional bulk reactors can be generally divided into two types: the slurry reactor and the immobilized reactor. For the slurry reactor, as shown on the left side in **Figure 4**, the catalyst particles are suspended in the solution forming a slurry. This type of reactors possesses the advantages of a large SA:V and fast mass transfer. However, the light distribution is non-uniform due to the disorganized suspension of catalysts particles which reduces the photoefficiency, and a filtration process is always needed to remove the suspended particles to ensure the purity of water. As for the immobilized reactor, catalyst is usually immobilized on the substrate as a thin-film. This kind of reactor does not need an additional step of filtration, and the uniform and fixed

catalysts lead to a good photon transfer. Compared with the slurry reactor, the immobilized catalysts lose some of the surface area due to its structure which causes a decrease in SA:V, and the decreasing ratio leads to harder interactions between contaminants and catalyst surfaces. Both designs of the conventional bulk reactors have the ability to break some of the limitations mentioned previously, but none of them can do it perfectly, hence more attentions are drawn on an atypical design of reactors – the microfluidic reactors.

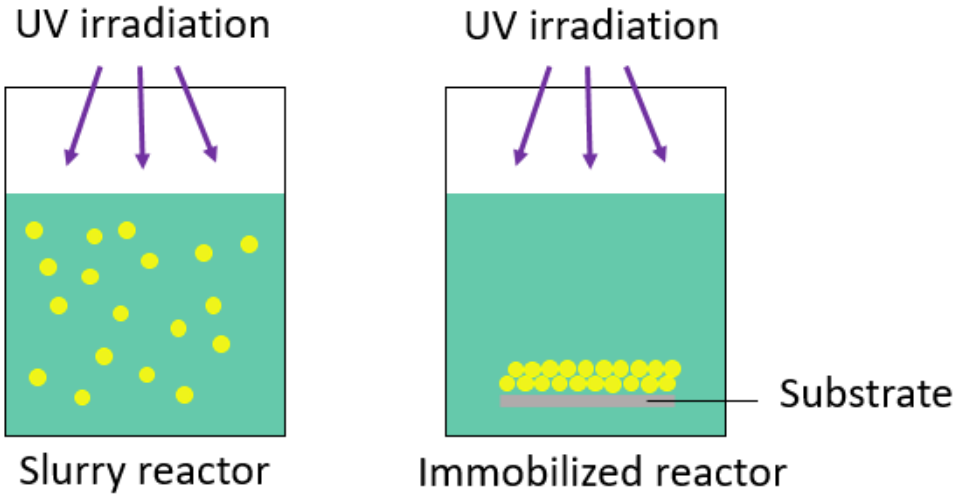

Figure 4. Schematics of slurry reactor (on the left) and immobilized reactor (on the right).

2.5. Microfluidic Reactors

To overcome the limitations owned by the conventional bulk reactors, a design of a miniaturized reactor with microfluid flowing inside the reaction chamber is brought up. Compared to the conventional bulk reactors, the volume of reaction site for the microfluidic reactors is usually at least three orders of magnitude smaller than the volume of bulk reactors. The small dimension of the reaction chamber lead to a dramatically large SA:V,

and as mentioned previously, larger SA:V can enhance the photocatalytic reaction rate. According to Wang et al., SA:V could be even larger if the photocatalyst is in nanoporous structure within a real microreactor.[64] The mass transfer also gets enhanced greatly due to the thin microfluidic layer which is usually around 100 μm thick. It is easy for a contaminant particle to have contact with the catalyst surface, thus more contaminants can be dissolved in general. The time for each contaminant flowing in the chamber is uniform because the microfluidic flow inside the reaction chamber is usually laminar, the flow time is defined as the residence time. Based on this phenomena, the residence time can be controlled by altering the flow rates of solution, it also makes the control of throughput feasible. Since catalysts are usually immobilized as a thin-film, the microfluidic reactor possesses the same advantage as the immobilized reactor does, the UV irradiation on the catalysts surface is uniform leading to high photoefficiency. A shorten reaction time is also obtained, it usually ranges from tens of seconds to hundreds of seconds while the conventional reactors usually need at least several hours of reaction time. Some other benefits brought in by the microfluidic reactors are self-refreshing effects, optimization of operating conditions and more functionalities.[64]

To have a deeper look at the microfluid flow inside the reaction chamber, a schematic is shown in **Figure 5** to present the mechanisms. In microfluidic reactors, liquid usually flows in a chamber sealed by a quartz disk on the top to ensure a good UV transmission, and a thin layer of photocatalyst is usually fixed on the bottom. The layer of flow is mostly about 100 μm thick and can be decomposed into three regions. In region 1 where the particles flow against the quartz disk, photolysis is most likely the dominant

reaction. Region 2 works as a medium zone, the thickness of this zone is dependent on the design of microreactors. Photocatalysis generally happens in the region 3 where catalysts interact with solutions, as photons hit the semiconductors such as TiO_2 used for this project and trigger the reaction, reactive free radicals (·OH and $O_2^{\cdot-}$) are generated and functions to degrade the organic contaminants in the solution. However, this laminar flow leads to one limitation where most of the contaminants removal happens in region 3, so the degradation reaction in region 1 and 2 is not as strong as what happens in region 3.

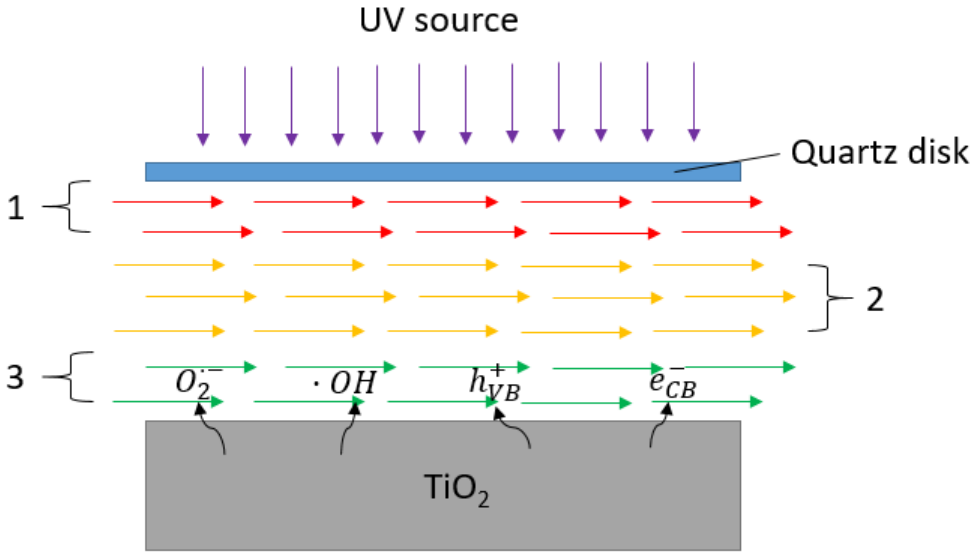

Figure 5. Schematic of the laminar flow within the microfluidic reactor chamber. Being divided into 3 regions, this laminar flow limits the efficiency of contaminants degradation.

Another major drawback of the microfluidic reactors is that the throughput of a single device is low due to the small scale of the reaction chamber. A common method to overcome this drawback is by connecting a number of devices in parallel so the throughput can be added up to reach a compelling value.[68] A study done by de Sa et al. aimed to

compare the effect of numbering-up and scale-up of microfluidic TiO_2 reactors on photocatalytic degradation of organic dyes. The system formed by six devices connected in parallel was able to achieve the highest degradation percentage under same reaction time compared to that by other experiment systems.[69] This result proves the feasibility of overcoming the throughput limitations by connect appropriate number of microreactors in parallel, specific researches are still required to find the best number to ensure a large throughput and a high degradation percentage being achieved simultaneously.

2.6. Review of Existing Microfluidic Reactors

In this section, a brief review of some microfluidic reactors reported in literatures are presented. In 2016, Liao et al. brought up with a biomimetic planar photocatalytic microreactor with 50 μm deep reaction chamber depth.[70] A schematic of this microreactor is presented in **figure 6 (a)**. This device had a reaction chamber with plane dimension of 1 cm × 1 cm, a layer of highly porous TiO_2 film was deposited onto the chamber bottom by using the manual painting method. The bifurcated system of this reactor was designed following the Murray's law, which made this system have the minimum energy loss while maintaining a constant shear stress. After fabricating and experimenting the devices, they found that the planar microreactor with the biomimetic bifurcated system design showed a 68% higher efficiency than the microreactor with non-biomimetic bifurcations.

Meanwhile another group intended to increase the planar microreactor's degradation efficiency by adding in more geometries for catalysts. Li et al. presented a

photocatalytic microfluidic reactor with TiO_2-coated fiberglass immersed in the reaction chamber.[71] **Figure 6 (b)** shows a schematic of the device. The TiO_2 colloid with Degussa P25 was first prepared and coated on the fiberglass. This bundle of fiberglass was stretched and collected, then sealed in the reaction chamber between the glass cover and PDMS chip. By introducing the TiO_2-coated fiberglass, this group believed that it would enhance the photocatalytic efficiency by reducing the mass transport length and inducing the perturbation to liquid flow. A conventional planar microreactor with TiO_2 coated on the chamber bottom was prepared for comparison. The degradation result illustrated that the TiO_2-coated fiberglass design was able to increase the degradation efficiency to at most 40% more compared to the efficiency of planar microreactor.

To further improve the performance of microreactors, a method through adding micropillar arrays into the reaction chamber was brought up by Li et al.[72] For this design, arrays of micropillars with 200 μm diameter, 250 μm height and 400 μm pitch were produced with a material of photoresist SU-8. Some basic molding and photolithography method were used. Photocatalyst Pt/TiO_2 nanoparticles were sprayed onto the reaction chamber surface. **Figure 6 (c)** presents a model of this reactor. By introducing the micropillar arrays, photocatalytic efficiency was enhanced due to the largely increasing SA:V and the reducing mass transfer distance. After testing the photocatalytic efficiency with water splitting, result was compared to the result collected by using a conventional planar microreactor, it turned out that a maximal increment of the reaction rate reached 56%. This study successfully presented the enhancements brought by the micropillar arrays; however, the size of micropillars has a potential to be reduced, and the micropillar

arrangements can be more compact. Tightened micropillar arrays can further enhance the SA:V and reduce the mass transfer distance thus increase the device efficiency more.

In 2018, Li et al. reported a microreactor with dual-film TiO_2 nanorods as photocatalysts.[73] The nanorods TiO_2 would benefit the photocatalysis by increasing the SA:V, reducing the mass transfer length and providing direct pathways for the photo-generated charge carriers. **Figure 6 (d)** shows the schematic of this reactor as well as the schematic of nanorod arrays. These TiO_2 nanorod arrays were prepared by a hydrothermal method and they were formed into a thin-film on two Fluorine-doped tin oxide (FTO) glasses. Then the FTO glasses were installed into a chamber made on a silicon wafer to form the final reaction chamber. It should be noted that the nanorods mentioned here was different from the micropillars mentioned previously, these nanorods were about 200 nm wide and 2.4 μm long, and grew in a crowed manner; the micropillars mentioned in the last reported study had larger sizes, and they grew uniformly on the substrate to form arrays. As for the result, this microreactor had two times higher photocatalytic degradation reaction rate than the rate of a conventional planar microreactor proving the enhancement brought by nanostructured TiO_2.

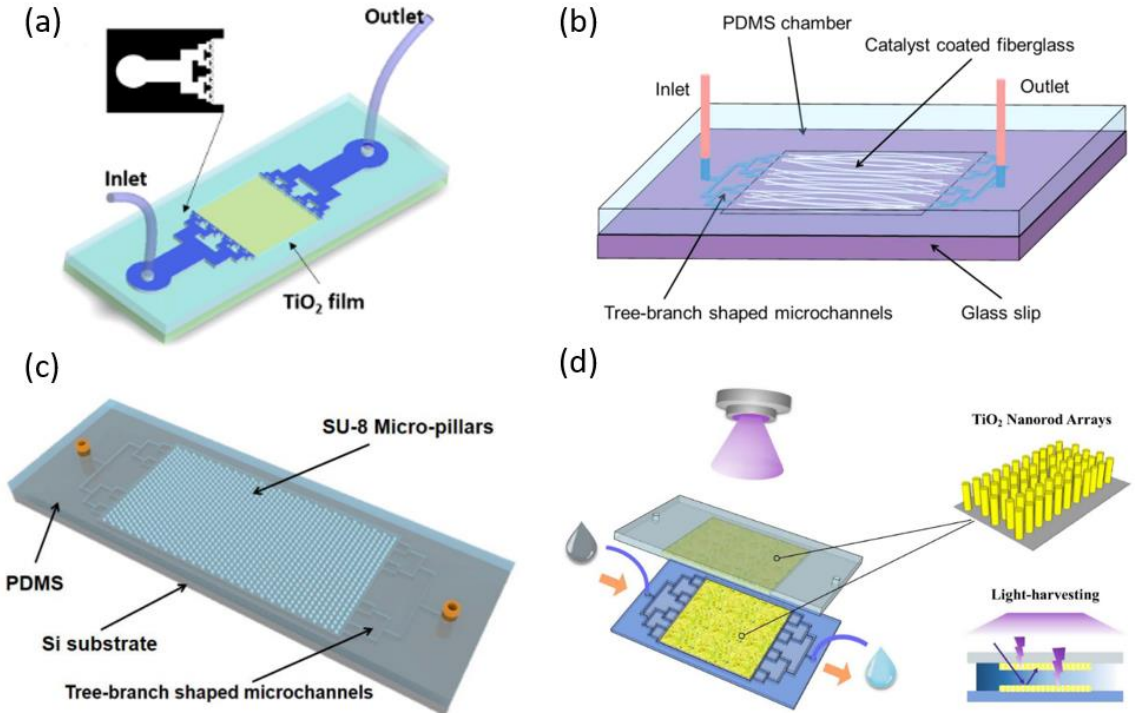

Figure 6. Schematics of four microreactors reported literatures. (a) biomimetic planar microreactor;[70] (b) TiO2-coated fiberglass microreactor;[71] (c) micropillar arrays enhanced microreactor;[72] (d) dual-film TiO2 nanorods microreactor.[73]

The four microreactors mentioned in this section are some representative and successful examples of the TiO_2 photocatalytic microreactors that have been reported so far. Although having different designs, all of these microreactors are intended to enhance the photocatalytic performance by mainly three ways: increasing SA:V, reducing mass transfer distance, and improving photon harvesting. Herein we present our novel design of the PMFR, it combines the advantages of bringing in intensified micropillar arrays and growing NPT on micropillar surfaces, which thus is capable of increasing the photocatalytic efficiency to a higher level.

3. Microreactor Design and Fabrication

3.1. Microreactor Design

For this project, we present a chip-based microreactor with one open reaction chamber in the center; two tree-branched flow distributor systems are connected to the chamber to ensure a uniform liquid flow through the chamber; two rounded holes at the endpoints of two distributor systems are created to work as inlet and outlet. This chip has a 60 mm × 40 mm planar dimension. **Figure 7** shows a CAD model of the microreactor chip and a photo of the chip. The reaction cite can be decomposed into two parts: the reaction chamber and the flow distributors.

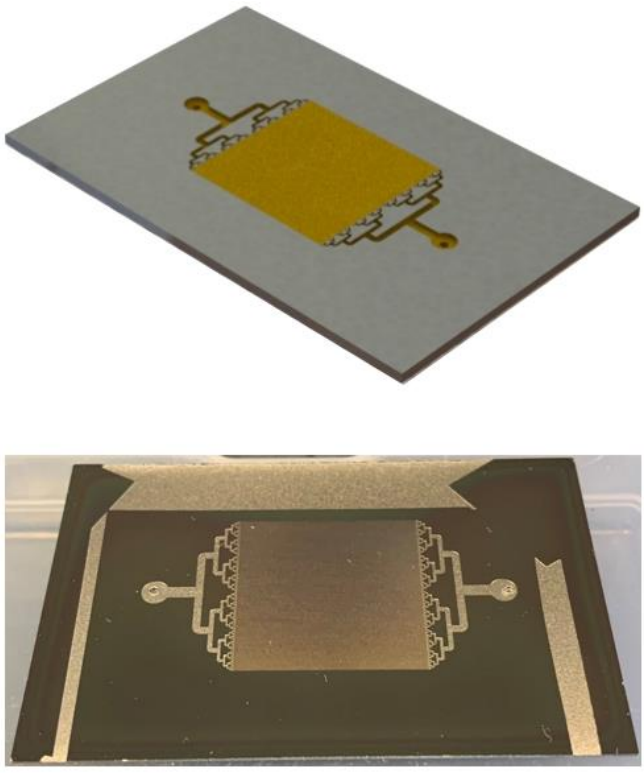

Figure 7. A CAD model of the microreactor chip (top) and a photo of the actual fabricated microreactor chip (bottom).

3.1.1. Reaction Chamber

For this proposed photocatalytic TiO_2 microreactor, the rectangular reaction chamber has a planar dimension of 2 cm × 2.048 cm. There are 512000 micropillars standing in the reaction chamber in an offset manner. A more detailed description of micropillars will be presented in a later section. Depths of the chamber depend on the micropillar heights. In order to study the effect of micropillar heights on photocatalysis efficiency, 50, 100 and 150 μm heights are selected, meaning that there are reaction chambers with these three different depths.

3.1.2. Micropillar Arrays

For the micropillars inside the reaction chamber, each of them has a 15 μm diameter and a 40 μm pitch. The original design of diameters was 20 μm, but the diameters were found to be around 15 μm after fabrication. All rows of micropillars are arranged in a staggered form to ensure the fluid flow being slowed down and there is adequate time for contaminant particles having contacting with photocatalysts. These micropillars have titanium as the substrate, NPT are grown and fully cover the surfaces of titanium pillars. **Figure 8** shows a schematic and a SEM image of the micropillar arrays. The grey part in **Figure 8 (a)** is the titanium substrate while the yellow part represents the NPT, the nanoporous structure and cracks can been seen on the micropillar sidewalls in **Figure 8 (b)**. The formation of cracks is common in thin-film TiO_2 after several hours oxidation in H_2O_2,

a former PhD student has done a study to find the perfect oxidation time to minimize the crack size.

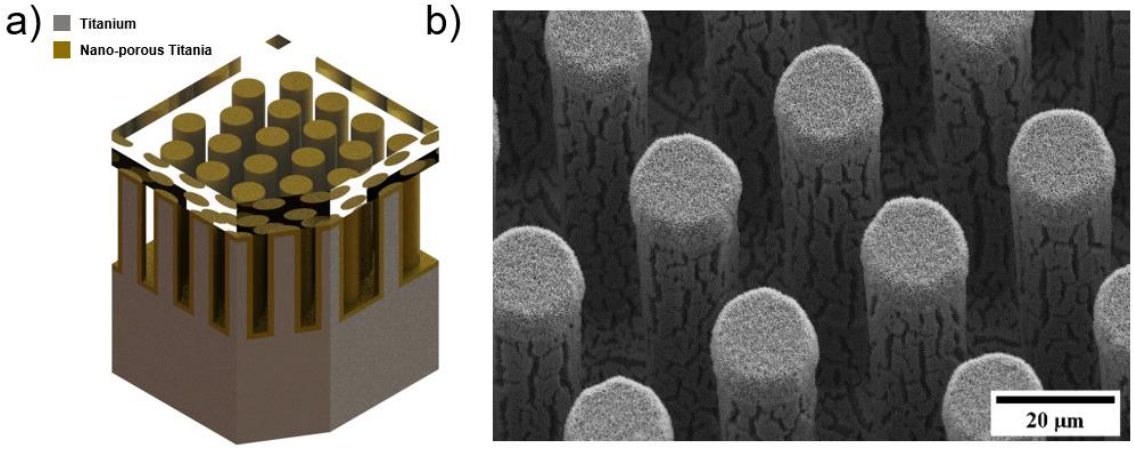

Figure 8. Presentation of NPT-coated micropillar arrays with: (a) a CAD model; (b) a SEM image. In the CAD model, yellow components stand for NPT and grey components represent Ti, the model top is covered with a transparent quartz slide.

3.1.3. Flow Distributors

The flow distributors are very important to the functioning of PMFR. If the reaction chamber is directly connected to reactor's inlet and outlet, the direct liquid flow coming out from the inlet would create a large pressure which might damage the micropillars. Moreover, the liquid flow rate would be high which can cause a shorten time for the contaminants to stay within the chamber, thus decreases the degradation efficiency. Only one liquid entrance for the chamber also negatively affects the flow within the chamber, based the mechanism of fluids, the two corners of chamber near the entrance would not be filled by the fluid, causing a significant waste of the photocatalyst surface area. Thus a tree-branched flow distributor is selected to eliminate these drawbacks. Tree-branched flow

distributors have been widely used by many studies.[70,73,74] This type of flow distributors provides two main advantages: low pressure drop and uniform liquid flow within the reaction chamber. For our proposed PMFR, flow distributors are divided into five tiers, the dimensions of the channels are decreased by a factor of 1.6 tier by tier, this dimension decreasing starts from the first channel which connects with the inlet/outlet. According to a study done by Vangelooven et al. in 2010, a channel dimension decreasing by a factor of 1.6 at each bifurcation could gradually slow down the flow as it proceeds into the distributor.[75] The slowing down flow speed guarantees a rational flow rate and a moderate pressure drop within the reaction chamber. Sixteen small channels uniformly spread over two sides of the chamber produces a uniform fluid flow within the chamber which ensures a consistent mass transfer distance for each contaminant particle. The SEM micrographs of the flow distributors are shown in **Figure 9**. A simulation done by this dissertation's author with COMSOL Multiphysics also proves the benefits brought by the tree-branched flow distributors.[76]

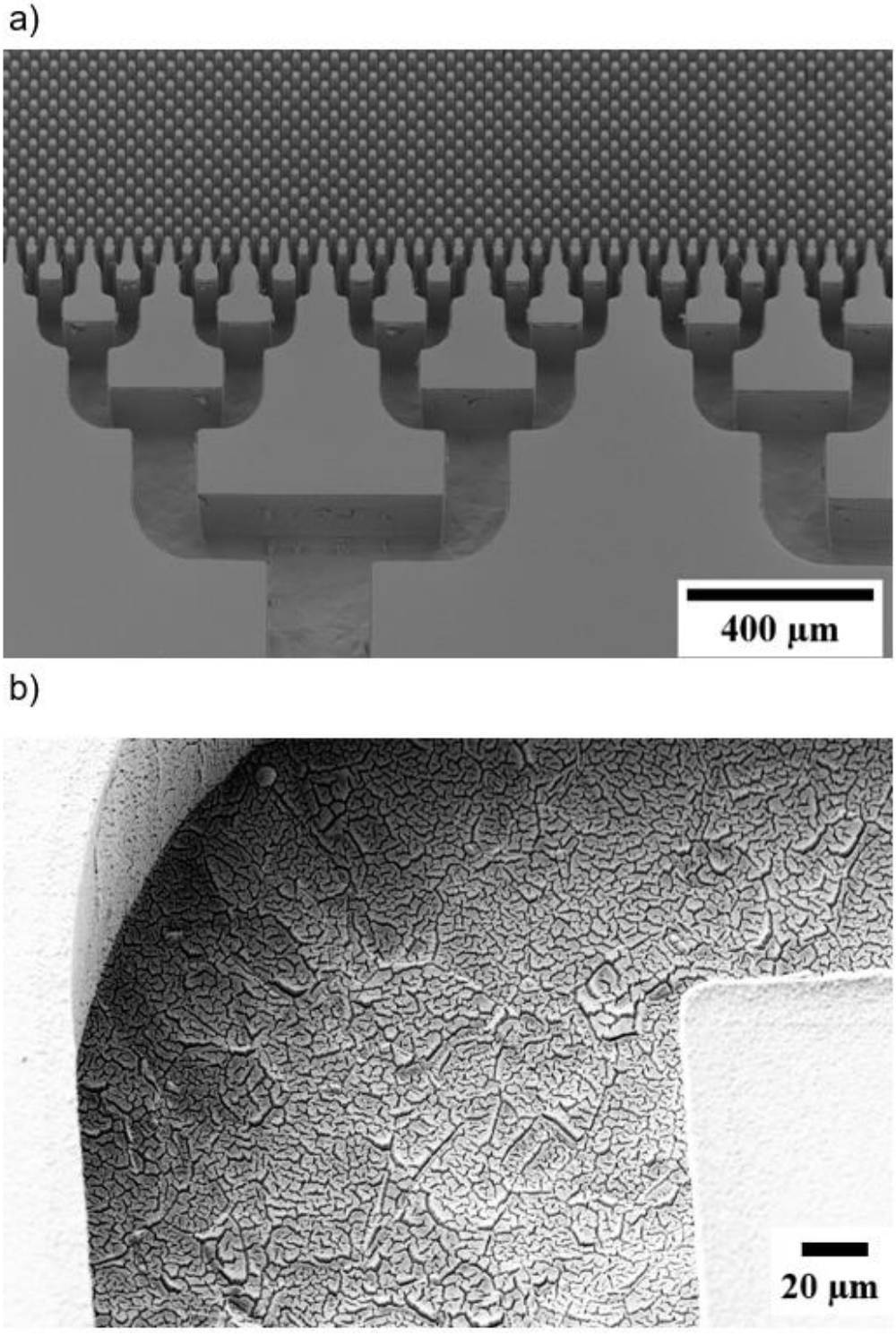

Figure 9. SEM images of (a) the tree-branched distributors; (b) zoom-in view of the flow distributors, sidewalls and ground of the flow distributor is also covered by NPT.

It is worth mentioning that, for examining the enhancement of photocatalytic degradation brought by micropillar arrays, a set of planar microreactors with 50, 100 and 150 μm depths are designed and fabricated to work as the comparison group. The dimension of planar microreactors is highly identical to that of their micropillar counterparts, the only difference is that there is no micropillar in their reaction chambers. The bottom of planar microreactor is in fully coverage of NPT which allows the happening of photocatalysis. Start from here through the whole dissertation, micropillar PMFRs (MP) with 50, 100, 150 μm will be written as "MP50", "MP100" and "MP150", and planar PMFRs (P) with 50, 100, 150 μm will be written as "P50", "P100" and "P150" for more intuitive reading. **Table 1** presents the calculated reaction chamber volumes of the six types of microreactors fabricated for this project, these calculations are made based on the exact dimensions of fabricated microreactors measured by precise instruments. After fabrication, the P50 shows a smaller depth that the MP50 which causes them have about the same chamber volume.

Microreactor	MP50	MP100	MP150	P50	P100	P150
Volume (μL)	24	49	73	24	42	65

Table 1. The chamber volumes for six PMFRs fabricated for this project.

3.2. Fabrication Techniques

Before introducing the microfabrication process, the first thing that is needed to be talked about is the microelectromechanical system (MEMS). This system has been one of

the most popular topic for both academic and industries since it came out, it is a process technology aiming to create micro scale integrated devices that combine mechanical and electrical components.[15] In order to install enough components on a small scale chip, a great variety of microfabrication processes have been developed and put into use. Among all microfabrication techniques, photolithography, film deposition, etching, and bonding are the most important ones.[77] Film deposition works on growing a layer of materials on the substrate to protect the base material from etching. Photolithography is an important process where desired patterns will be transferred to the substrate. This process is consist of several steps, the key part is dissolving of photoresist under UV exposure. To sculpture 3-D geometries on the substrate, the etching process is used. Etching is able to generate 3-D geometries from the patterns produced by photolithography through either physical or chemical methods. Last but not the least, bonding is capable of creating tight bonds between microstructures, this technique is important for making devices with complex geometries. Herein, we introduce the three major microfabrication steps for this project in the following sections.

3.2.1. Hardmask Patterning

In order to produce micropillars from Ti chips, desired patterns which guide the etching are needed to be created on the surface of Ti chips. Since etching is a top-down process, different etch rates are required for patterns and un-patterned areas to create 3-D structures. The ratio between substrate etching rate and the mask (used for patterning) etch

rate is called selectivity. A high selectivity describes that two materials etch at significantly different etch rates, the substrate material etches at a relatively higher rate compared to what the mask material does. Using a high selectivity can help promote an anisotropic etching and prevent etching on the under-layer. When two materials etch at similar rates, the selectivity is near 1:1, it can be defined as a low selectivity. This selectivity is usually applied for the situation where the mask shaped is reproduced in the material being etched. For this project, the selectivity between Ti and the SPR 220-7 photoresist is about 1-2:1, which leads to two issues if directly using photoresists as the etching mask: the difficulties of creating a 150 μm layer of photoresists on Ti wafer for etching 150 μm depth chambers; and the possibility that all photoresists being degraded by plasma before finishing etching Ti. To solve this problem, a hardmask is required to etch desired geometries. A hardmask is on the contrary to the "soft" material masks such as photoresists, it usually is in the material like oxides. The selectivity between Ti and oxide hardmasks is typically 40:1, which allows the oxide hardmasks to be more slowly etched during etching process compared to Ti, thus hardmasks can protect the Ti underneath hardmasks from being etched. The un-etched Ti forms into the desired micropillars in the end. For this project, SiO_2 was chosen as the material for hardmasks, Plasma Enhanced Chemical Vapor Deposition (PECVD) process was used to deposit the SiO_2 onto Ti wafers.

3.2.2. Inductively Coupled Plasma - Reactive Ion Etching

Inductively Coupled Plasma – Reactive Ion Etching (ICP-RIE) is one of the most widely used etching techniques in the field of semiconductor fabrication. This dry etching technique uses a combination of reactive species for chemical etching and ions for physical etching. With the addition of separate ICP RF power source connected to the cathode that generates DC bias and attracts ions to the wafer, a more controllable etching is achieved. Compared with regular RIE, ICP-RIE is able to be operated under lower pressure, offer higher etch rates, has better selectivity, and provide wider range of process control.[78] The anisotropic etching provided by ICP-RIE is also what is needed for the fabrication of micropillars with good shapes. Because of these benefits, ICP-RIE has been used for etching with oxide hardmasks in several studies.[79–81] For this project, ICP-RIE was used to etch the SiO_2 hardmask.

3.2.3. Titanium ICP Deep Etching

Titanium has attracted lots of attentions as one of the best befitting materials for bio-MEMS according to its high fracture toughness, great biocompatibility, good self-protection ability, and wonderful surface-modification potential.[82] In 2004, the metal anisotropic reactive ion etching with oxidation (MARIO) process was found to perform high-aspect-ratio bulk micromachining of titanium. **Figure 10** shows a flowchart of the MARIO process. By doing repetitive cycles of a Cl/Ar-based slightly isotropic etch step and an oxygen plasma-based passivation formation step, MARIO process was capable of

creating straight sidewalls and microscale features on titanium. This process produced about 0.5 μm/min etch rate, a selectivity of 40:1 between Ti/TiO_2 and a 1 μm minimum feature size.[83] However, two major limitation existed due to the etching mechanisms: a. relatively low etching rates because of the parallel plate system; b. scallops forming on the sideways on account of passivation steps.

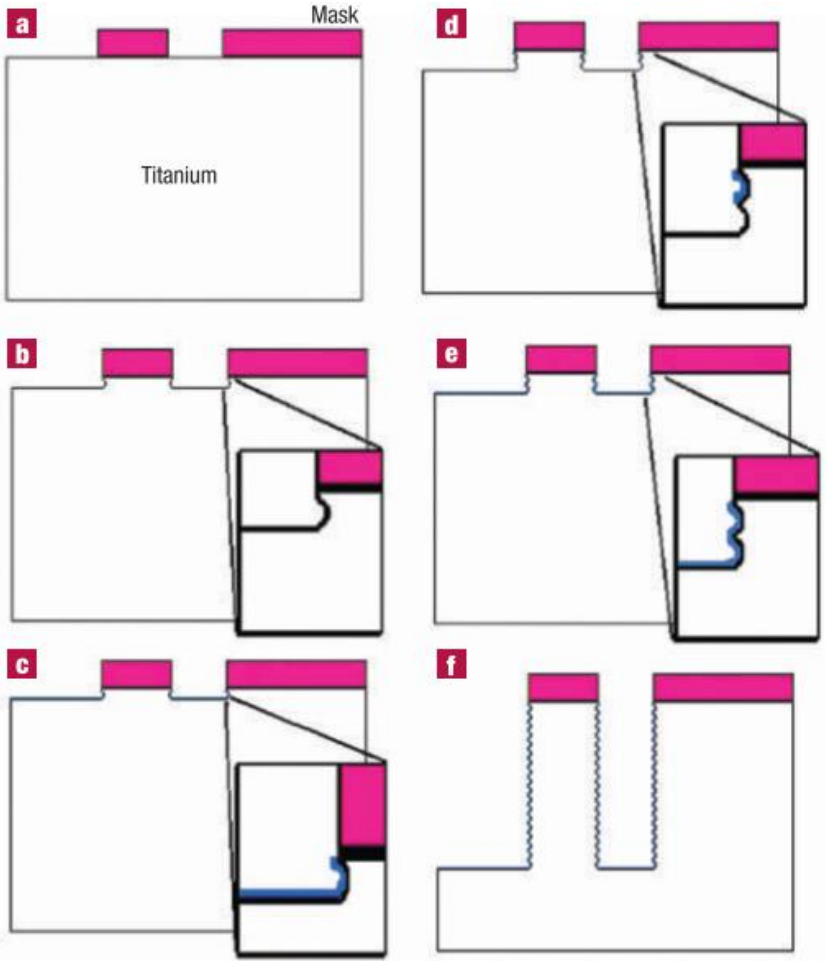

Figure 10. A flow chat describes MARIO process: a. oxide hardmasks on the top of titanium to define patterns; b. initial etch step slightly undercuts hardmasks; c. oxidation plasma creates passivation layer after each etching step; d. etch step starts again and slightly undercuts the oxidation layer; e. oxidation plasma produces passivation layer repetitively; f. high-aspect-ratio structures with scalloped sidewalls are obtained after cycles.[83]

One year later, studies were conducted to overcome shortcomings owned by MARIO process. Important etching parameters such as ICP source power, sample RF power, process pressure, and gas flow rates were optimized to obtain the desired titanium etching results. After research and analysis, the titanium ICP deep etch (TIDE) was developed, this process could reach a bulk titanium etch rates of 2 μm/min and 40:1 selectivity between Ti and TiO_2. Even better, smooth sides were obtained because of the elimination of scallops.[84] The development of TIDE process improved the bulk titanium etch quality and provided more application possibilities for Ti based MEMS. This technique had been used to fabricate microscale channels for a Ti based multi-frequency traveling wave dielectrophoresis (DEP) device for bioparticles separation,[85] and it also had been used to develop a Ti based microneedle devices for drug delievery.[79] For this project, TIDE process was used to fabricate micropillars with smooth sidewalls from Ti chips.

3.2.4. Wet Etching

As mentioned in previous section, passivation layer will be formed on micropillar sidewalls according to the mechanisms of TIDE process. The chemical composition of this layer are titanium, chlorine, and oxygen because of the use of Cl_2 during etching steps and O_2 during oxidation steps. The passivation layer will contaminate the NPT if growing NPT directly from this layer. In order to remove the passivation layer and expose the Ti underneath, wet etching is considered to be used. By putting the object into liquid reactant, certain materials can be dissolved through chemical reactions. Some advantages provided

by wet etching are: low price, almost no damage to purely chemical nature, and high selectivity. For removing the passivation layer, wet etching's poor anisotropy will not affect the results since these layers fully cover every surface of reaction chamber. Hence wet etching was adopted to remove the passivation layer for this project. Hydrofluoric acid (HF) is one of the most widely used wet etching reactant, it is capable of etching amorphous oxides, glass, and Ti at relatively high etch rates. For the fabrication of PMFRs, 2.3% HF was used in the passivation layer wet etching to make sure the process was controllable and not damaging the Ti substrate.

3.2.5. NPT Growing

According to DeRosa et al., NPT was able to be created by submerging Ti wafers into 10% aqueous H_2O_2 solution following an appropriate annealing.[57] In order to figure out the best condition to grow NPT with maximum reaction rate and minimum average crack size, a former PhD student conducted a Taguchi study. Based on the results, a 10% H_2O_2 concentration, 80 °C oxidation temperature and 5 hours oxidation time led to the optimal NPT growing rate and the smallest crack size. These parameters were used for the production of NPT for PMFRs.

3.3. PMFR Fabrication Process

The wafers used for this project were 100 mm thick Grade 1 commercially pure titanium wafers. First step was to deposit 4.2 μm silicon dioxide (SiO_2) onto the Ti wafers to form a protection layer. This SiO_2 was able to protect the Ti layer while wafer being diced, and also works as the hard mask in the later etching step. To do this, each wafer was put into a large enough flat beaker, Acetone, Isopropanol (IPA) and deionized (DI) water were poured into the beaker in sequence following by about 1 minute gently shaking to clean the wafer. Then the cleaned wafers were put into the chamber of Plasmatherm 790 system for the PECVD process. This process used two parallel electrodes – a grounded electrode and an RF-energized electrode to excite the reactant gases into plasma, which led to a deposition chemical reaction on the substrate surface.

With the SiO_2 covered Ti water, the next step was to dice each wafer into two pieces of 6 cm × 4 cm rectangular chip. Before dicing, the wafer was attached to a silicon (Si) wafer for strengthening purpose, 3M double-sided thermally conductive tapes were used for a good adhesion. Without the Si wafer as the substrate, the dicing residual Ti might stack on dicing blades which could damage the blades, Si wafer was capable of re-sharpening the blade to ensure a proper performance. A layer of photoresist SPR 220-3 was then spun coated onto the wafer to protect the wafer surface. Then a Disco DAD 321 Automatic Dicing Saw was used to perform the dicing. Scribed lines were created on the wafer with a process tools, then a dicing blade cut through wafer following the lines to obtain the chips. Acetone, IPA and DI water combined with an ultrasonic cleaner were then used to remove the photoresist and clean the diced chips.

Photolithography was the next step where desired patterns would be delineated on the chips. To do this, photoresists needed to be coated on the chip surfaces. First, the hexamethyldisilazane (HMDS) was spun onto the chip to form a uniform layer which ensured that the surface was hydrophobic, it promoted good photoresist-to-wafer adhesion. Then the photoresist SPR 220-7 was spun onto the same chip to get a 5.5 μm thick layer. This spin coating process was performed using a spin coater, where the chip was put onto a rotated substrate, the vacuum connected to the back of this substrate would keep the chip fixed on the substrate while it started rotation. Rotation speed, acceleration, and spin time were adjusted based the viscosity of photoresists to define the thickness of photoresist layer. After confirming that there was no defect on the photoresist, the chips were put into the Karl SUSS MA-6 Mask Aligner to get the UV exposure. The patterns of MP and P were controlled by two photomasks made by L-Edit. In the mask aligner, Ti chips were placed under the photomask, and UV irradiation from above passed through the transparent areas on the photomask and dissolved the photoresist. Then the Ti chips were put into AZ 300 MIF developer to get rid of the residual dissolved photoresists. After photolithography, patterns were examined using an optic microscope to ensure a good quality.

After the previous step, patterns were printed on Ti chips in the form of photoresists. The next step was plasma etching which could be decomposed into two parts: SiO_2 etching and Ti etching. An Oxford Cobra Plasma Model 100 Silicon Trench Etch system was used to perform the SiO_2 etching. Each Ti chip was attached to a thoroughly cleaned Si substrate wafer, and then put into the reaction chamber. Etching was running with C_4F_8 gas plasmas under the Cryo mode with -20 °C reaction temperature. After SiO_2 etching, Ti chips were

cleaned with Acetone, IPA and DI water to remove the left-over photoresist. With this step, the patterns were transferred from photoresists to the SiO_2 hardmask. For the fabrication of all three planar microreactors and MP50, an Oxford Cobra Metal Trench Etching system was used to do the Ti etching. With the Ti chips attached to Si substrate wafers being put into the chamber, etching ran with Cl_2/O_2 gas plasmas at 20 °C temperature. As for the MP100 and MP150, Ti etching was performed using a Panasonic E626I ICP System with Cl_2/Ar gas plasmas at UC Santa Barbara. The reason why two different Ti etching systems were used was that the Oxford system at UC Riverside offered higher ICP power and higher Cl_2 flow rates compared to the Panasonic systems, which led to more aggressive etching. After Ti etching at UCR, the middle region of 100 μm and 150 μm micropillars had smaller diameters compare to other regions of the micropillar causing an irregular shape, some pillars even broke apart since the etching was too aggressive. To ensure a perfect cylinder shape for micropillars in all devices, two Ti etching systems were used. Devices were put into a beaker with Acetone for 3 days to separate Ti chips and the substrate Si chips. Inlets and outlets were then drilled on all microreactors with an electric drill.

Ti chips were then submerged into 2.3% diluted HF for removing the passivation layer formed during Ti etching process. Wet etching was performed using the acid bench inside UCR nanofabrication facility to avoid danger caused by the highly corrosive HF. While chips being submerged in HF, a large amount of bubbles were generated from the reaction chamber, this was caused by the gases generated from reaction between HF and passivation layer. Ti chips were then picked out by plastic tweezers and rinsed with DI water immediately. Afterwards an ultrasonic cleaner was used to clean Ti chips for 5

minutes to ensure that there was no HF left on chips. After removing passivation layers, NPT was grown by submerging Ti chips into H_2O_2 solution. 400 mL 10% solution was prepared and stored in a large glass beaker, a Corning PC-420D stirring hot plate was used to heat up the solution and maintain an 80 °C temperature. The solution temperature was monitored by a chemical safe thermometer during the whole time. After 5 hours, Ti chips were taken out from H_2O_2 solution and rinsed with DI water, then they were annealed at 300 °C for 8 hours using a Lindberg Blue M Box Furnace. Finally each Ti chip was examined using a Zeiss STEM Scanning Transmission Electron Microscopy to make sure there was no apparent defect on these devices. **Figure 11** shows a flowchart about the brief fabrication process of PMFRs.

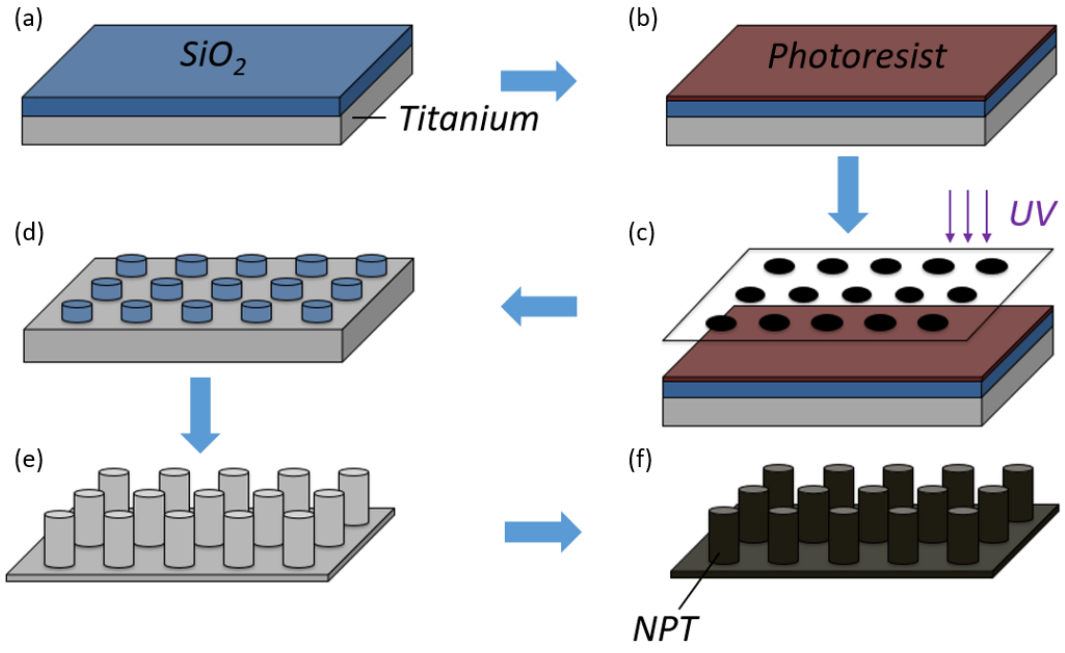

Figure 11. A flowchart of the fabrication for micropillar microreactors. (a) SiO_2 hardmask deposited onto Ti wafer using PECVD; (b) photoresist SPR 220-7 spun onto chips; (c) patterns transferred from photomask to photoresist under UV exposure; (d) patterns transferred from photoresist to SiO_2 hardmask through ICP-RIE process; (e) Ti micropillars etched through TIDE process; (f) NPT grew on reaction chamber after removal of passivation layer.

4. Study 1: Photocatalytic Degradation Performance of Organic Dyes With Micropillar/Planar Microreactors

4.1. Introduction

As introduced in the Background chapter, with the fast development of industries, wastewater effluents has been one of main reasons why drinkable water faces severe safety challenges. Among all contaminants in wastewater effluents, organic dyes have abilities to hydrolyze and have reaction with other contaminants to generate harmful byproducts, the carcinogenicity of these byproducts makes them not only bad for environment but also extremely harmful for peoples' health.[86] Painting and textile industries are in favor of using organic dyes and discharging wastewater effluents to the environment.[87] Some harmful organic dyes that can be commonly found in industrial effluents include Rhodamine B, Acid Red 114, ethyl violet and methylene blue.[88–90] Using conventional purification methods such as filtration, ozonation etc., has very low efficiency on removing these dyes On the contrary, photocatalysis has been proved to work well on dissolving organic dyes.[91] This topic has been popular for both academics and industries for a long time, and organic dyes have gradually become a commonly used target contaminant to examine the activity of photocatalysis for all types of photocatalysis reactors. The two benefits about using organic dyes to evaluate photocatalysis are: a. the fast reaction rate between organic dyes and photocatalysis products (ions, electron holes, and free radicals) can present the real-time reaction as solution flows in microreactors; b. concentrations of dyes can be easily determined by measuring the light absorbance of collected samples.

Methylene blue (MB) has been used the most in photocatalysis studies among all organic dyes. The textile industry heavily uses this cationic dye for dyeing wool, cotton and silk, and human consumption of MB may lead to vomiting, diarrhea, nausea and burning sensation in eyes.[92] Studies have been conducted by researchers to investigate the pathway of TiO_2/UV-based photocatalytic degradation on MB. Results show that the photocatalysis products mainly the hydroxyl radicals (·OH) are capable of dissolving and eventually fully mineralizing MB particles into final products - CO_2, NH_4^+, NO_3^- and SO_4^{2-} companying with decolorization.[86,93] This mechanism makes MB a superb target contaminants to evaluate photocatalysis efficiency. For this study, MB was selected as the target contaminant, performance of both MP and P were both evaluated based on MB concentrations. The MB degradation performance of six microreactors with different chamber depths and geometries were examined. For each microreactor test, five residence times were used (5, 10, 20, 30, 40 seconds), the trend of MB degradation performances at different residence times would illustrate how different variables affected photocatalysis. It was worth mentioning again that the residence time measured how long a contaminant particle could stay in the reaction chamber before flowing out. There are two objectives for this study: first, proving the enhancement on photocatalysis brought by the addition of NPT micropillars through comparing the MB degradation performances of MP and P; second, verifying the superiority of the PMFR design by comparing the best PMFR's MB photocatalytic degradation performance to the performances of microreactors from various published literatures.

4.2. Methods

4.2.1. Experiment Devices and Setup

4.2.1.1. Microreactor Fixture

To test the proposed microreactors, an aluminum fixture was designed and fabricated to offer a water-sealed and gas-tight environment for the reaction chamber. This aluminum fixture was consisted of a top and a bottom parts. The top fixture owned a stratified structure which could be decomposed into two levels. Top level had 100.2 mm length, 74.8 mm width and 10 mm total height, it worked as the connection part to the bottom fixture. Bottom level had 60 mm length and 40 mm width same as the plan view dimensions of microreactor chips, and it had height of 4 mm. In the center of top fixture, a window with slightly larger dimension than the dimension of reaction chambers was created vertically penetrating the fixture. This window would allow UV irradiation to reach reaction chambers while running experiments. The bottom level was designed to be pressed on the chips to offer a desired working environment. As for the bottom part of the fixture, it was in a perfect rectangular shape with 100.2 mm length, 74.8 mm width and 12 mm height. Two 2 mm diameter, 5 mm depth holes with 39.7 mm pitch were created in the center of the bottom fixture from top; two 3.94 mm diameter, 7 mm depth holes with thread were created at the same locations from the bottom. These holes were linked to be used as the flow inlet and the outlet for experiments, threads allowed the installation of tubing fittings which kept tubing fixed in the inlet and outlet. On both fixtures, ten 5 mm diameter M5 thread holes were created with uniform pitch.

In order to seal the reaction chamber, a 60 mm long, 40 mm wide and 1 mm thick quartz slide bonded with 250 μm thick PDMS gasket was laid over the microreactor chip. Quartz slides had excellent UV transparency, UV irradiation would not be affected by putting them on the microreactors. The addition of thin PDMS gasket helped eliminate any leakage possibilities which ensured no disturbing on photocatalysis inside the chamber. Meanwhile, two 1 mm thick PDMS gaskets were used to provide protection for microreactor chips and quartz slides against the pressure created by aluminum fixtures. These thick PDMS gaskets could absorb some of the forces directly generated by the fixtures, they were able to prevent quartz glass from being broken and offer enough pressure to keep reaction chamber sealed in the meantime. An exploded view of experiment fixture model and a side-view schematic are presented in **Figure 12**. From up to down, the fixture had layers in the sequence of the top aluminum fixture, the top thick PDMS gasket, a quartz slide bonded by a thin PDMS gasket, microreactor chip, the bottom thick PDMS gasket and the bottom aluminum fixture. After installation, ten M5 screws were used to tight the fixture.

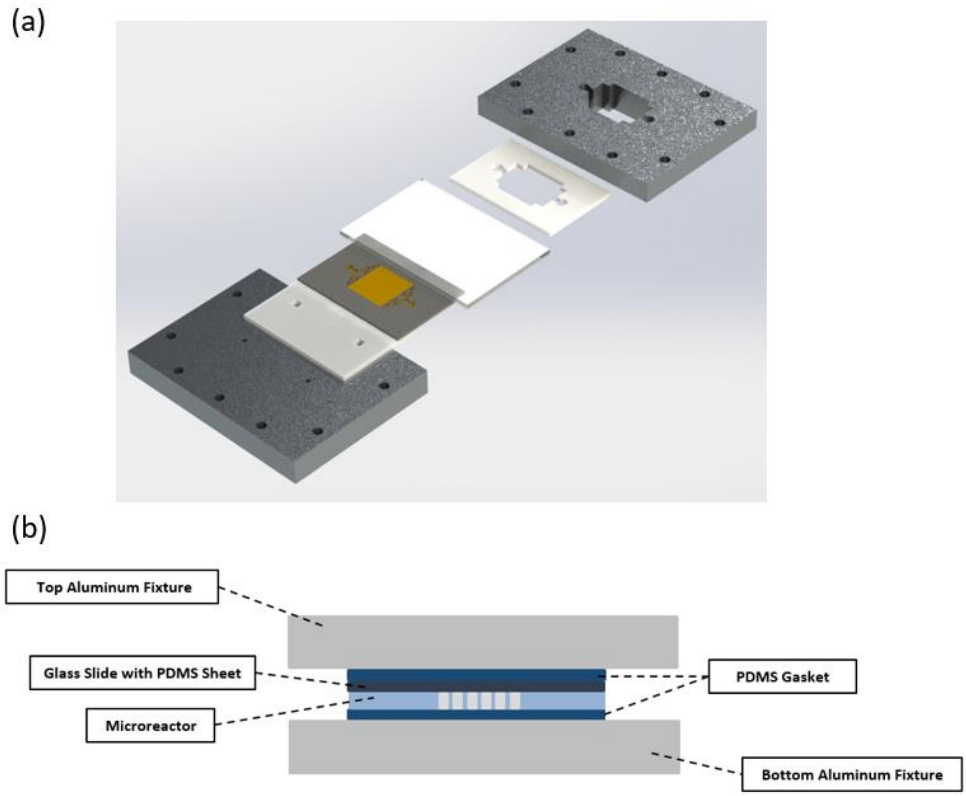

Figure 12. Presentation of the experiment fixture: (a) a CAD model to show the exploded view. From up to down, layers are top aluminum fixture, top thick PDMS gasket, a quartz slide bonded by a thin PDMS gasket, microreactor chip, bottom thick PDMS gasket, bottom aluminum fixture; (b) a side-view schematic of all layers.

4.2.1.2. Experiment Setup

With the microreactor fixture being installed, an experiment system was assembled to run the photocatalytic degradation experiments. A schematic of the experiment setup was shown in **Figure 13**. A Harvard Apparatus PHD 2000 syringe pump combined with the 10 mL Hamilton gas tight syringes were used to produce the liquid flow. This programmable syringe pump was able to control the MB solution flow rates. The gas tight syringe eliminated the possibility of air bubbles forming in the reaction chamber, which

ensured the reaction chamber work at its best condition. Two 0.01” ID tubing were connected to tube fittings which allowed them to be installed onto the inlet and outlet on bottom fixture. MB solution was able to flow through the tubing and enter the reaction chamber. A Black-Ray B-100A UV lamp with 365 nm wavelength and 100 W power was placed 1” above the microreactor fixture to provide the UV irradiation. The light intensity through the thin PDMS gasket bonded quartz slide was measured to be 5.5 mW/cm^2. In order to prevent the microreactor fixture from being heated by the UV, the fixture was placed in a water bath while running the experiments. The outlet port of the tubing would be placed in an Erlenmeyer flask to collect the effluent MB solution. A cuvette was then used to collect 1.5 mL of MB, then the solution was sent to a UV-Vis Thermo Scientific Evolution 60 spectrometer for concentration measurements at 665 nm wavelength. Each cuvette was thoroughly cleaned by ethanol and DI water after measurements.

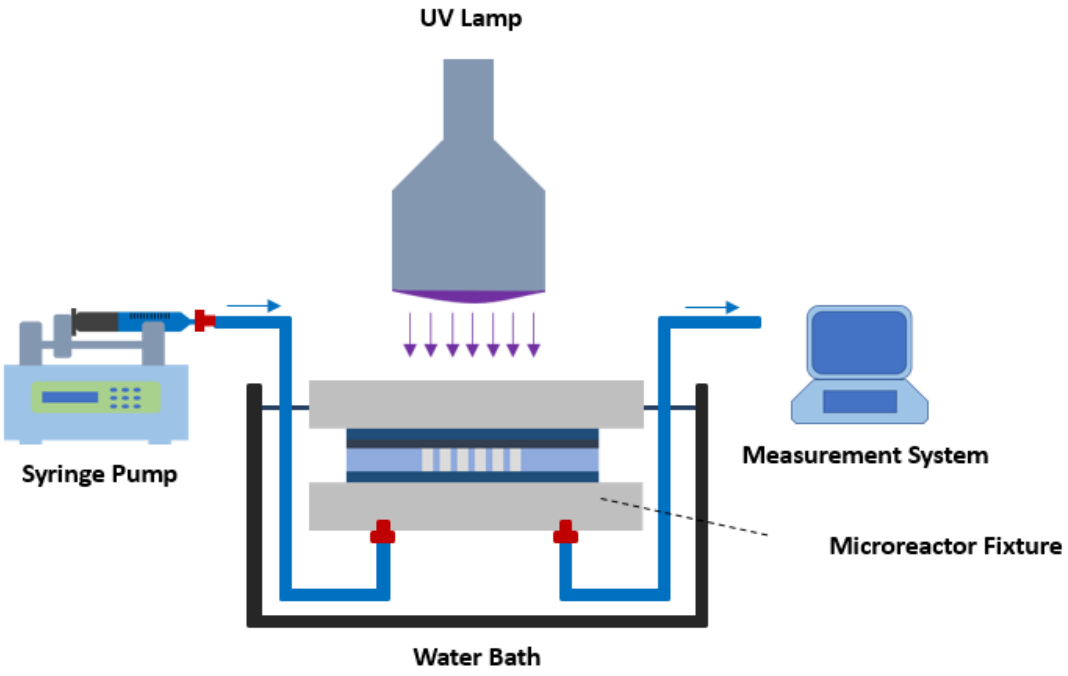

Figure 13. A schematic of the photocatalytic degradation experiment setup. Syringe pump controls the flow rate. UV lamp provides the UV illumination. Water bath keeps the operating temperature at normal. The outflow solution is collected and analyzed with different instruments based on the requirements.

4.2.2 Experiment Process

The target MB concentration used in this study was 20 µM, this concentration was selected based on the fact that it was double the ISO standard for MB degradation test.[94] As mentioned in previous sections, six microreactors – MP50, MP100, MP150, P50, P150, and P150 were put into use for this study. For each microreactor, the degradation performances of microreactor at five residence times were investigated. These residence times were controlled by adjusting the flow rates offered by the syringe pump, flow rates

for each device at different residence times were presented in **Table 2**, calculation was made based on reaction chamber volumes and residence times.

Microreactor	MP50	MP100	MP150	P50	P100	P150	Residence Time (s)
Flow Rates (μL/min)	36	63	97.5	36	73.5	109.5	40
	48	84	130	48	98	146	30
	72	126	195	72	147	219	20
	144	252	390	144	294	438	10
	288	504	780	288	588	876	5

Table 2. Flow rates for each microreactor at different residence time.

The experiment started with a purge of the system, 2 mL KOPTEC 200 Pure Ethanol 200 Proof was flowed through at the fastest flow rate. Ethanol helped eliminate all the air and potential residual particles inside the system to prevent forming of air bubbles and pollution. Then 2 mL DI water was flowed through the system to clear away the ethanol. The next step was for evaluating the dark adsorption effect, the experiment fixture was covered by a large piece of aluminum foil to ensure that the microreactor was in an absolute dark environment, MB was flowed through system at the slowest flow rate time for 1 hour, 1.5 mL MB effluent was collected for UV-Vis measurement afterwards. This step was performed to verify that the adsorption effect created by the microreactor geometries would

not observably affect the MB degradation performance. For the next step, the aluminum foil was removed and the turned-on UV lamp was placed above the reaction chamber window. 1 mL of MB was flowed through the system with desired flow rate to guarantee that the system was filled with MB being in the reaction chamber at the desired residence time. Then 1.5 mL of MB effluent was collected and measured. This step was cycled for all five residence times in the sequence of 40, 30, 20, 10 and 5 seconds. After collecting all desired solutions, the experiment system was purged by 5 mL ethanol and 5 mL DI water flowing at the highest flow rate, it would remove most of MB particles physically adsorbed by the system and assure that the next experiment would receive minimum influence by the residual created during the current study. Each experiment was run three times on the same microreactor to minimize errors. Between each experiment, the thin PDMS coated quartz slide was replaced with a new one to ensure the best degradation effects.

4.3. Results and Discussions

For evaluating the photocatalytic degradation performances of the six microreactors produced for this study, two performance metrics were used. It is worth noting that there is no standard model for evaluating the microreactor's performance. The decrease in contaminant concentrations is most reported performance metric which has been reported by some previous reported photocatalytic degradation of organic contaminants over TiO_2 studies.[95,96] In this study, for a better comparison of the performance by PFMRs with other reported microreactors, a novel metric – degradation

activity was used. The activity measures the mass of MB being degraded per minute and then being normalized to the chamber volume, this metric is able to normalize the MB degradation performance of reactors using different chamber volume and flow rates to the same unit, thus making the comparison among different devices possible. These two metrics were measured at five different residence times for each microreactor, comparisons and discussions were made based on the results.

4.3.1. Degradation Percentage

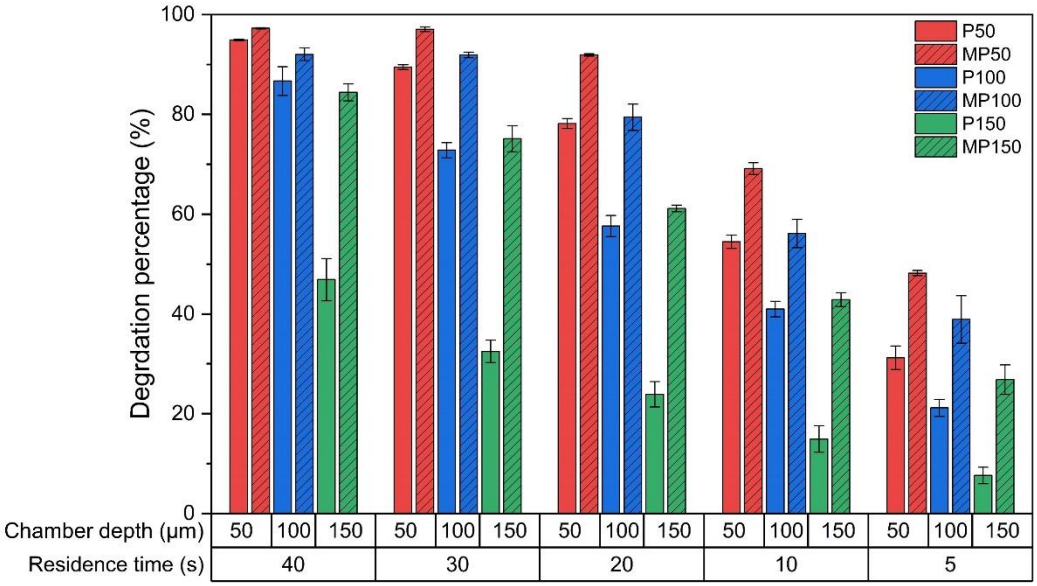

Figure 14. MB degradation percentage for each microreactor at different residence time.

Figure 14 presents the degradation percentage of MB for each device at different residence times. For MP and P with the same chamber depth, MP always achieved higher degradation percentages compared the planar counterparts. This was mainly because of the

addition of micropillar arrays, micropillars largely increased the SA:V ratio of the catalyst which allowed MB molecules to have easier access to the catalyst surface thus enhancing the degradation reaction.

As for the influence of chamber depths, for both MP and P, larger depths led to lower degradation percentages. For the reactor with micropillar arrays, the main factor that caused this circumstance was the limitation of photon penetration. Larger depths made photons have more difficulties to penetrate to the bottom of reaction chamber, a long penetration distance caused a large amount of photons to lose their energy while being scattered or absorbed by pillars. Without enough photon energy, the amount of free radicals generated by NPT in the deeper region of chamber was limited, which weakened the degradation reactions in this region. For planar reactors, the main limiting factor was the laminar flow. The generated hydroxyl free radicals stayed close to the catalyst surface, which meant MB molecules needed to diffuse to the bottom of planar reactor to have reaction with ·OH. Larger chamber depths increased the diffusion length for MB molecules, which negatively influenced the degradation percentage.

Residence time also largely affected the MB degradation. For each device, higher degradation percentage was obtained with longer residence time. MB molecules had more time to diffuse to the catalyst surface and have reaction with ·OH when residence time was longer. It was worth mentioning that for MP50 at 30 and 40 seconds residence times, only 1.99% differentiation was noticed, this was mainly because the degradation of MB almost reached saturation at both conditions, the degradation was not as aggressive as it was at

lower residence times. All in all, MP50 reached the highest MB degradation percentage of 97.26 ± 0.15% at 40 seconds residence time.

4.3.2. Degradation Activity

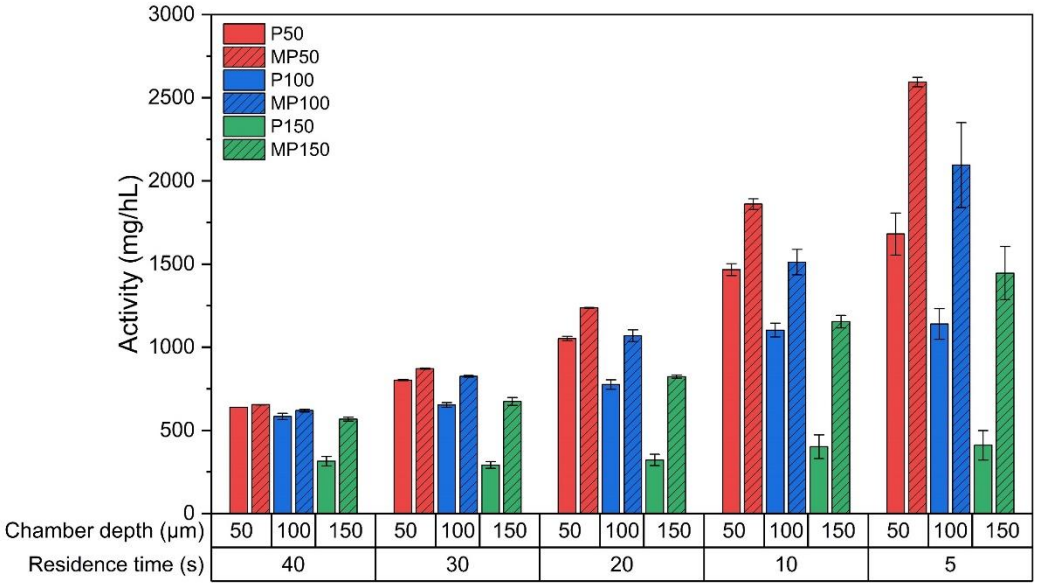

Figure 15. Degradation activity for each microreactor at different residence time.

The degradation activity for each microreactor is presented in **Figure 15**. This metric was adopted to exhibit the mass degradation of MB normalized by residence time and chamber volume. It was clear that micropillar reactors presented higher degradation activity compared to their counterparts, and this differential increased as the residence time became shorter. And the microreactor with lighter reaction chamber always showed higher degradation activity than the one with deeper chamber at the same residence time. MP50

at 5 seconds of residence time presented the highest activity among all devices of 2595 ± 28 mg/hL, it was about 79.58% higher than the activity of MP150 at 5 seconds of residence time and 531% higher than that of P150 at 5 seconds of residence time. For micropillar reactors, limitation of photon penetration in the deeper reaction chamber mainly contributed to this differential, almost all the NPT on the surfaces of MP50's micropillars and chamber ground were accessed by photons during experiments, causing MB molecules have intense reaction with ·OH in every corner of the reaction chamber, thus leading to high activity. As for MP150, on the contrary, the amount of photons which could reach the lower part of the pillar and the chamber ground was limited, which meant that less ·OH were generated at those locations, thus some volume of the chamber being lack of having efficient degradation reactions limited the activity of this reactor. Residence time also played an important role in influencing the degradation activity. For each reactor except P150, the degradation activity increased as residence time decreased. In order to decrease the residence time, the flow rate needed to be increased. Higher flow rate was able to push more MB molecules into the reaction chamber and it allowed more degradation reactions to happen, thus increasing the degradation activity. In conclusion, for this MB study, the highest degradation activity was achieved by MP50 at residence time of 5 seconds. This activity result would also be used for comparison with the activity collected from other reported microreactors.

Herein, a summarization of some identical comparable photocatalytic microreactor studies are presented in **Table 3**. Some important parameters for MB degradation study with photocatalytic microreactors – conditions of light source, MB concentration, and the

volume of reaction chamber are listed. Light intensity has been proven to be one of the main influence factors for photocatalytic degradation of organic pollutants. Since the UV radiation is a key ingredient for the photocatalysis process, high light intensity UV leads to the generation of high concentrations of ·OH.[97] The degradation rate is expected to be increased with increasing light intensity; however, one study claims that the impact of light intensity becomes negligible at high doses.[98] For our study, the influence of light intensity was not looked into because of the target operating environment. This device is expected to be used on the ISS where there is enough UV irradiation, so it can be assumed that the light intensity would reach its saturation when the reactor is being used on the ISS. The light intensity produced by the UV lamp used for this study is relatively low, hence the degradation of MB is mainly due to photocatalysis generated through the combination of formal coverage of TiO_2 catalysts and photons. Light intensities for UV irradiation of different studies are also reported here for a comparison.

The four devices reported in the Table 3 are all microreactors, the first three of them have already been briefly introduced in the Background chapter. The TiO_2 dual-film optofluidic microreactor intended to enhance the specific area of catalyst and enlarge the mass transfer by creating TiO_2 nanorod arrays on both the top and bottom internal wall of the reaction chamber.[73] The dual-film design also allowed the incident light to be harvested at both top and bottom of the chamber which reduced the waste of photons. By conducting degradation experiments with the same concentration of MB as what we used, they found that the degradation reaction rate constant of the dual-film microreactor was 2 times higher than that of the conventional planar counterpart. However, this device obtained 646 mg/hL

as the highest activity, and it was about 4 times smaller than the highest activity of MP50. The main limitation of the dual-film microreactor was the size of nanorod arrays. These nanorods had an average length of around 2.4 μm, they were immobilized on the reaction chamber with a depth of 200 μm. Most of ·OH could not reach the space in the middle of the chamber, causing some MB molecules not to be degraded before flowing out of the chamber. As for MP50, since the micropillars had the same height as the chamber, a higher SA:V and greater mass transfer rate were generated, leading to a relatively higher activity.

As for the biomimetic microreactor proposed by Liao et al., it was a planar reactor with a bifurcated microchannel designed based on the Murray's law.[70] This design was supposed to create a larger flow velocity fluctuation than what the reactor with conventional bifurcating channels could do, and they found a 68% increase in the degradation efficiency compared to the no-biomimetic ones. As a planar microreactor, it generated a maximum activity of 1380 mg/hL, about 47% lower than that of MP50. It was worth noting that this device only had a 5 μL reaction volume, which led to a high mass transfer rate but very low throughput; the light intensity used for this study was 100 mW/cm^2, which was extremely high compared to the light intensity used for MP50 and other devices reported here. These two factors might contribute to their decent activity result, though as a planar reactor. The PMFRs including MP50 all adopted the biomimetic design for the bifurcating microchannels, with the addition of NPT-coated micropillar arrays, a higher degradation activity was achieved with greater throughput under lower intensity light source.

The conventional planar microreactor was facing a problem of limited mass transfer rate due to the laminar flow, the optofluidic microreactor designed by Li et al. tended to overcome the drawback by adding in TiO_2-coated fiberglass.[71] Such design offered two benefits: first, the mass transfer rate was increased by adding in more scaffolding of catalysts; second, perturbation was added to liquid flow to enhance the performance. The degradation efficiency of the microreactor with fiberglass observed a 25% increase compared to that of the conventional microreactor. And this reactor reached a maximum activity of 808 mg/hL, which was about 4 times lower than the highest activity of MP50. Although both micropillars arrays and fiberglass tried to enhance mass transfer through adding in more scaffolding of TiO_2, the micropillar arrays were more uniform placed and offered more surface of catalysts compared to the one with fiberglass.

The last microreactor was using a stainless steel mesh-supported ZnO disc as the catalyst.[99] It was claimed that most of the surface of the catalyst was not in contact with the MB molecules, most of degradation happened on the eternal non-polar edges of the ZnO nanosheets. This phenomenon was mainly caused by the hydrophobicity of the nanosheets polar faces and the low MB pH. However, this microreactor still presented superior MB degradation performance compare with microfluidic reactors reported in other literatures, a maximum activity of 1305 mg/hL was obtained by this device. MP50 still owned a maximum activity almost 2 times higher than that of this reactor. What was noteworthy was that this author reported activity as the evaluation metric for the comparison of MB degradation performance by different microreactors. Not only that, another report about a metal-ion doped TiO_2-coated planar microreactor also did

comparisons for MB degradation with different microreactors in the metric of activity, where they named it as degradation rate per unit reaction volume (DRPRV).[100] These examples showed that activity was a good metric to be used for the comparison of degradation performance with microreactors owning different sizes and various experiment conditions.

Device	Light Source	MB (mg/L)	Reaction Volume (μL)	Flow Rate (μL/min)	Residence Time (s)	Activity (mg/hL)
MP50 (this work)	100 W, 5.5 mW/cm^2	7.478	24	288	5	2595
TiO_2 dual-film optofluidic MR[73]	150 W, 2 mW/cm^2	7.478	40	120	20	646
TiO_2 biomimetic MR[70]	150 W, 100 mW/cm^2	11.217	5	25	12	1380
TiO_2 fiberglass optofluidic MR[71]	150 W, 2 mW/cm^2	7.478	50	200	15	808
ZnO thin-film MR[99]	400 W, 9.9 mW/cm^2	10	99	333.3	17.8	1305

Table 3. A summarization of the test conditions and degradation activities for MP50 (this work) and microreactors reported in other literatures. It is worth noting if the activity of a certain device cannot be found in the cited report, it is calculated based on the device dimensions and experiment results claimed by the report.

Since the microreactor is aiming to be used on the ISS where space is very precious, the best microreactor should be able to degrade most amount of MB molecules in a unit of time and volume. Hence, the device with the highest activity suits best for this project's requirement. Judging from the comparison result, the MP50 at 5 seconds residence time has a maximum activity almost 2 times higher than the highest activity that other reported reactors can get. The results of MB degradation percentages and the degradation rate constants also demonstrate the superior performance of microreactors with NPT-coated micropillar arrays than that of their planar counterparts. MP50 shows the best performance among all PMFRs fabricated for this study based on the two performance metrics. A reduction of photon penetration after the depth exceeds 50 μm has been proved by a Monte-Carlo ray tracing model performed by our collaborator,[101,102] as well as a ray tracing model created by the author of this dissertation using COMSOL Multiphysics.[76] All in all, the MP50 has a great potential to be used for the WPA system on ISS. An organic contaminants removal module can be formed by setting numerous of MP50 in parallel to ensure a decent throughput. For confirming MP50's ability on degrading the contaminants required by NASA, studies about quantifying the ·OH generated by MP50 system as well as degradation studies with real toxic organic compounds instead of organic dyes are conducted for the next step.

5. Study 2: Measurement of Steady-State Hydroxyl Radicals Concentration and VOCs Half-Lives Estimation

5.1. Introduction

Photocatalysis has been proved to be one of the most effective ways to degrade organic pollutants in aqueous solution. The electrons and holes generated on the catalyst's heterogeneous surfaces lead to the redox reactions that produce reactive species such as hydroxyl radical (·OH), superoxide anion radical ($\cdot O_2^-$), and hydrogen peroxide (H_2O_2). The degradation reactions take place through the oxidative and reductive reactions involving these radicals.[103] Among all free radicals, ·OH has been proved to play the most important role in the photocatalytic degradation of organic contaminants. These radicals can have rapid reactions with electron rich sites of organic compounds, and these reactions initiate more complex radical chain reactions to break the chemical bonds as a consequence.[104] The fact that ·OH is able to react with more than 600 organic molecules with rate constants on orders ranging from 10^6 to 10^9 M^{-1} s^{-1} makes them have very low selectivity towards organic compounds.[105] For organic dyes, in general, the decolorization takes place mainly because of aromatic ring structures being attacked by ·OH.[106] When it comes to the stubborn organic chemicals such as 1,4-dioxane, ·OH dominates the degradation reaction compared to other reactive species.[107] As for inactivation of bacteria like *E. Coli*, ·OH has been proved to be able to initiate oxidizing reaction to the cell wall and cell membrane which causes severe morphological and structural injuries, thus kill the bacteria.[108]

This project is motivated by the current problem existed in the WPA system on ISS as described in the Introduction chapter. For testing the current thermal catalytic reactor, several Ersatz solutions were designed based on the ISS wastewater components by research groups from NASA.[109] In 2016, one group worked on developing a new catalysts that could make the thermal catalytic reactor work at lower temperature and pressure brought up three types of optimized Ersatz solutions for testing their new catalysts. The type II Ersatz solution simulated the wastewater collected on ISS, and it was a slightly simplified specimen that imitated the ISS wastewater and it was designed for the laboratory test. This solution was consisted of 10 harmful VOCs with different concentrations resulting in a total TOC level of 35.75 mg/L. Considering the unexpected increasing transport time caused by the COVID-19 pandemic for getting the 10 VOC solutions, an estimation model was prompted to evaluate the PMFR's degradation performance on the type II Ersatz solution.

This estimation model is based on predicting half-lives of each VOC from the Ersatz solution according to the steady-state hydroxyl radical concentration within the reaction chamber. Based on the fact that the degradation kinetics of VOCs is largely affected by the ·OH, the steady-state hydroxyl radical concentration ($[\cdot OH]_{SS}$) and the 2nd-order rate constant $k_{\cdot OH}$ are able to determine the half-life time of VOC while being in the reaction chamber. According to the United States Environmental Protection Agency (EPA), the half-life indicates the time required for the concentration of a solute to drop 50% in a solution, it has been used to characterize the degradation of contaminants in certain solutions for a long time.[110] A shorter half-life means that a certain contaminant needs less

time to be degraded to half of its original concentration, indicating a better system degradation performance. While the PMFR is working, the ·OH generated by photocatalysis will finally reach saturation and the concentration of ·OH will remain at a steady-state, this steady-state concentration can be calculated by using a competition kinetic method which is going to be introduced in later sections. There are two objectives for this study: first, finding the $[\cdot OH]_{SS}$ for the best performance PMFR while in operation; second, evaluating the PMFR degradation performance on VOCs from the type II Ersatz solution through estimating the half-lives.

5.2. Methods

5.2.1. Experiment Process

The PMFR used for this study was MP50 based on its best photocatalytic degradation performance among performances by all 6 microreactors. The experiment fixture and setup were identical to the MB degradation tests. Nitrobenzene was selected as the ·OH scavenger probe because of its extremely high reactivity with ·OH and relatively low reactivity with other reactive radicals.[111] It was also one of the most widely used ·OH detection probes for lots of related studies.[112–114] For this study, nitrobenzene was diluted to 8 µM for the probe purpose. This concentration was selected based on a low 5.5% branching ratio, the branching ratio reflected the contribution of each organic matter on the consumption of ·OH, and it was assumed that a branching ratio of nitrobenzene at 5.5%

would not affect the steady-state [·OH] while ·OH having reactions with most kinds of the VOCs. All nitrobenzene solutions were collected for 1.8 mL and stored in 2 mL Screw Thread Autosampler Vials covered by 9 mm Screw Thread Autosampler Caps. These samples were then sent to an Agilent 1200 Series High Performance Liquid Chromatograph equipped with a diode array detector for the nitrobenzene concentration measurement.

In order to minimize the influence brought by the system physical adsorption of nitrobenzene particles, a dark adsorption test was performed at the very start. 15 mL DI water was flowed through the system to purge air and possible contaminants, then 8 μM nitrobenzene solution was pumped into the system at the highest flow rate of 288 μL/min. The experiment fixture was covered by an aluminum foil during this experiment to eliminate any light. The highest flow rate was used because it could allow most amount of nitrobenzene particles to flow through the system in the same amount of time. This process was run for 3 hours, and effluents were collected every 30 minutes for measurements. An adequate time to avoid physical adsorption effects was decided based on the results.

For collecting the concentrations of nitrobenzene after reaction with different residence times, it began with the same process under dark environment. The system was purged by 15 mL DI water, followed by 8 μM nitrobenzene solutions flowing for the time decided from the previous step. Then 1.8 mL effluent was collected to verify that the concentration was not affected by the dark adsorption. The UV lamp was turned on and the aluminum foil was removed afterwards. For obtaining the nitrobenzene concentrations at different residence times, four different residence times 5, 10, 20 and 30 seconds were used.

The experiments proceeded from the longest residence time to the shortest residence time. This sequence was chosen because of the reason that solution at lower concentration would not affect solution with higher concentration. After collecting the effluent which went through 30 seconds residence time, the flow rate was switched to provide 20 seconds residence time, 5 mL of nitrobenzene was allowed to flow through the system before the collection of effluent. By doing this, it could make sure that all solution from the previous collection was pushed out, and this process was repeated every time after changing the flow rate. After collecting all desired solutions, 20 mL DI water was flowed through the system at highest flow rate to clean off all the residual nitrobenzene. This experiment was run three times to minimize the errors.

5.2.2. Steady-State Hydroxyl Radicals Concentration Calculation

It has been proved by many researches that the degradation reaction between hydroxyl radicals and organic compounds, even bacteria is a pseudo-1st -order reaction.[115–118] A pseudo-1st-order reaction is a simplified way to inspect a 2nd-order reaction to avoid more complicated experiments and calculations. This reaction is overall a 2nd-order reaction but is 1st-order with respect to two reactants. For a pseudo-1st-order reaction with two reactants A and B, the rate of disappearance of A can be calculated through

$$\frac{d[A]}{dt} = -k[A][B] \qquad (4)$$

In this equation, the brackets represent the instant concentration of the reactants, and *k* stands for the 2nd-order rate constant for the reaction between the reactants. And for a 2nd-order reaction with two reactants, when the initial concentrations are not the same, the integrated rate equation is:

$$\frac{1}{[B]_0-[A]_0} ln \frac{[B][A]_0}{[A][B]_0} = kt \quad (5)$$

where $[A]_0$ and $[B]_0$ stand for the initial concentration of reactant A and B. When $[B]_0 >> [A]_0$, the influence of reactant A on reactant B would be negligible so it can be assumed that the $[B]$ remains constant through the whole reaction thus $[B]_0 = [B]$. Then the equation 5 becomes

$$\frac{1}{[B]} ln \frac{[A]_0}{[A]} = kt \quad (6)$$

By doing simple transition, equation 6 can be written as

$$\ln\left(\frac{[A]}{[A]_0}\right) = -k[B]t \quad (7)$$

For this study, the two reactants are the nitrobenzene and ·OH, and since the ·OH is being constantly generated by photocatalysis, it can be assumed that the concentration of ·OH will be essentially constant and it will not be affected by other reactants. Following equation 4, the rate of disappearance of nitrobenzene can be written as

$$\frac{d[NB]}{dt} = -k_{(NB+\cdot OH)}[NB][\cdot OH]_{SS} \quad (8)$$

where $[\cdot OH]_{SS}$ is the steady-state hydroxyl radical concentration, and $k_{(NB + \cdot OH)}$ is the 2nd-order rate constant between ·OH and nitrobenzene. And they can be substituted into equation 7 to get

$$\ln(\frac{[NB]}{[NB]_0}) = -k_{(NB+ \cdot OH)}[\cdot OH]_{SS}t \quad (9)$$

where the ratio between $\ln([NB]/[\mathrm{NB}]_0)$ and residence time t can be represented by the right side of this equation. After obtaining the nitrobenzene concentrations after degradation with different residence times, values of $\ln([NB]/[\mathrm{NB}]_0)$ are calculated and plotted as the y-axis; the residence times are plotted on the x-axis. A linear plot will be presented with slope being calculated as

$$slope = \frac{\ln(\frac{[NB]}{[NB]_0})}{t} = -k_{(NB+\cdot OH)}[\cdot OH]_{SS} \quad (10)$$

Thus the steady-state hydroxyl radical concentration can be found through:

$$[\cdot OH]_{SS} = -\frac{slope}{k_{(NB+ \cdot OH)}} \quad (11)$$

where $k_{(NB + \cdot OH)}$ can be found in a heavily cited review literature as 4.0×10^9 M^{-1} s^{-1}.[119] The method has been proved to be effective, and used in several studies for quantifying the steady-state hydroxyl radicals in aqueous solutions.[120–122]

5.2.3. VOCs Half-Lives Estimation Model

Since ·OH plays the most important roles in the degradation of organic compounds, the half-lives of these compounds are largely dependent on the $[\cdot OH]_{SS}$ in the solution.[123] Based on the pseudo-1st-order reaction kinetics between ·OH and VOCs, it is relatively easy to derive the relation among VOCs half-lives, $[\cdot OH]_{SS}$ and the 2nd-order reaction rate constant between ·OH/VOCs - $k_{(VOCs+\cdot OH)}$. For each VOC, by using equation 4, the reactions can be presented as

$$\frac{d[VOC]}{dt} = -k_{(VOCs+\cdot OH)} \times [VOC] \times [\cdot OH]_{SS} \quad (8)$$

Then through equation 7, the time needed for completing the reaction is

$$t = -\frac{\ln(\frac{[VOC]}{[VOC_0]})}{k_{(VOCs+\cdot OH)} \times [\cdot OH]_{SS}} \quad (9)$$

For estimating the half-lives, it is when the instant concentration of VOC is half of the initial VOC concentration. So the final equation for half-lives $t_{1/2}$ is written as

$$t_{\frac{1}{2}} = -\frac{\ln(50\%)}{k_{(VOCs+\cdot OH)} \times [\cdot OH]_{SS}} \quad (10)$$

After acquiring the 2nd-order rate constants between ·OH and each VOC, the half-life of each VOC while being in the operating PMFR system is able to be estimated by using this equation. These half-lives will be listed and discussed in the later section. This half-lives estimation model has been used in several studies, after acquiring the steady-state ·OH concentrations in their photocatalysis systems, the half-lives of target

contaminants in different systems were predicted and compared for their research purposes.[124–126] This estimation model helped reduce the complexity and cost for running repetitive experiments, and provided an intuitional way to predict the photocatalytic degradation performance on different VOCs.

5.3 Results and Discussions

5.3.1. Steady-State Hydroxyl Radicals Concentration

Figure 16 presents the Napierian logarithms of relative nitrobenzene concentrations at different residence times. A linear regression model was fitted to the data points. The slope of the fitted line was found to be -0.0627 with an R square of 0.992. Then the equation 7 was used, this slope was divided by the negative 2nd-order rate constant (4.0 × 10^{9} M^{-1} s^{-1}) of reaction between nitrobenzene and hydroxyl radicals, and the steady-state ·OH concentration in the functioning MP50 system was 1.57 × 10^{-11} M. A detailed calculation process is presented in **Appendix C**.

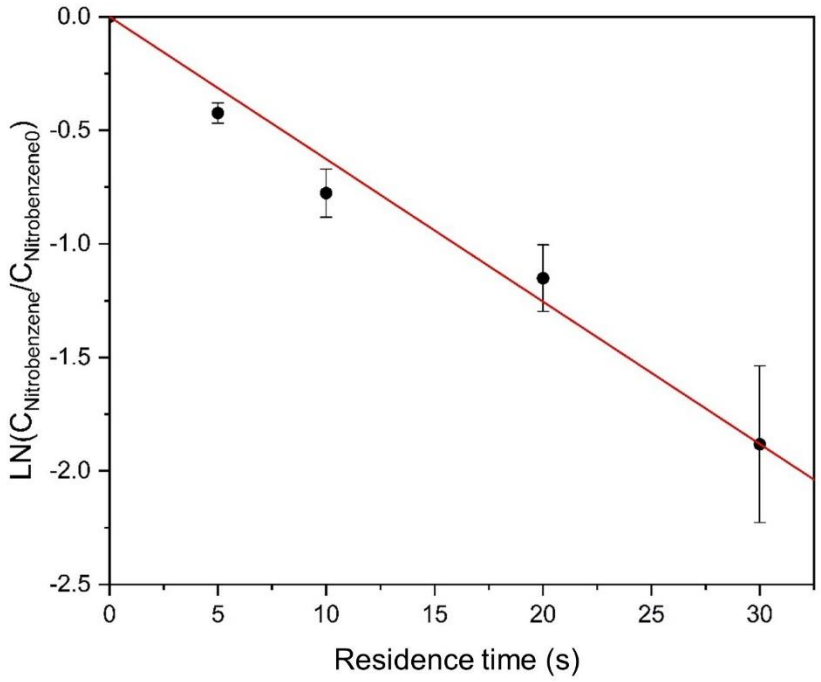

Figure 16. Plot of the Napierian logarithm of relative nitrobenzene percentages at different residence time in MP50. The best-fit slope of this linear regression was used to estimate the steady-state ·OH concentration in the MP50 system.

5.3.2. Predicted Half-Lives of VOCs

After acquiring the steady-state ·OH concentration, the estimated half-lives of VOCs in MP50 can be estimated by using equation 10. In order to verify the reliability of this estimation model, MB is used as the first test object for this model. Since the MB degradation test with MP50 has already been performed, the practical half-life of MB during the period of this experiment can be calculated. Based on the MB degradation result, the practical half-life of MB in MP50 is found to be 6.66 seconds. Then by knowing that

the 2nd-order reaction rate constant of reaction between ·OH and MB is 2.1×10^{10} M^{-1} s^{-1},[119] the theoretical MB half-life is found to be 2.10 seconds. It is clear that the practical half-life and the theoretical half-life of MB are in the same order of magnitude, which indicates the viability of using this model to estimate the half-lives of VOCs.

For presenting the potential of PMFRs to be used for the VOCs removal on the ISS, the half-life estimation model is used to predict half-lives of VOCs from the NASA type II Ersatz solution. The 2nd-order reaction rate constants between different VOCs and ·OH are collected from one authoritative published report.[119] The concentrations of VOCs from type II Ersatz solution are collected from the literature reported by NASA.[127] The estimation model following equation 10 is used to make the prediction, and the estimated half-lives are listed in **Table 4**. Most of VOCs are able to be degraded to 50% under 50 seconds, the three exceptions are Methanol (CH_3OH), acetaldehyde (C_2H_4O) and acetone (C_3H_6O), the first one needs 77.46 seconds while the second and third ones require 88.3 and 401.36 seconds. Acetone is one of the hardest VOCs to be oxidized because of its strong C-bond, the destruction of the carbon skeleton of the acetone molecule is required for oxidizing it. This also explains why the acetone has a relatively much longer half-life compare to other VOCs. These estimates of VOC half-lives demonstrate the excellent ability of micropillar PMFRs to remove VOCs in aqueous solution. With further optimization, the micropillar reactor has the potential to be applied towards water purification on the ISS or other areas of need.

	Rate constant with ·OH [M^{-1} s^{-1}]	Concentration [mg/L]	UV exposure time needed to degrade 50% of target [s]
Acetaldehyde	5.00×10^8	1.8	88.30
Acetone	1.10×10^8	4.6	401.36
Ethanol	1.00×10^9	25.4	44.15
Methanol	5.70×10^8	5.3	77.46
Propylene Glycol	1.80×10^9	23.5	24.53
Ethylene Glycol	1.50×10^9	4.1	29.43
Formaldehyde	1.00×10^9	3.8	44.15
1-propanol	2.30×10^9	0.3	19.20
2-propanol	2.30×10^9	2.7	19.20
1-butanol	4.10×10^9	1	10.77

Table 4. Estimated half-lives of different VOCs based on the Ersatz solutions created by NASA using the prediction model introduced in the study. All the rate constants with ·OH listed in the table were collected from one widely cited report.[119]

6. Study 3: Photocatalytic Degradation Performance of Volatile Organic Compounds

In the previous study, the half-lives of different VOCs were estimated, and the result showed a great potential for the PMFRs to be used for photocatalytic degradation of the organic contaminants in waste water. This study was designed and performed to verify the theory that PMFRs could degrade VOCs at a decent rate. Two typical VOCs – ethanol and 1,4-dioxane were used for this study.

6.1. Photocatalytic Degradation Performance of Ethanol

6.1.1. Introduction

Ethanol is one of the most common VOCs in daily life, and it has caused various issues for the environment and human health. From a macro point of view, ethanol has been widely used as an industrial solvents, which makes it largely exist in the lots of water resources as a result of industry wastewater being emitted into the environment. Adding ethanol to pure fuel can increase fuel density, flash point temperature, viscosity, and octane number while reducing fuel vapor pressure.[128] The immoderate using of ethanol as a fuel additive makes ethanol being abundant in the atmosphere as well as water sources, leading to a damage to the environment. Research has shown that the emission of ethanol took up 4% of the total anthropogenic emissions in UK in 1993, causing ethanol to be a trouble for the environment.[129] On the micro scale, ethanol emitted from wet-wipes is the main VOC that affect the quality of airstreams in flight cabin, and it can hardly be eliminated by most

of the filtration systems, making it harmful to air passengers.[130] Meanwhile, in the type II Ersatz solution introduced in the previous study, ethanol holds the highest concentration among all VOC components, the carbons offered by ethanol takes up to 37.03% of the solution's total organic carbon (TOC).[127] The TOC level measures the total amount of organic compounds contained in a water sample, and it is a very important parameter to evaluate the level of cleanness for purified water.[131] Constantly consumption of ethanol shows harmful effects to human health, it can bring damage to some vital organs such as brain, heart, liver, intestinal, pancreatic, and teratogenic.[132] To ensure the safety of ISS crew members, it is essential to make sure that ethanol is removed from the recycled wastewater. For this study, ethanol was diluted to the same concentration as what the Ersatz solution ethanol had, and TOC level was measured for evaluating the degradation performance. The objective of this study is to investigate the practical degradation performance of MP50 on ethanol, the result would be used to evaluate the practicality of MP to be used for water purification.

6.1.2. Experiment Methods

The PMFR used for this study was MP50 based on its best MB photocatalytic degradation performance. 25.4 mg/L of ethanol was prepared using the 200 proof ethanol and DI water. This concentration was selected based on the ethanol concentration from the NASA type II Ersatz solution.[127] This concentration of ethanol resulted in an approximate 13.24 ppm TOC level. Based on the 44.15 seconds estimated half-life of ethanol in the

PMFR system, a residence time 300 seconds was chosen for this study. This residence time was more than six-times the half-life of ethanol while being in the system, it was supposed to get around 99% degradation of ethanol theoretically.[133] To obtain this residence time, a flow rate of 4.8 µL/min was used, this flow rate was dramatically slower compared to the flow rates used for the previous MB degradation study, which led to a much longer sample collection time. The experiment fixture and setup were identical to what was used in previous studies.

This experiment began with DI water flowing through the system at 288 µL/min for 30 min to purge all the air in the system. Then the syringe pump let 25.4 mg/L ethanol solution run through the system at 288 µL/min for 1 hour. This step was performed to make the system's physical adsorption of ethanol particles in a dark environment reach its saturation, one sample was collected for measurement after 1 hour of solution flow to confirm if the saturation had been approached. UV lamp was turned on afterwards to provide UV irradiation. For the experiment groups, 1 mL of ethanol was first run through the system at 4.8 µL/min to ensure all solution left by the previous dark adsorption step being purged. Then the sample collection began, effluents were collected in a 20 mL glass vial with its opening covered by a piece of parafilm to prevent contaminants coming from air. For each sample, it took 70 hours to collect 20.16 mL ethanol effluents for the measurement. After collecting the sample for each experiment group, a control group experiment was run subsequently, the only difference for control tests was that these tests were performed under an environment without any light, which stopped the happening of photocatalysis. The experiments for both the experiment group and the control group were

performed three times to minimize the errors, after each experiment, DI water was flowed through the system at 288 µL/min for 1 hour to clean out all the residuals. Six samples were collected in total and sent to a Shimadzu TOC-VCPH/CPN TOC analyzer for measurements of TOC level. Samples were prepared for TOC analysis by acidifying samples to pH 2-3, then sparging gas was bubbled through the sample to eliminate the inorganic carbon (IC) component. The remaining total carbon (TC) was measured to determine total organic carbon, and the result is generally referred to as TOC.

By comparing the TOC level of ethanol solution before and after the photocatalytic reaction, a TOC degradation percentage could be found, this percentage could also be called the mineralization percentage. Mineralization of organic compounds meant the breakdown of organic compounds into CO_2, H_2O, and harmless inorganic anions. The measurements of decreases of certain types of VOCs only quantified the destruction of the chromophore group or the rearrangement of conjugate bonds, the intermediate products might still be organic compounds which could be detected by TOC analyzers.[134] The ·OH was also known to be one of the main contributors to the photocatalytic mineralization process.[135,136] Thus the mineralization percentage was used as the performance metric for this study, it helped evaluate the PMFR's ability to not only degrade ethanol but also the ability to completely break down this VOC.

6.1.3. Results and Discussions

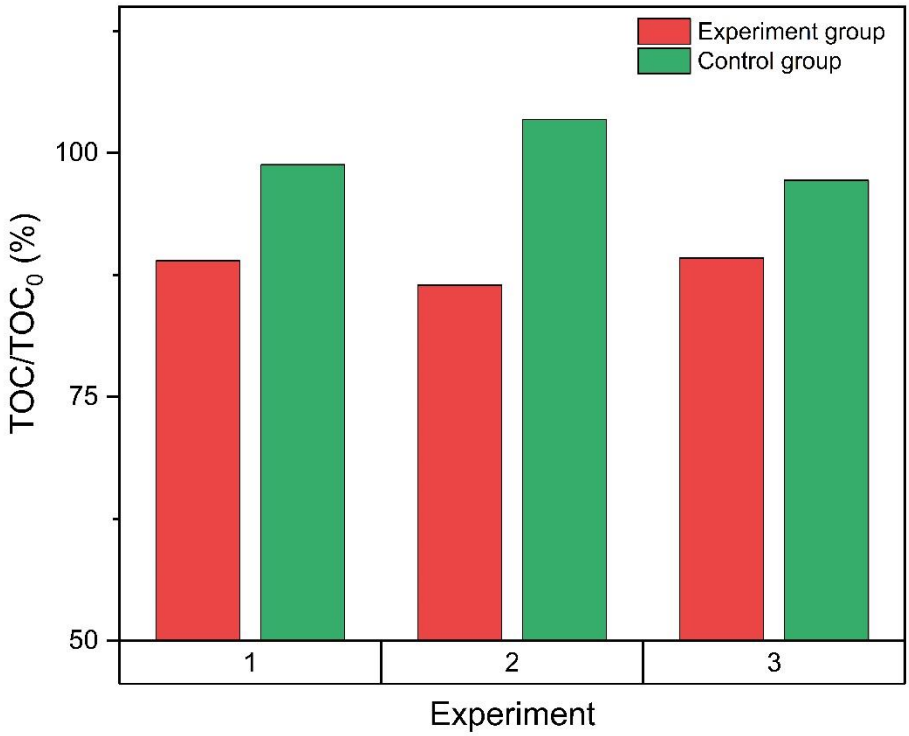

Figure 17. The relative TOC level for the experiment group and control group of each degradation test. The experiment group always observed lower TOC level than that of the control group.

Results for both the experiment group and the control group are shown in **Figure 17**. A ratio between TOC levels of samples collected after experiment/control tests and TOC levels of samples collected after the dark adsorption step was shown on the y-axis. Judging from this column graph, it was obvious that the column representing the control group results were always higher than the ones representing experiment group results, meaning that the complete photocatalytic mineralization of ethanol took place during the

tests. For the experiment group, because of the degradation reaction happening between ethanol and ·OH, the average percentage of TOC dropped to 88.22 ± 0.02%; while the average percentage of TOC for the control group remained at a high level of 99.81 ± 0.03%. The control group result clearly showed that only a minimum amount of ethanol was absorbed by the system when photocatalysis did not take place. The MP50 was able to mineralize 11.78 ± 0.02% of ethanol at a residence time of 300 seconds.

Looking at this result, it seems like the mineralization percentage is much lower compared to the estimated ethanol degradation percentage, this happens because of the differences in measurement standards between the mineralization percentage and the ethanol degradation percentage. Basing on the photocatalytic degradation reaction mechanisms of ethanol, acetaldehyde is the first intermediate product. Then the acetaldehyde undergoes photocatalytic degradation through at least two parallel pathways. First pathway is: acetaldehyde → acetic acid → CO_2 + formaldehyde → formic acid → CO_2; while the second pathway is: acetaldehyde → formaldehyde → formic acid → CO_2.[137] A flow chart of the pathways is presented in **Figure 18**. As both the descriptions and the flow chart of pathways show, acetaldehyde is the main and starting intermediate product for the photocatalytic degradation of ethanol, it is still an organic compound which can be detected the TOC analyzer. As for some of the subsequent intermediate products such as acetic acid, formaldehyde, and formic acid, they are also detectable to the TOC analyzer. The mineralization percentages calculated based on the TOC results only measures the percentage of ethanol being completely degraded into CO_2 and H_2O, while the theoretical degradation percentage estimated based on the half-life of ethanol measures

the percentage of ethanol being decomposed by ·OH regardless of products. Because of this difference, the estimated degradation percentage ought to be larger than the mineralization percentage. Two studies also suggest that ·OH plays a main role in degrading acetaldehyde and the reaction's byproducts into CO_2 when water vapor is in the presence.[138,139] It indicates that a certain amount of ·OH was occupied by degradation reactions for acetaldehyde and other organic byproducts, and these reactions took place concurrently with the photocatalytic degradation of ethanol, thus less ·OH was used for the ethanol degradation. When the half-life of ethanol in the PFMR system was estimated, it was assumed that the reaction was under an ideal situation where all radicals were used for the degradation of ethanol, this also explained why the practical mineralization percentage was very different from the estimated ethanol degradation percentage.

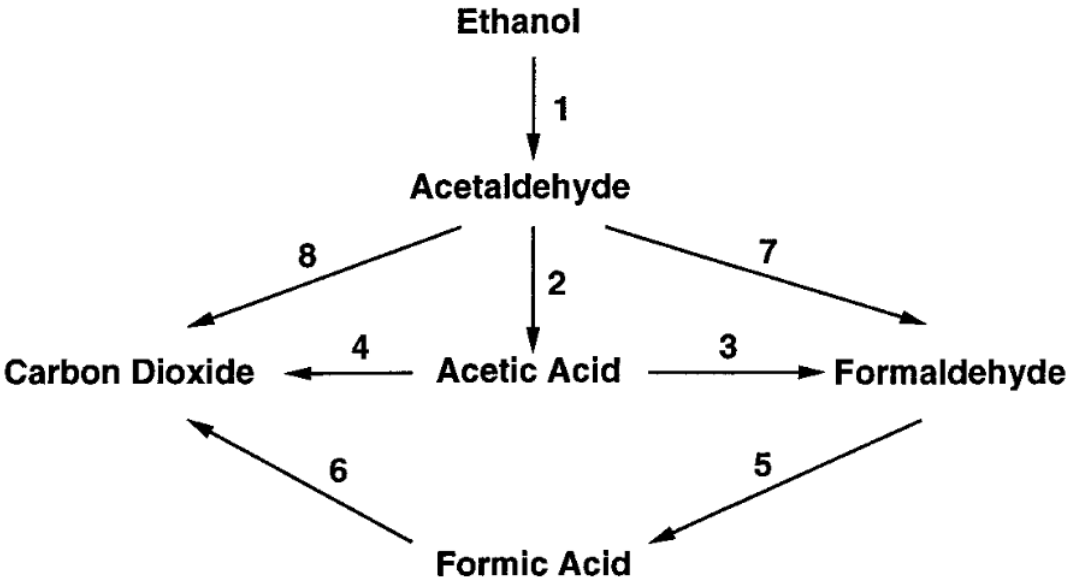

Figure 18. Pathways of photocatalytic degradation of ethanol.[140]

6.2. Photocatalytic Degradation Performance of 1,4-Dioxane

6.2.1. Introduction

Although ethanol works well as a target VOC contaminant to test the PMFR's photocatalytic degradation performance, a lack of severe toxicity makes it not as problematic as some other VOCs in real life. In order to figure out the application of MP on treating some VOCs that is prejudicial to human health, 1,4-dioxane was selected to be the target contaminant for this study. This ring-structured organic compound is widely used as a solvent for many types of cellulose, resins, oils, waxes, and dyes. 1,4-dioxane's high solubility and volatility make it have high accessibility for the environment, it has been commonly detected in both surface water and groundwater. According to EPA, being exposed to high levels of 1,4-dioxane can cause vertigo, drowsiness, headache, anorexia and irritation of human eyes, nose, throat, and lungs.[141] Studies also mention that short-term exposing to high levels of 1,4-dioxane is relevant to severe kidney and liver damage in both humans and animals. As for chronic effects, animal studies have observed lesions in kidney, liver, nose, testes, lungs and spleen.[142] Some researches even claim 1,4-dioxane being one of the principal chemical components of Agent Orange is the main cause of the cancers found in Vietnam military personnel, which increases the chance of getting breast and endometrial cancer, stress-related illness and lower sperm counts.[143] These toxicities possessed by 1,4-dioxane make it be classified as a Group B2, probable human carcinogen by EPA.[141]

Several studies have been done to investigate removal approaches for 1,4-dioxane. Biodegradation did not work on removing this organic compound at all based on the results of biochemical oxygen demand tests.[144] Using oxidation with chlorine or permanganate was proved to be ineffective, and what was worse was that this process could lead to the formation of more toxic compounds.[145] One group in Netherlands tried to use a conventional water purification system composed of reverse osmosis and activated carbon filtration to remove 1,4-dioxane, results showed an extremely low removal efficiency due to this chemical's high hydrophilicity.[146] In addition, another study was done to investigate the effectiveness of nine on-site industrial wastewater treatment plants on removing several micropollutants, this research group found that the high hydrophilicity of 1,4-dioxane resulted in a low removal efficiency for it in most of treatment processes.[147] Judging from all these studies, 1,4-dioxane is obviously one stubborn VOC that can hardly be removed by conventional water purification methods.

Advanced oxidation processes (AOPs) have become a popular topic when it comes to the degradation of 1,4-dioxane in aqueous solution, and they have been considered as one of the most effective methods. AOPs manage to degrade or even mineralize organic pollutants in aqueous solution through the generation of reactive free radicals, and ·OH has been proved to be one of the strongest oxidants.[148,149] One common approach to conduct AOPs is trough photolysis, UV illumination are applied to activate oxidants to form ·OH. However, the practical application of photolysis is limited by its low ·OH generation efficiency. Many researches have tried to increase the production rate of ·OH by adding in external oxidants, some commonly used techniques include using UV/H_2O_2, UV/Fe^{3+},

UV/O_3, UV/S_2O_8, and UV/chlorine.[150–153] These methods are able to help enhance the generation of ·OH and thus increase the degradation efficiency, but the introducing of external reagents challenges the safety of purified water for human consumption.

Herein the UV/TiO_2 photocatalytic system has become a favourable approach to overcome these drawbacks. Triggered by photon energy, a decent number of ·OH are constantly generated near the surface of TiO_2 photocatalyst, leading to a continuous decompose of VOCs in aqueous solution, and the fixed photocatalysts eliminate the concern about bringing external pollutants into the purified solution. Numerous researches have been done to investigate the photocatalytic degradation of 1,4-dioxane using TiO_2 as the catalyst, and it is claimed that photocatalytic oxidation systems are able to obtain higher organic pollutants degradation efficiency compared to the photolysis system, most of these systems tend to improve their treatment efficiency through enhancing the ·OH generation activity by modifying TiO_2 with other transition metals like tungsten (W), nickel (Ni), copper (Cu), etc.[39,154,155] It is worth noting all the reported researches related to UV/TiO_2 photocatalytic degradation of 1,4-dioxane were using conventional bulk reactors, no report about any photocatalytic microreactor's degradation of 1,4-dioxane study has been published up to this point. The main reason why this happens is that the reaction between ·OH and 1,4-dioxane is less intense compared to the reaction between ·OH and commonly used organic dyes, for example, the 2^{nd}-order reaction rate constant of ·OH/MB is approximately 10 times larger than the rate constant of ·OH/1,4-dioxane, this lower reaction rate will not result in a good degradation result if the proposed microreactor is not able to generate enough ·OH. As mentioned in the Background chapter, compared to

conventional reactors, the reaction volume of microreactor is usually several orders of magnitude smaller, which leads to two main advantages: larger SA:V ratio and shorter mass diffusion length, these merits allow microreactors to get a relatively higher 1,4-dioxane degradation efficiency hypothetically.

The mechanism of the degradation of 1,4-dioxane by photocatalysis has been studied in several previously published reports. This reaction is initiated by ·OH, these radicals attack the 1,4-dioxane to create 1,4-dioxan-α-oxyl radical which is believed to be the precursors for further reactions. Then ·OH tends to continue the attack on 1,4-dioxan-α-oxyl at different α-C positions to produce further oxidation reactions and posterior ring-opening reactions. There are two main reaction routes for the oxidation of 1,4-dioxan-α-oxyl. For the route A, under the attack of radicals, the molecule is dissolved into 1,2-ethanediol diformate (EDF), 1,2-ethanediol monoformate (EMF), and formaldehyde, these intermediates are further oxidized into formic acid by ·OH afterwards. The route B is through the oxidation of C-centered radical, two intermediates – formaldehyde and formic acid are generated, then the formaldehyde reacts with ·OH and turns into formic acid.[154,156] **Figure 19** shows a simplified schematic of the two routes of 1,4-dioxane degradation by photocatalysis. It is clear that the main by-product of the photocatalytic degradation of 1,4-dioxane is formic acid, if an sufficient quantity of ·OH is provided to produce fully mineralization, 1,4-dioxane will finally be mineralized into CO_2 and water. This mechanism also indicates the use of HPLC instead of TOC analyzer as the analysis instrument for this study. If the by-product formic acid cannot be fully mineralized, barely any change will be observed in the TOC levels, as what happened in the previous ethanol

study. By using HPLC, an intuitive change of the 1,4-dioxane concentration will be observed regardless of the intermediate products, which can provide a better understanding of PMFR's degradation performance on 1,4-dioxane.

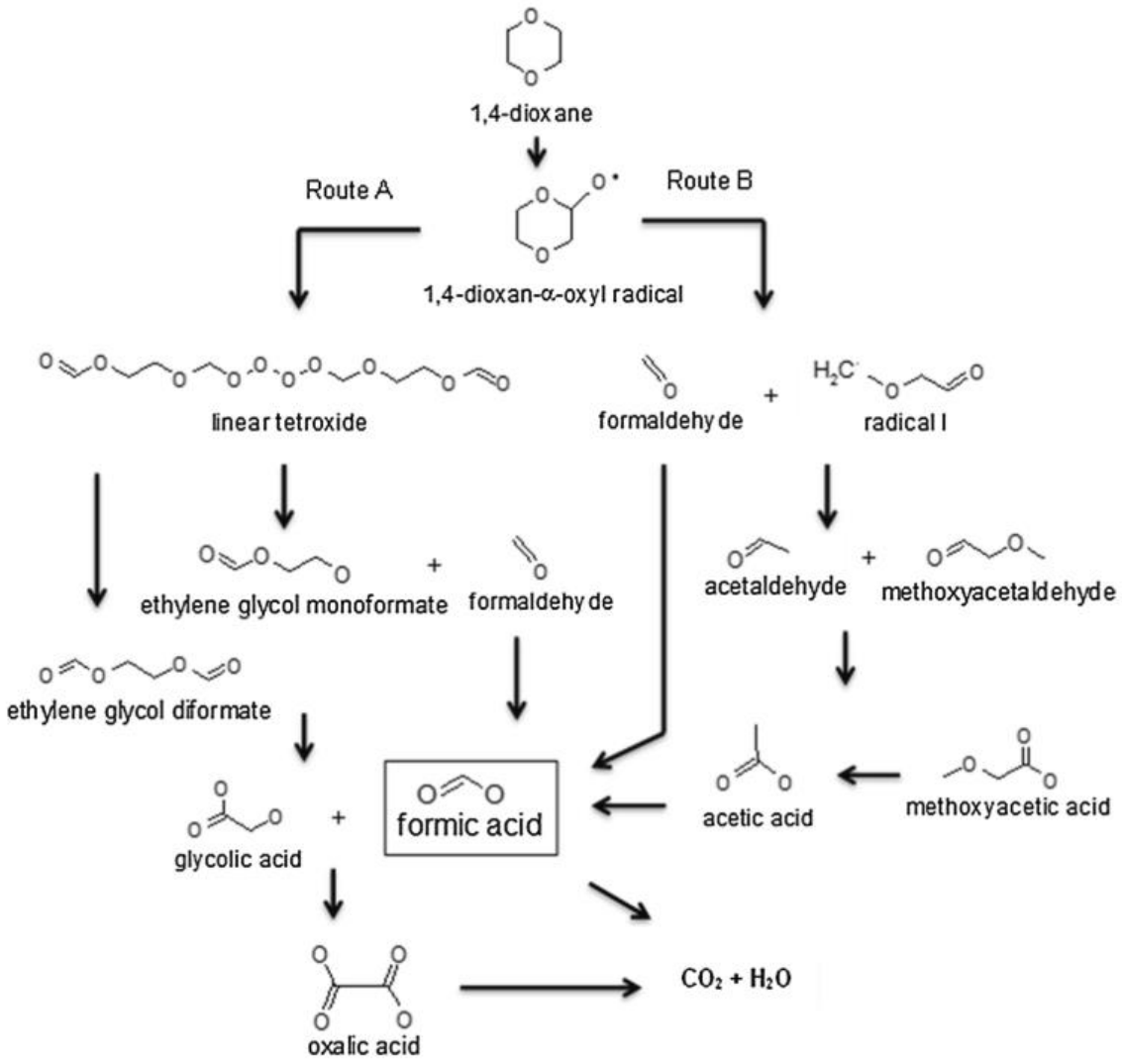

Figure 19. Pathways of photocatalytic degradation of 1,4-dioxane.[154]

In this study, the PMFR's degradation performance on the stubborn VOC – 1,4-dioxane was examined. The initial contaminant concentration was identical to one of the

recent 1,4-dioxane degradation studies with conventional reactors.[107] Results of this study were compared to the results of several most recent published photocatalytic conventional reactor 1,4-dixoane degradation studies, and discussions were conducted to illustrate the superiority of PFMR's degradation performance. This was also the first microreactor device that was reported to successfully degrade 1,4-dioxane in aqueous solution to a relatively low level.

6.2.2. Experiment Methods

The experiment fixture and set up were identical to the previous degradation studies. 1,4-dioxane solution with a concentration of 100 μM was prepared for the study. The microreactor used for this study was only MP50 according to its highest degradation activity in the MB degradation performance study. In order to inspect the PFMR's degradation performances at different residence times, 40, 60, 80, 100, 120 seconds residence times were used, these residence times were approximately three, four, five, six, and seven times the estimated half-life of 1,4-dixoane, respectively. The half-life was calculated using the estimation model introduced in the chapter 5, the 2nd-order rate constant for the reaction between ·OH and 1,4-dioxane was found to be 2.8×10^9 M^{-1} s^{-1}, a half-life of 15.77 seconds was calculated.[119] Hypothetically, these five residence times were able to generate degradation percentages of 87.5%, 93.75%, 96.88%, 98.44% and 99.22%.

To start the experiment, DI water was flowed through the experiment system at 288 µL/min for 30 min to purge all the air. Then the liquid was switched to 1,4-dioxane, it was flowed at the same flow rate for 1 hour under a dark environment to perform the dark adsorption step. This step aimed to let the system's physical adsorption reach a saturation so that the adsorption effect on degradation results could be negligible. After 1 hour, 1.8 mL of effluent was collected in a 2 mL glass vial for the concentration measurement. If the effluent's concentration was close to 100 µM, it meant that the effect created by system's adsorption would be ignored. UV lamp was then turned on to provide light irradiation, 1,4-dioxane was flowed through the system at flow rates from the slowest to the fastest, which prevented the higher concentration solution's effluence on the lower concentration solution. Before collecting 1.8 mL effluents for the flow at every residence time, 2 mL of 1,4-dioxane solution was allowed to flow through the system at the desired flow rate to push out all the solution left by the previous run. All experiments at different residence times were run three times to minimize the errors. The collected solutions were sent to a HPLC for 1,4-dioxane concentrations measurements.

6.2.3. Results and Discussions

For the dark adsorption test, less than 5% decrease in the concentration of 1,4-dioxane was observed, which implied that the impact of system's physical adsorption was negligible. **Figure 20** shows the degradation of 1,4-dioxane using MP50. Longer residence time led to higher 1,4-dioxane degradation percentage, the degradation percentage reached

its highest at the longest residence time as an average of 78.83 ± 1.4%. This trend was accord with the hypothesis that longer residence time would allow contaminant particles to stay longer in the reaction chamber thus was more likely to have reaction with ·OH. The negative Napierian logarithm of relative 1,4-dioxane percentages at different residence times is shown in **Figure 21**. A best-fit linear regression model was also created, the pseudo-1st-order reaction rate constant was determined from the slope, this constant was found to be 1.23×10 min^{-1} with a linear regression coefficient of 0.99715. Based on this result, it is obvious that MP50 is capable of removing 1,4-dioxane in the aqueous solution. However, further analysis is still needed to determine if this degradation performance is superior compared to other reported devices.

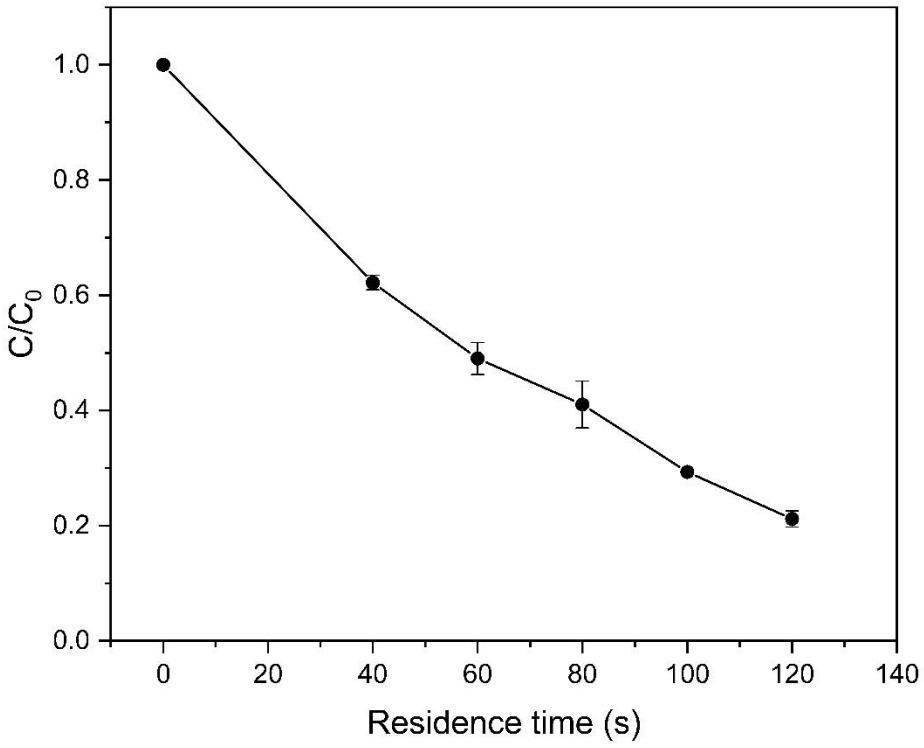

Figure 20. Degradation of 1,4-dioxane by MP50. Longer residence time led to better degradation performance.

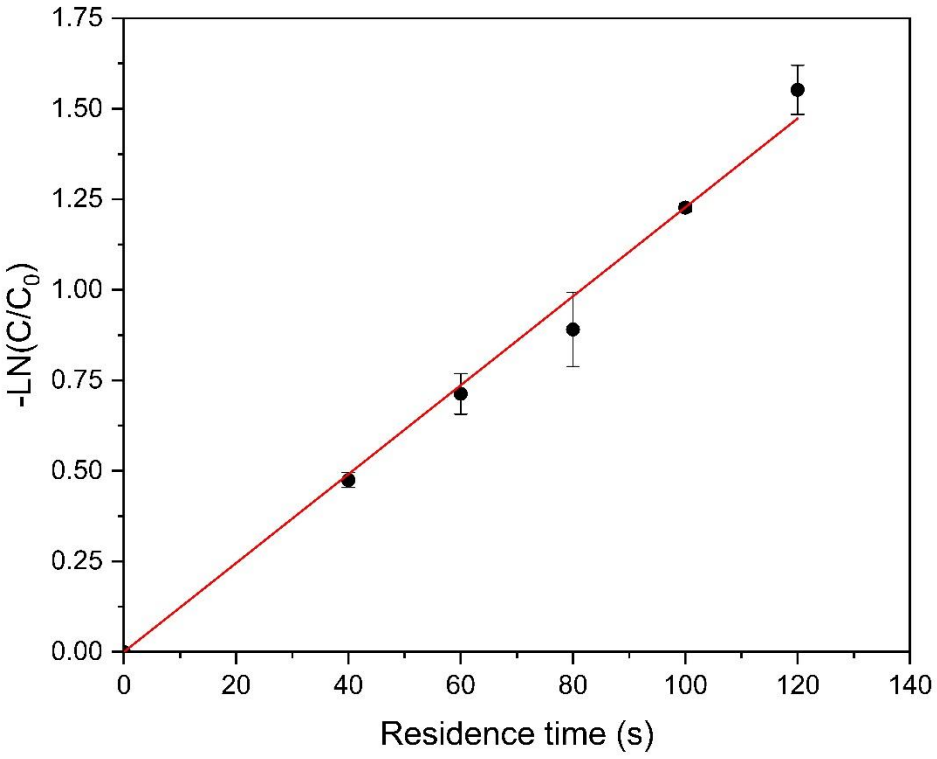

Figure 21. Napierian logarithm of relative 1,4-dioxane percentage at different residence times by MP50.

In order to evaluate the degradation performance of MP50, the author collected four recent reported publications using TiO_2 bulk reactors to degrade 1,4-dioxane. The best degradation results and the pseudo-1st-order reaction rate constants of these reported devices were compared to those of the MP50. The first bulk reactor was reported by H. Barndõk et al., this reactor was designed to degrade 1,4-dioxane through photocatalysis by an immobilized nitrogen and fluorine co-doped titanium dioxide (NF-TiO2) composite with monodisperse TiO2 nanoparticles.[156] The NF-TiO_2 composite used in this study was

prepared by a modified sol-gel method. A concentration of 140 mg/L (1588.92 μM) 1,4-dioxane was prepared as the target contaminant solution. The degradation test was carried out in a 50 mL borosilicate glass vessel reactor which had 5 photocatalytic films with a total catalyst area of 75 cm^2. The UV irradiation was provided by a Xe lamp with a wavelength ranging from 315 to 400 nm and light intensity of 80 mW/cm^2. A gas-liquid chromatography (GLC) was used to quantify 1,4-dioxane and its possible degradation product. The blue trend line in **Figure 22** shows the best 1,4-dixoane degradation performance for this study. A degradation percentage of 90% was reached after 7 hours of experiment, after fitting a linear regression model to the negative Napierian logarithms of related concentrations, a pseudo-1^{st}-order reaction rate constant of 9.33×10^{-5} min^{-1} was found, the linear regression coefficient for this fit was 0.99759.

In 2021, Byrne et al. reported a 1,4-dioxane degradation study by using the modification of anatase TiO_2 with tungsten (W).[154] The photocatalyst W-TiO_2 with different composing proportion was created through sol-gel method to investigate the influence of W on 1,4-dioxane degradation. A 50 mL bulk reactor was used for the degradation study while the initial 1,4-dioxane concentration was prepared to be 100 mg/L (1134.94 μM). Under irradiation of 5 mW/cm^2 UVA light, the degradation of 1,4-dioxane is shown in Figure 22. This device reported almost 100% degradation at the longest reaction time of 4 hours. **Figure 23** presents the negative Napierian logarithm of relative concentrations and the best-fit linear regression model. The best pseudo-1^{st}-order reaction rate constant of this device was calculated to be 1.80×10^{-4} min^{-1} with an R square of 0.94921. This group has also reported another study on the degradation of 1,4-dioxane

using Cu-doped TiO_2 as the photocatalyst.[39] They hypothetically assumed that the copper doping of TiO_2 would improve the performance of photocatalytic degradation. In order to perform the tests, a 50 mL bulk reactor was used, and the target 1,4-dioxane concentration was 75 mg/L (851.21 μM). UV irradiation was provided by a Xe lamp with light intensity of 15 mW/cm^2. As for the result, the Cu-doped reactor performed worse compared to the control reactor (TiO_2 without Cu). The 1,4-dioxane degradation of the pure TiO_2 reactor was shown in Figure 22, the highest degradation percentage was found after 4 hours reaction time, which was about 95.5% according to the result figure provided by the report. And the highest reaction rate constant was about 1.95×10^{-4} min^{-1} based on the slope of linear regression model as shown in Figure 23, the regression coefficient was about 0.97933.

The last device was proposed to increase the generation of reactive species by using photoelectrolysis, this process was deemed to combine the benefits of photocatalysis and electrolysis, the reaction efficiency was expected to have a boost through this process. A TiO_2/g-C_3N_4 (TCN) film electrode was used as the photocatalyst, it helped generate reactive species through both photocatalysis and electrolysis.[107] 10 mg/L (113.49 μM) of 1,4-dioxane was prepared for the degradation test, and the test was performed in a 15 mL plexiglass bulk reactor. An LED visible light with light intensity between 80 and 85 mW/cm^2 was used as the light source. They found that the reactor with TiO2/g-C3N4/CQDs nanorod arrays (TCNC NRAs) film conducted the best degradation performance, 77.9% of 1,4-dioxane was eliminated after 6 hours of reaction time as shown

in Figure 22. For this device, the pseudo-1st-order reaction rate constant was determined to be 7.75×10^{-5} min^{-1} with an R square of 0.99157.

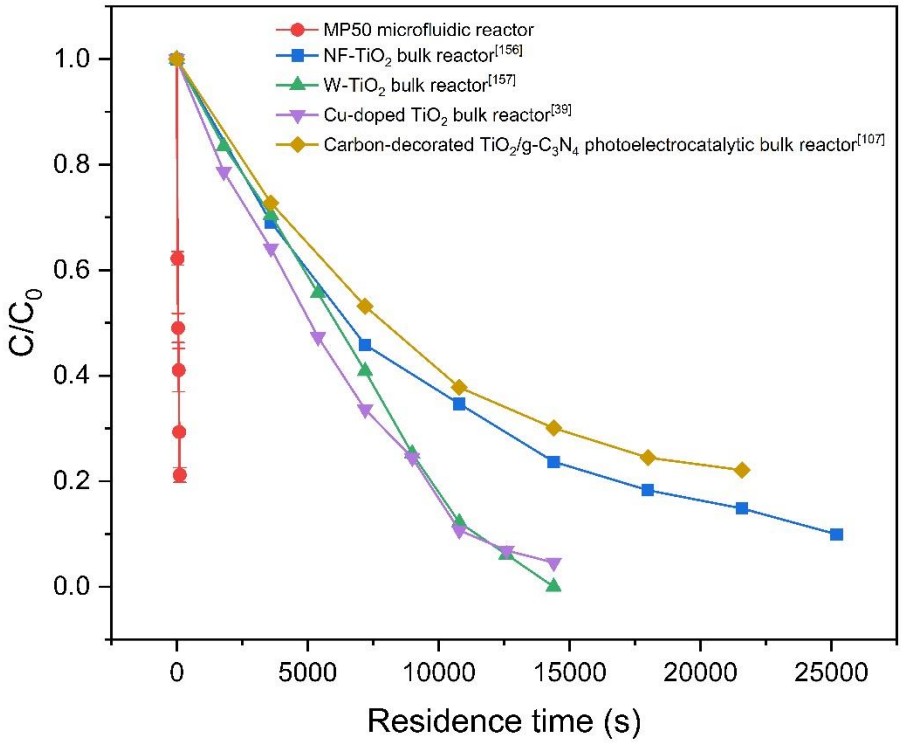

Figure 22. Degradation of 1,4-dioxane by MP50 (this work) and four reported conventional bulk TiO2 photocatalytic reactors. A comparable highest degradation percentage was achieved by MP50 in a significantly shorter time.

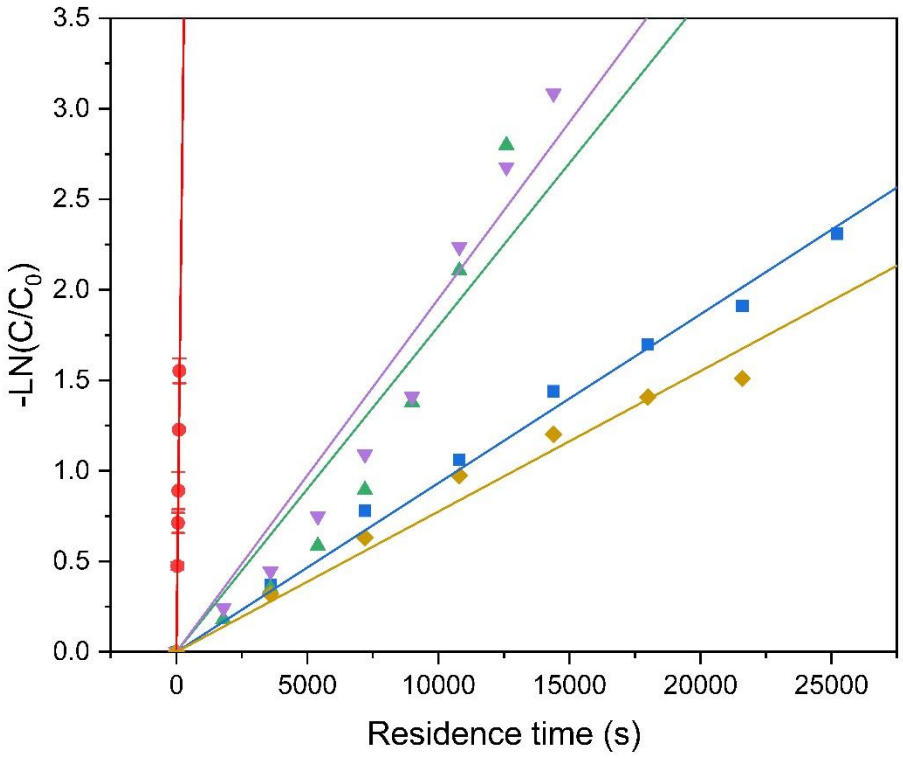

Figure 23. Plot of the negative Napierian logarithm of relative 1,4-dioxane percentages at different residence times by MP50 (this work) and four reported conventional bulk TiO_2 photocatalytic reactors. A pseudo-1st-order reaction rate constant for each device was determined from slope of the best-fit linear regression model. MP50 showed the highest reaction rate constant thus yielded the highest reaction rate among all devices presented in the plot. The legend is identical to the legend of Figure 22.

Judging from Figure 22, although the MP50 does not reach a 1,4-dioxane degradation percentage as high as some of the reported devices, its degradation performance is still comparable, and the highest degradation percentage of 78.83 ± 1.4% may be limited by the longest used residence time. By further increasing the residence time, 1,4-dioxane has a good chance to be degraded to around 10% according the rule of pseudo-

1^{st}-order reaction. The reason why the trend line of MP50 points is almost vertically downward is that MP50 achieved this decrease of 1,4-dioxane concentration in a dramatically shorter residence or reaction time compared to the other four devices presented in the figure. Residence time describes the time available for a contaminant particle to have degradation reaction within a microreactor, it can be considered identical to the reaction time while evaluating a bulk reactor. The comparable decrease of 1,4-dioxane concentration in much shorter time presented by MP50 proves that MP50 possesses significantly higher photocatalytic degradation efficiency compared to the reported bulk reactors.

In order to better quantify the reaction efficiency, the pseudo-1^{st}-order reaction rate constants of MP50 as well as the four recent reported bulk reactors were summarized in **Table 5**, these constants were calculated based on the best-fit linear regression models presented in Figure 23. It is clear that the linear fit line of MP50 has the largest slope among all the fit lines, indicating that it has the largest reaction rate constant. According to the table, the pseudo-1^{st}-order reaction rate constant of MP50 is two to three orders of magnitude higher than the rate constant of the reported bulk reactors, proving the advanced reaction rate provided by MP50. This result is in keep with the hypothesis that microfluidic reactor has higher reaction efficiency compared to conventional bulk reactors. For this study, compared to bulk reactors, the main advantages that MP50 has are significantly larger SA:V ratio, dramatically shorter mass diffusion length and more uniform UV light irradiation, all of these merits contribute to the better degradation efficiency of MP50, and it further proves the benefit of using PMFRs. However, it is worth noting that although the

microfluidic reactor has been proven to produce higher photocatalytic degradation efficiency for water purification compared to conventional bulk reactors, the low throughput is still one major limitation. It is hypothetical that this drawback can be overcome by setting up a large amount of PMFRs in parallel, it should provide great purification efficiency as well as decent throughput for water purification. Further experiments are still needed to prove this hypothesis.

Device	$-\ln(C/C_0) = k't$	k' [s^{-1}]	R^2
MP50 (this work)	$-\ln(C/C_0) = 1.23 \times 10^{-2}t$	1.23×10^{-2}	0.99715
NF-TiO_2 bulk reactor[156]	$-\ln(C/C_0) = 9.33 \times 10^{-5}t$	9.33×10^{-5}	0.99759
W-TiO_2 bulk reactor[157]	$-\ln(C/C_0) = 1.80 \times 10^{-4}t$	1.80×10^{-4}	0.94921
Cu-doped TiO_2 bulk reactor[39]	$-\ln(C/C_0) = 1.95 \times 10^{-4}t$	1.95×10^{-4}	0.97933
C-decorated TiO_2/g-C_3N_4 bulk reactor[107]	$-\ln(C/C_0) = 7.75 \times 10^{-5}t$	7.75×10^{-5}	0.99157

Table 5. Summary table of the pseudo-1st-order reaction rate constants (k') and linear regression coefficients (R^2) for 1,4-dioxane for the current work and four most recent published reports for 1,4-dioxane degradation using different bulk TiO_2 photocatalytic reactors. Important note: In cases where k' were not reported explicitly in the cited studies, these were estimated based upon experimental results reported therein.

7. Conclusions

7.1. Summary of Current Work

For overcoming the short-life problem of the thermal catalytic reactor currently used on ISS, a novel photocatalytic microreactor with micropillar arrays has been proposed in this study. The micropillar arrays work as the scaffolding for NPT, they largely increase the SA:V ratio, enhance the mass transfer rate, and promote the light trapping. Hence the generation of ·OH receives a huge boost, which increases the degradation reaction of VOCs. The titanium-based microreactor with microscale micropillars are fabricated by using MEMS technologies, and its degradation performance are researched with different organic contaminants. For the MB organic dye, MP50 degrades the most amount of MB among all fabricated PMFRs and it also has the highest reaction rate constant. For the MB degradation activity, MP50 performs about twice better compared to other reported microreactors, showing the great efficiency enhancement offered by the novel design of micropillar microreactors. For investigating the potential of MP50 to be used for removing the various VOCs that exist in the ISS wastewater, the main reactant of the degradation reaction - ·OH is quantified by using a well-established kinetic model and nitrobenzene as the probe. Based on the steady state concentration of ·OH, an estimation model was created to predict the half-lives of VOCs when they are within the reaction chamber of MP50. This model indicates that MP50 has the ability to degrade required VOCs in an appropriate amount of time. Ethanol is adopted as the first target VOC for the degradation test, a small amount of mineralization of this chemical is observed, discussions are conducted about why the

mineralization results is not as good as the estimated degradation result. Lastly, the degradation study with 1,4-dioxane, a toxic VOC, presents a decent removal performance. The reaction rate constant possessed by MP50 is 2 to 3 orders of magnitude higher than that of other conventional bulk reactors published in literatures, it reveals the superior performance of PMFRs with micropillar arrays on degrading a real problematic VOC. All studies conducted in this dissertation indicates that this novel designed titanium-based photocatalytic microreactor has great potential to be used for wastewater purification. With further investigation about assembling this device in parallel with large quantities, this device is expected to be applied to the WPA system on ISS or even broader fields.

7.2. Future Work

Although the proposed micropillar PMFR has been proved to have satisfying water purification performance, some future studies have the potential to further improve the purification capability of PMFR, and bring PMFR to broader application fields. First of all, a detailed degradation study of MB and 1,4-dioxane with different UV illumination light intensities could be conducted. As the author mentioned in the MB degradation study chapter, the influence of one crucial parameter – light intensity, has not been studied in this project due to the hypothetical working environment and the lack of varieties of UV equipment. The light intensity used in this project is 5.5 mW/cm^2, this intensity is relatively low considering some of other reported studies are using UV light source with much higher light intensity. Hypothetically, photons can penetrate deeper into the reaction chamber with

a higher UV light intensity, thus the degradation reaction can be enhanced in more space of the chamber. There is a possibility that the increased light intensity can allow MP100 and MP150 to have better degradation performance. If the PMFRs with deeper chamber depth can have comparable performance as what MP50 has, a higher throughput can be achieved at the same residence time, which make removing more pollutants in the same amount of time possible. Hence, conducting a study with higher light intensity has the potential to enhance the degradation performance of micropillar PMFRs, and make them be more suitable for practical usage.

Another potential study is the optimization of geometry for micropillars. As discussed in this dissertation, dimensions of pillars have large impact on the efficiency of the reactor. According to the Monte-Carlo simulation model run by our collaborator, diameter, height, and pitch highly influence the photon adsorption and mass transfer of contaminants, which largely affect the degradation reaction as a result. It is worth mentioning that the simulation shows that a larger pitch allows more photons to penetrate to the bottom of chamber. However, the enlarged pitch will reduce the amount of pillars, leading to a decrease in the total surface area of photocatalyst. Hence, a more comprehensive and detailed simulation can be conducted to find out the perfect combination of diameter, height and pitch to make the reactor obtain the best light adsorption and highest mass diffusion. Some preliminary experiments about physically altering the micropillar dimensions have been done with the method of HF etching and ion milling. Preliminary results show that HF etching can successfully remove the NPT, and ion milling is capable of slowly tapering the pillars. For the potential study, optimization

of pillar arrays can be made based on new simulation results, and the PMFRs with optimized micropillar arrays can be used for more degradation studies with MB or 1,4-dioxane. The results can be compared to what has been collected in this report.

Last but not the least, in order to examine the capability of PMFRs to be used for more broad areas of water purification, degradation experiments with bacteria and viruses can be conducted. Apart from VOCs, microbial contamination in drinking water creates another huge risk towards human health. Waterborne diseases caused by microorganisms such as diarrhea lead to around a million deaths every year. The most widely used purification method is by using chlorine or ozone to inactivate those microorganisms. However, these conventional purification techniques usually result in various byproducts which is still harmful to people. Therefore, many attentions have been attracted to develop a new type of water purification system to remove microorganisms without introducing new toxic chemicals. Researches have stated that ·OH generated by photocatalysis has the ability to create damage to cell membranes and make microorganisms inactivated.[158] Researches about using photocatalytic bulk reactor as well as microfluidic reactor to lower the microorganism contaminant level in water have been done by many groups, some good degradation results have been observed.[158–160] The two most commonly used target microorganism contaminants are *Escherichia coli* (*E. coli*) and MS2. *E. coli* is a common virus which can be usually found in polluted water, this virus processes a relatively high UV resistance, which makes it a perfect target contaminant for photocatalysis study. As for the bacteriophage MS2, it has a similar structure as that of many pathogenic enteric viruses and has been widely used as a surrogate for enteric viruses.[161] Traditional membrane

filtration does not work well on removing MS2 due to its small size, and UV with wavelengths greater than 295 nm is not able to inactivate MS2 due to the good UV resistance.[162] ·OH, on the other hand, has been proved to work well on dissolving MS2 through oxidation.[163] Hence, for future study, the micropillar PMFRs can be used for the degradation of *E. coli* and MS2. According to results collected from this dissertation, this novel designed microreactor shows greater photocatalytic performance compared to other reported devices. Hypothetically, the micropillar PMFR has the potential to outperform other existing microfluidic reactors in the field of microorganism inactivation. Studies like this can exhibit the potential of micropillar PMFRs to be applied to broader fields of water purification.

Bibliography

1. Guppy L, Anderson K. Global Water Crisis: the Facts. *United Nations Univ Inst Water, Environ Heal Hamilton, Canada*. Published online 2017. http://inweh.unu.edu/wp-content/uploads/2017/11/Global-Water-Crisis-The-Facts.pdf

2. Kresic N. Groundwater Contamination. *Hydrogeol Groundw Model*. Published online 2020:425-468. doi:10.1201/9781420004991-9

3. Act NTA. National Space Exploration Campaign Report Pursuant. 2018;432(September):1-21. https://www.nasa.gov/sites/default/files/atoms/files/nationalspaceexplorationcampaign.pdf

4. Carr MH, Garvin J. Mars exploration. *Nature*. 2001;412(6843):250-253. doi:10.1038/35084200

5. NASA. Mars 2020 Perseverance Launch Press Kit | Introduction. 2020;(June). https://www.jpl.nasa.gov/news/press_kits/mars_2020/launch/

6. NASA, MSFC. Environmental Control and Life Support System (ECLSS). Published online 2017:1-2. https://www.nasa.gov/sites/default/files/atoms/files/g-281237_eclss_0.pdf

7. NASA. Closing the Loop: Recycling Water and Air in Space 9–12. Published online 2000:1-7. http://www.nasa.gov/audience/foreducators/9-12/features/F_Recycling_on_the_ISS.html.%0Awww.nasa.gov

8. EPA. EPA Guidlines for Water Reuse U.S. Environmental Protection Agency. *Guidel water reuse*. 2012;(September):643.

9. Carter L. Status of the regenerative ECLS water recovery system. *40th Int Conf Environ Syst ICES 2010*. Published online 2010. doi:10.2514/6.2010-6216

10. Carter L, Brown C, Orozco N. Status of ISS water management and recovery. *43rd Int Conf Environ Syst*. Published online 2013:1-11. doi:10.2514/6.2013-3509

11. Bagdigian RM, Layne Carter D, Sitler G. Status of the regenerative ECLSS water recovery system. *SAE Tech Pap*. Published online 2008. doi:10.4271/2008-01-2133

12. John Steele, Mark Wilson, Janice Makinen CMO. Antimicrobials for Water Systems in Manned Spaceflight – Past, Present, and Future Applications and Challenges. *Int Conf Environ Syst*. 2018;(July).

13. Carter L, Brown C, Orozco N. Status of ISS water management and recovery. 2018;(July 2017):1-16. doi:10.2514/6.2013-3509

14. Bagdigian RM, Dake J, Gentry G, Gault M. International Space Station Environmental Control and Life Support System Mass and Crewtime Utilization In Comparison to a Long Duration Human Space Exploration Mission. *45th Int Conf Environ Syst*. 2015;(July):1-16. https://ttu-ir.tdl.org/handle/2346/64374

15. Mezghani B, Tounsi F, Rekik AA, Mailly F, Masmoudi M, Nouet P. *An Introduction to MEMS (Micro-Electromechanical Systems) MEMS*. Vol 44.; 2013. doi:10.1016/j.mejo.2013.06.006

16. Vierinen K. Microsystems, MEMS-applications, manufacturing methods for MEMS. 2018;(February).

17. Wu CH, Chang CL. Decolorization of Reactive Red 2 by advanced oxidation processes: Comparative studies of homogeneous and heterogeneous systems. *J Hazard Mater*. 2006;128(2-3):265-272. doi:10.1016/j.jhazmat.2005.08.013

18. Guo Q, Zhou C, Ma Z, Yang X. Fundamentals of TiO2 Photocatalysis: Concepts, Mechanisms, and Challenges. *Adv Mater*. 2019;31(50). doi:10.1002/adma.201901997

19. Xu C, Rangaiah GP, Zhao XS. Photocatalytic degradation of methylene blue by titanium dioxide: Experimental and modeling study. *Ind Eng Chem Res*. 2014;53(38):14641-14649. doi:10.1021/ie502367x

20. Matthews RW. Photooxidation of organic impurities in water using thin films of titanium dioxide. *J Phys Chem*. 1987;91(12):3328-3333. doi:10.1021/j100296a044

21. Li Q, Mahendra S, Lyon DY, et al. Antimicrobial nanomaterials for water disinfection and microbial control: Potential applications and implications. *Water Res*. 2008;42(18):4591-4602. doi:10.1016/j.watres.2008.08.015

22. Zhao J, Chen C, Ma W. Photocatalytic Degradation of Organic Pollutants Under Visible Light Irradiation. *Top Catal*. 2005;35(3-4):269-278. doi:10.1007/s11244-005-3834-0

23. Nakata K, Fujishima A. TiO2photocatalysis: Design and applications. *J Photochem Photobiol C Photochem Rev*. 2012;13(3):169-189. doi:10.1016/j.jphotochemrev.2012.06.001

24. Titanium Dioxide Whites. WebExhibits. http://www.webexhibits.org/pigments/indiv/history/tiwhite.html#:~:text=History of Titanium Dioxide Whites,it could be mass produced.

25. Jacobs JF, van de Poel I, Osseweijer P. Sunscreens with Titanium Dioxide (TiO2) Nano-Particles: A Societal Experiment. *Nanoethics*. 2010;4(2):103-113. doi:10.1007/s11569-010-0090-y

26. Hamad S, Catlow CRA, Woodley SM, Lago S, Mejías JA. Structure and Stability of Small TiO $_2$ Nanoparticles. *J Phys Chem B*. 2005;109(33):15741-15748. doi:10.1021/jp0521914

27. Lee SY, Park SJ. TiO2 photocatalyst for water treatment applications. *J Ind Eng Chem*. 2013;19(6):1761-1769. doi:10.1016/j.jiec.2013.07.012

28. Ophus EM, Rode L, Gylseth B, Nicholson DG, Saeed K. Analysis of titanium pigments in human lung tissue. *Scand J Work Environ Heal*. 1979;5(3):290-296. doi:10.5271/sjweh.3104

29. Mahyad B. Biomedical Applications of TiO 2 Nanostructures : Recent Advances. Published online 2020.

30. Hashemzadeh H, Allahverdi A, Sedghi M, Vaezi Z. PDMS Nano-Modified Sca ff olds for Improvement of Stem Cells Proliferation and Di ff erentiation in Microfluidic Platform.

31. Skocaj M, Filipic M, Petkovic J, Novak S. Titanium dioxide in our everyday life; Is it safe? *Radiol Oncol*. 2011;45(4):227-247. doi:10.2478/v10019-011-0037-0

32. A Fujishima KH. Electrochemical photolysis of water at a semiconductor electrode. *Nature*. 1972;238(5358):38-40. doi:10.1038/238038a0

33. HERRMANN J-M. Water Treatment By Heterogeneous Photocatalysis. Published online 1999:171-194. doi:10.1142/9781848160613_0009

34. Byrne JA, Davidson A, Dunlop PSM, Eggins BR. Water treatment using nano-crystalline TiO2 electrodes. *J Photochem Photobiol A Chem*. 2002;148(1-3):365-374. doi:10.1016/S1010-6030(02)00064-3

35. Shen W, Zhao W, He F, Fang Y. TiO2-based photocatalysis and its applications for waste water treatment. *Prog Chem*. 1998;10(4).

36. Ben Chobba M, Messaoud M, Weththimuni ML, et al. Preparation and characterization of photocatalytic Gd-doped TiO2 nanoparticles for water treatment. *Environ Sci Pollut Res*. 2019;26(32):32734-32745. doi:10.1007/s11356-019-04680-7

37. Periyat P, Pillai SC, McCormack DE, Colreavy J, Hinder SJ. Improved high-temperature stability and sun-light-driven photocatalytic activity of sulfur-doped anatase TiO2. *J Phys Chem C*. 2008;112(20):7644-7652. doi:10.1021/jp0774847

38. Hanaor DAH, Sorrell CC. Review of the anatase to rutile phase transformation. doi:10.1007/s10853-010-5113-0

39. Byrne C, Moran L, Hermosilla D, et al. Effect of Cu doping on the anatase-to-rutile phase transition in TiO2 photocatalysts: Theory and experiments. *Appl Catal B Environ*. 2019;246(December 2018):266-276. doi:10.1016/j.apcatb.2019.01.058

40. Luttrell T, Halpegamage S, Tao J, Kramer A, Sutter E, Batzill M. Why is anatase a better photocatalyst than rutile? - Model studies on epitaxial TiO2 films. *Sci Rep*. 2015;4:1-8. doi:10.1038/srep04043

41. Nakata K, Fujishima A. TiO 2 photocatalysis: Design and applications. *J Photochem Photobiol C Photochem Rev*. 2012;13(3):169-189. doi:10.1016/j.jphotochemrev.2012.06.001

42. Pelaez M, Nolan NT, Pillai SC, et al. A review on the visible light active titanium dioxide photocatalysts for environmental applications. *Appl Catal B Environ*. 2012;125:331-349. doi:10.1016/j.apcatb.2012.05.036

43. Yu JC, Ho W, Lin J, Yip H, Wong PK. Photocatalytic activity, antibacterial effect, and photoinduced hydrophilicity of TiO2 films coated on a stainless steel substrate. *Environ Sci Technol*. 2003;37(10):2296-2301. doi:10.1021/es0259483

44. Nam HJ, Amemiya T, Murabayashi M, Itoh K. Photocatalytic activity of Sol-Gel TiO2 thin films on various kinds of glass substrates: The effects of Na+ and primary particle size. *J Phys Chem B*. 2004;108(24):8254-8259. doi:10.1021/jp037170t

45. Yu J, Zhao X, Zhao Q. Effect of surface structure on photocatalytic activity of TiO2 thin films prepared by sol-gel method. *Thin Solid Films*. 2000;379(1-2):7-14. doi:10.1016/S0040-6090(00)01542-X

46. Dong S, Feng J, Fan M, Pi Y, Hu L, Han X. RSC Advances Recent developments in heterogeneous photocatalytic water treatment using visible light- responsive photocatalysts : a review. Published online 2015:14610-14630. doi:10.1039/c4ra13734e

47. Brezesinski T, Wang J, Polleux J, Dunn B, Tolbert SH. Templated Nanocrystal-Based Porous TiO 2 Films for Next-Generation Electrochemical Capacitors. 2009;(11):1802-1809.

48. Chen M, Chu JW. NOx photocatalytic degradation on active concrete road surface - From experiment to real-scale application. *J Clean Prod*. 2011;19(11):1266-1272. doi:10.1016/j.jclepro.2011.03.001

49. Li Puma G, Bono A, Krishnaiah D, Collin JG. Preparation of titanium dioxide photocatalyst loaded onto activated carbon support using chemical vapor deposition: A review paper. *J Hazard Mater*. 2008;157(2-3):209-219. doi:10.1016/j.jhazmat.2008.01.040

50. Keshmiri M, Mohseni M, Troczynski T. Development of novel TiO2 sol-gel-derived composite and its photocatalytic activities for trichloroethylene oxidation. *Appl Catal B Environ*. 2004;53(4):209-219. doi:10.1016/j.apcatb.2004.05.016

51. Shi YL, Zhang XG, Li HL. Liquid phase deposition templates synthesis of nanostructures of anatase titania. *Mater Sci Eng A*. 2002;333(1-2):239-242. doi:10.1016/S0921-5093(01)01844-5

52. Perillo PM, Rodríguez DF, Boggio NG. TiO2 Nanotubes for Room Temperature Toluene Sensor. *OALib*. 2014;01(07):1-7. doi:10.4236/oalib.1101040

53. Tomoko Kasuga,* Masayoshi Hiramatsu, Akihiko Hoson, Toru Sekino and KN. Titania Nanotubes Prepared by Chemical Processing. *Adv Mater*. Published online 1999. Accessed February 20, 2022. https://onlinelibrary.wiley.com/doi/epdf/10.1002/%28SICI%291521-4095%28199910%2911%3A15%3C1307%3A%3AAID-ADMA1307%3E3.0.CO%3B2-H

54. Dai S, Wu Y, Sakai T, Du Z, Sakai H, Abe M. Preparation of highly crystalline TiO 2 nanostructures by acid-assisted hydrothermal treatment of hexagonal-structured nanocrystalline titania/cetyltrimethyammonium bromide nanoskeleton. *Nanoscale Res Lett*. 2010;5(11):1829-1835. doi:10.1007/s11671-010-9720-0

55. Hu Y, Tsai HL, Huang CL. Effect of brookite phase on the anatase-rutile transition in titania nanoparticles. *J Eur Ceram Soc*. 2003;23(5):691-696. doi:10.1016/S0955-2219(02)00194-2

56. Wu J-M. Low-temperature preparation of titania nanorods through direct oxidation of titanium with hydrogen peroxide. *J Cryst Growth*. 2004;269(2–4):347-355. doi:10.1016/j.jcrysgro.2004.05.023

57. DeRosa DM, Zuruzi AS, MacDonald NC. Formation of Nanostructured Titania: Effect of Thickness on Oxidation Kinetics of Titanium Thin Films in Aqueous Hydrogen Peroxide. *Adv Eng Mater*. 2006;8(1-2):77-80. doi:10.1002/adem.200500186

58. Gollwitzer H, Haenle M, Mittelmeier W, Heidenau F, Harrasser N. A biocompatible sol–gel derived titania coating for medical implants with antibacterial modification by copper integration. *AMB Express*. 2018;8(1). doi:10.1186/s13568-018-0554-y

59. Paunesku T, Rajh T, Wiederrecht G, et al. Biology of TiO2-oligonucleotide nanocomposites. *Nat Mater*. 2003;2(5):343-346. doi:10.1038/nmat875

60. Grätzel M. Applied physics: Solar cells to dye for. *Nature*. 2003;421(6923):586-587. doi:10.1038/421586a

61. Armor JN. Membrane catalysis: Where is it now, what needs to be done? *Catal Today*. 1995;25(3-4):199-207. doi:10.1016/0920-5861(95)00073-O

62. Herrmann JM. Heterogeneous photocatalysis: Fundamentals and applications to the removal of various types of aqueous pollutants. *Catal Today*. 1999;53(1):115-129. doi:10.1016/S0920-5861(99)00107-8

63. Van Gerven T, Mul G, Moulijn J, Stankiewicz A. A review of intensification of photocatalytic processes. *Chem Eng Process Process Intensif*. 2007;46(9 SPEC. ISS.):781-789. doi:10.1016/j.cep.2007.05.012

64. Wang N, Zhang X, Wang Y, Yu W, Chan HLW. Microfluidic reactors for photocatalytic water purification. *Lab Chip*. 2014;14(6):1074-1082. doi:10.1039/c3lc51233a

65. Sauer T, Cesconeto Neto G, José HJ, Moreira RFPM. Kinetics of photocatalytic degradation of reactive dyes in a TiO2 slurry reactor. *J Photochem Photobiol A Chem*. 2002;149(1-3):147-154. doi:10.1016/S1010-6030(02)00015-1

66. Noorjahan M, Reddy MP, Kumari VD, Lavédrine B, Boule P, Subrahmanyam M. Photocatalytic degradation of H-acid over a novel TiO 2 thin film fixed bed reactor and in aqueous suspensions. *J Photochem Photobiol A Chem*. 2003;156(1-3):179-187. doi:10.1016/S1010-6030(02)00408-2

67. Kuo HP, Wu CT, Hsu RC. Continuous reduction of toluene vapours from the contaminated gas stream in a fluidised bed photoreactor. *Powder Technol*. 2009;195(1):50-56. doi:10.1016/j.powtec.2009.05.010

68. Lindstrom H, Wootton R, Hes A. High Surface Area Titania Photocatalytic Microfluidic Reactors. *AIChE J*. 2007;53(3):695-702. doi:10.1002/aic.11096

69. de Sá DS, Vasconcelos LE, de Souza JR, et al. Intensification of photocatalytic degradation of organic dyes and phenol by scale-up and numbering-up of meso- and microfluidic TiO2reactors for wastewater treatment. *J Photochem Photobiol A Chem*. 2018;364(May):59-75. doi:10.1016/j.jphotochem.2018.05.020

70. Liao W, Wang N, Wang T, et al. Biomimetic microchannels of planar reactors for optimized photocatalytic efficiency of water purification. *Biomicrofluidics*. 2016;10(1). doi:10.1063/1.4942947

71. Li L, Chen R, Zhu X, et al. Optofluidic microreactors with TiO2-coated fiberglass. *ACS Appl Mater Interfaces*. 2013;5(23):12548-12553. doi:10.1021/am403842b

72. Li L, Chen R, Liao Q, Zhu X, Wang G, Wang D. High surface area optofluidic microreactor for redox mediated photocatalytic water splitting. *Int J Hydrogen Energy*. 2014;39(33):19270-19276. doi:10.1016/j.ijhydene.2014.05.098

73. Li L, Tang D, Song Y, Jiang B. Dual-film optofluidic microreactor with enhanced light-harvesting for photocatalytic applications. *Chem Eng J*. 2018;339(November 2017):71-77. doi:10.1016/j.cej.2018.01.074

74. Azzouz I, Habba YG, Capochichi-Gnambodoe M, et al. Zinc oxide nano-enabled microfluidic reactor for water purification and its applicability to volatile organic compounds. *Microsystems Nanoeng*. 2018;4(March 2017):17093. doi:10.1038/micronano.2017.93

75. Vangelooven J, De Malsche W, De Beeck JO, Eghbali H, Gardeniers H, Desmet G. Design and evaluation of flow distributors for microfabricated pillar array columns. *Lab Chip*. 2010;10(3):349-356. doi:10.1039/b916126k

76. Xia K. UNIVERSITY OF CALIFORNIA RIVERSIDE Simulation of a Photocatalytic Microreactor with COMSOL Multiphysics. Published online 2018.

77. Betancourt T, Brannon-Peppas L. Micro-and nanofabrication methods in nanotechnological medical and pharmaceutical devices. *Int J Nanomedicine*. 2006;1(4):483-495. doi:10.2147/nano.2006.1.4.483

78. Lishan DG. LPCVD VS . Plasma Etching : HDPCVD PE , Comparing RIE and ICP-RIE. *Plasma Therm*. 2020;(October).

79. Parker ER, Rao MP, Turner KL, Meinhart CD, MacDonald NC. Bulk micromachined titanium microneedles. *J Microelectromechanical Syst*. 2007;16(2):289-295. doi:10.1109/JMEMS.2007.892909

80. Noemaun AN, Mont FW, Cho J, Schubert EF, Kim GB, Sone C. Inductively coupled plasma etching of graded-refractive-index layers of TiO 2 and SiO 2 using an ITO hard mask . *J Vac Sci Technol A Vacuum, Surfaces, Film*. 2011;29(5):051302. doi:10.1116/1.3620494

81. Messow F, Welch C, Eifert A, et al. Deep single step vertical ICP-RIE etching of ion beam sputter deposited SiO2/Si multilayer stacks. *Microelectron Eng*. 2014;113:70-73. doi:10.1016/j.mee.2013.07.018

82. Chircov C, Grumezescu AM. *Microelectromechanical Systems (MEMS) for Biomedical Applications*. Vol 13.; 2022. doi:10.3390/mi13020164

83. Aimi MF, Rao MP, MacDonald NC, Zuruzi AS, Bothman DP. High-aspect-ratio bulk micromachining of titanium. *Nat Mater*. 2004;3(2):103-105. doi:10.1038/nmat1058

84. Parker ER, Thibeault BJ, Aimi MF, Rao MP, MacDonald NC. Inductively Coupled Plasma Etching of Bulk Titanium for MEMS Applications. *J Electrochem Soc*. 2005;152(10):C675. doi:10.1149/1.2006647

85. Zhang Y, Parker ER, Rao MP, Aimi MF, Mezic I, MacDonald NC. Titanium bulk micromachining for biomems applications: A DEP device as a demonstration. *Am Soc Mech Eng Micro-Electro Mech Syst Div MEMS*. Published online 2004:45-48. doi:10.1115/IMECE2004-62136

86. Akpan UG, Hameed BH. Parameters affecting the photocatalytic degradation of dyes using TiO2-based photocatalysts: A review. *J Hazard Mater*. 2009;170(2-3):520-529. doi:10.1016/j.jhazmat.2009.05.039

87. Abdellah MH, Nosier SA, El-Shazly AH, Mubarak AA. Photocatalytic decolorization of methylene blue using TiO2/UV system enhanced by air sparging. *Alexandria Eng J*. 2018;57(4):3727-3735. doi:10.1016/j.aej.2018.07.018

88. Ahmad M, Ahmed E, Hong ZL, Khalid NR, Ahmed W, Elhissi A. Graphene-Ag/ZnO nanocomposites as high performance photocatalysts under visible light irradiation. *J Alloys Compd*. 2013;577:717-727. doi:10.1016/j.jallcom.2013.06.137

89. Nikazar M, Gholivand K, Mahanpoor K. Photocatalytic degradation of azo dye Acid Red 114 in water with TiO2 supported on clinoptilolite as a catalyst. *Desalination*. 2008;219(1-3):293-300. doi:10.1016/j.desal.2007.02.035

90. Wang J, Zhang G, Zhang Z, et al. Investigation on photocatalytic degradation of ethyl violet dyestuff using visible light in the presence of ordinary rutile TiO2 catalyst doped with upconversion luminescence agent. *Water Res*. 2006;40(11):2143-2150. doi:10.1016/j.watres.2006.04.009

91. Vasiljevic ZZ, Dojcinovic MP, Vujancevic JD, et al. Photocatalytic degradation of methylene blue under natural sunlight using iron titanate nanoparticles prepared by a modified sol-gel method: Methylene blue degradation with Fe2TiO5. *R Soc Open Sci*. 2020;7(9). doi:10.1098/rsos.200708

92. Moosavi S, Li RYM, Lai CW, et al. Methylene blue dye photocatalytic degradation over synthesised fe3 o4 /ac/tio2 nano-catalyst: Degradation and reusability studies. *Nanomaterials*. 2020;10(12):1-15. doi:10.3390/nano10122360

93. Houas A, Lachheb H, Ksibi M, Elaloui E, Guillard C, Herrmann J. Photocatalytic degradation pathway of methylene blue in water. 2001;31:145-157.

94. Mills A. An overview of the methylene blue ISO test for assessing the activities of photocatalytic films. *Appl Catal B Environ*. 2012;128:144-149. doi:10.1016/j.apcatb.2012.01.019

95. Gaya UI, Abdullah AH. Heterogeneous photocatalytic degradation of organic contaminants over titanium dioxide: A review of fundamentals, progress and problems. *J Photochem Photobiol C Photochem Rev*. 2008;9(1):1-12. doi:10.1016/j.jphotochemrev.2007.12.003

96. Zhao Y, Zhang X, Zhai J, et al. Enhanced photocatalytic activity of hierarchically micro-/nano-porous TiO2 films. *Appl Catal B Environ*. 2008;83(1-2):24-29. doi:10.1016/j.apcatb.2008.01.035

97. Zeghioud H, Khellaf N, Djelal H, Amrane A, Bouhelassa M. Photocatalytic Reactors Dedicated to the Degradation of Hazardous Organic Pollutants: Kinetics, Mechanistic Aspects, and Design – A Review. *Chem Eng Commun*. 2016;203(11):1415-1431. doi:10.1080/00986445.2016.1202243

98. Faramarzpour M, Vossoughi M, Borghei M. Photocatalytic degradation of furfural by titania nanoparticles in a floating-bed photoreactor. *Chem Eng J*. 2009;146(1):79-85. doi:10.1016/j.cej.2008.05.033

99. Fernández-Pérez A, Rodríguez-Casado V, Valdés-Solís T, Marbán G. A new continuous flow-through structured reactor for the photodegradation of aqueous contaminants. *J Environ Chem Eng*. 2018;6(4):4070-4077. doi:10.1016/j.jece.2018.06.018

100. Lin C, Liu M, Yang Z. Performance of a Metal Ion-Doped Titania-Coated Planar Photocatalytic Microreactor. *Chem Eng Technol*. 2016;39(1):88-96. doi:10.1002/ceat.201400776

101. Mirabedini PS, Truskowska A, Ashby DZ, Rao MP, Greaney PA. Coupled Light Capture and Lattice Boltzmann Model of TiO 2 Micropillar Array for Water Purification . *MRS Adv*. 2019;4(50):2689-2698. doi:10.1557/adv.2019.467

102. Mirabedini PS. LightCapture_Model. LightCapture_Model.

103. Nosaka Y, Nosaka AY. Generation and Detection of Reactive Oxygen Species in Photocatalysis. *Chem Rev*. 2017;117(17):11302-11336. doi:10.1021/acs.chemrev.7b00161

104. Khare M. Reactivity of hydroxyl radical : mechanistic insight into the reactivity with dissolved organic matter. Published online 2016.

105. Farhataziz AB. Selected Specific Rates of Reactions of Transients From Water in Aqueous Solution. Iii. Hydroxyl Radical and Perhydroxyl Radical and Their Radical Ions. *Natl Bur Stand Natl Stand Ref Data Ser*. 1977;(59).

106. Alpert SM, Knappe DRU, Ducoste JJ. Modeling the UV/hydrogen peroxide advanced oxidation process using computational fluid dynamics. *Water Res*. 2010;44(6):1797-1808. doi:10.1016/j.watres.2009.12.003

107. Su Y, Liu G, Zeng C, Lu Y, Luo H, Zhang R. Carbon quantum dots-decorated TiO2/g-C3N4 film electrode as a photoanode with improved photoelectrocatalytic performance for 1,4-dioxane degradation. *Chemosphere*. 2020;251:126381. doi:10.1016/j.chemosphere.2020.126381

108. Hou Y, Li X, Zhao Q, Chen G, Raston CL. Role of hydroxyl radicals and mechanism of escherichia coli inactivation on Ag/AgBr/TiO2 nanotube array electrode under visible light irradiation. *Environ Sci Technol*. 2012;46(7):4042-4050. doi:10.1021/es204079d

109. Nalette T, Bedard J, Carter L. Catalyst development for the space station Water Processor Assembly. *SAE Tech Pap*. 2002;(724). doi:10.4271/2002-01-2362

110. Jayaraj SK, Sadishkumar V, Arun T, Thangadurai P. Enhanced photocatalytic activity of V2O5 nanorods for the photodegradation of organic dyes: A detailed understanding of the mechanism and their antibacterial activity. *Mater Sci Semicond Process*. 2018;85(April):122-133. doi:10.1016/j.mssp.2018.06.006

111. Watts RJ, Yu M, Teel AL. Reactive oxygen species and associated reactivity of peroxymonosulfate activated by soluble iron species. *J Contam Hydrol*. 2017;205(August):70-77. doi:10.1016/j.jconhyd.2017.09.001

112. Watts RJ, Teel AL. Hydroxyl radical and non-hydroxyl radical pathways for trichloroethylene and perchloroethylene degradation in catalyzed H2O2 propagation systems. *Water Res*. 2019;159:46-54. doi:10.1016/j.watres.2019.05.001

113. Lee Hong-Kyun, Do Si-Hyun KS-H. The Role of Magnetite Nano Particle (MNP) to Oxidize Nitrobenzene using Heterogeneous Fenton Reaction. *Lect Notes Eng Comput Sci*. 2010;2187(1):717-720.

114. Furman OS, Teel AL, Ahmad M, Merker MC, Watts RJ. Effect of Basicity on Persulfate Reactivity. *J Environ Eng*. 2011;137(4):241-247. doi:10.1061/(asce)ee.1943-7870.0000323

115. Odling G, Robertson N. BiVO4-TiO2 Composite Photocatalysts for Dye Degradation Formed Using the SILAR Method. *ChemPhysChem*. Published online 2016:2872-2880. doi:10.1002/cphc.201600443

116. Sun P, Tyree C, Huang CH. Inactivation of Escherichia coli, Bacteriophage MS2, and Bacillus Spores under UV/H2O2 and UV/Peroxydisulfate Advanced Disinfection Conditions. *Environ Sci Technol*. 2016;50(8):4448-4458. doi:10.1021/acs.est.5b06097

117. Wu J-M, Qi B. Low-Temperature Growth of a Nitrogen-Doped Titania Nanoflower Film and Its Ability To Assist Photodegradation of Rhodamine B in Water. *J Phys Chem C*. 2007;111(2):666-673. doi:10.1021/jp065630n

118. Bora L V., Mewada RK. Visible/solar light active photocatalysts for organic effluent treatment: Fundamentals, mechanisms and parametric review. *Renew Sustain Energy Rev*. 2017;76:1393-1421. doi:10.1016/j.rser.2017.01.130

119. Buxton G V., Greenstock CL, Helman WP, Ross AB. Critical Review of rate constants for reactions of hydrated electrons, hydrogen atoms and hydroxyl radicals (·OH/·O− in Aqueous Solution. *J Phys Chem Ref Data*. 1988;17(2):513-886. doi:10.1063/1.555805

120. Stone D, Whalley LK, Heard DE. Tropospheric OH and HO2 radicals: Field measurements and model comparisons. *Chem Soc Rev*. 2012;41(19):6348-6404. doi:10.1039/c2cs35140d

121. Lallement A, Vinatier V, Brigante M, Deguillaume L, Delort AM, Mailhot G. First evaluation of the effect of microorganisms on steady state hydroxyl radical concentrations in atmospheric waters. *Chemosphere*. 2018;212:715-722. doi:10.1016/j.chemosphere.2018.08.128

122. Allen JM, Lucas S, Allen SK. Formation of hydroxyl radical (˙OH) in illuminated surface waters contaminated with acidic mine drainage. *Environ Toxicol Chem*. 1996;15(2):107-113. doi:10.1002/etc.5620150206

123. Chin YP, Miller PL, Zeng L, Cawley K, Weavers LK. Photosensitized degradation of bisphenol A by dissolved organic matter. *Environ Sci Technol*. 2004;38(22):5888-5894. doi:10.1021/es0496569

124. Analitica C, Torino U, Giuria VP. A MODEL TO PREDICT THE STEADY-STATE CONCENTRATION OF HYDROXYL RADICALS IN THE SURFACE LAYER OF NATURAL WATERS. Published online 2007. doi:10.1002/adic.200790053

125. Mahmoud MA, Poncheri A, Badr Y, Abd El Waned MG. Photocatalytic degradation of methyl red dye. *S Afr J Sci*. 2009;105(7-8):299-303. doi:10.4102/sajs.v105i7/8.86

126. Muirhead DL, Marshall GC, Flight S. A Simple Model to Estimate the Hydroxyl Radical Concentration and Associated DMSD Production Rates from Volatile Methyl Siloxanes in the ISS Atmosphere. 2018;(July).

127. Yu P, Nalette T, Kayatin MJ. Development of Advanced ISS-WPA Catalysts for Organic Oxidation at Reduced Pressure/Temperature. *46th Int Conf Environ Syst*. Published online 2016:1-12.

128. Kurji HJ, Imran MS, Bded AS. The impact of using pure ethanol additives on gasoline fuel with respect to SI engine emissions. *IOP Conf Ser Mater Sci Eng*. 2021;1067(1):012090. doi:10.1088/1757-899x/1067/1/012090

129. Meroni D, Ardizzone S, Cappelletti G, et al. Photocatalytic removal of ethanol and acetaldehyde by N-promoted TiO 2 films: The role of the different nitrogen sources. *Catal Today*. 2011;161(1):169-174. doi:10.1016/j.cattod.2010.08.013

130. Wisthaler A, Strøm-Tejsen P, Fang L, et al. PTR-MS assessment of photocatalytic and sorption-based purification of recirculated cabin air during simulated 7-h flights with high passenger density. *Environ Sci Technol*. 2007;41(1):229-234. doi:10.1021/es060424e

131. Bisutti I, Hilke I, Raessler M. Determination of total organic carbon - An overview of current methods. *TrAC - Trends Anal Chem*. 2004;23(10-11):716-726. doi:10.1016/j.trac.2004.09.003

132. Natarajan SK, Pachunka JM, Mott JL. Role of microRNAs in alcohol-induced multi-organ injury. *Biomolecules*. 2015;5(4):3309-3338. doi:10.3390/biom5043309

133. Levy RH, Bauer LA. *Basic Pharmacokinetics*. Vol 8. INC; 1986. doi:10.1097/00007691-198603000-00010

134. Regmi C, Lotfi S, Espíndola JC, Fischer K, Schulze A, Schäfer AI. Comparison of photocatalytic membrane reactor types for the degradation of an organic molecule by TiO2-coated PES membrane. *Catalysts*. 2020;10(7). doi:10.3390/catal10070725

135. Carp O, Huisman CL, Reller A. Photoinduced reactivity of titanium dioxide. *Prog Solid State Chem*. 2004;32(1-2):33-177. doi:10.1016/j.progsolidstchem.2004.08.001

136. Cambié D, Bottecchia C, Straathof NJW, Hessel V, Noël T. Applications of Continuous-Flow Photochemistry in Organic Synthesis, Material Science, and Water Treatment. *Chem Rev*. 2016;116(17):10276-10341. doi:10.1021/acs.chemrev.5b00707

137. Muggli DS, McCue JT, Falconer JL. Mechanism of the photocatalytic oxidation of ethanol on TiO2. *J Catal*. 1998;173(2):470-483. doi:10.1006/jcat.1997.1946

138. Takeuchi M, Deguchi J, Sakai S, Anpo M. Effect of H2O vapor addition on the photocatalytic oxidation of ethanol, acetaldehyde and acetic acid in the gas phase on TiO2 semiconductor powders. *Appl Catal B Environ*. 2010;96(1-2):218-223. doi:10.1016/j.apcatb.2010.02.024

139. Ohko Y, Tryk DA, Hashimoto K, Fujishima A. Autoxidation of acetaldehyde initiated by TiO2 photocatalysis under weak UV illumination. *J Phys Chem B*. 1998;102(15):2699-2704. doi:10.1021/jp9732524

140. Sauer ML, Ollis DF. Photocatalyzed oxidation of ethanol and acetaldehyde in humidified air. *J Catal*. 1996;158(2):570-582. doi:10.1006/jcat.1996.0055

141. U.S. Environmental Protection Agency. Integrated Risk Information System (IRIS) on 1,4-Dioxane. *Natl Cent Environ Assessment, Off Res Dev Washington, DC*. 1999;(2):6-9.

142. Industrial N, Notification C, Scheme A. 1,4-Dioxane: Priority Existing Chemical No. 7. 1998;(7).

143. Coleman HM, Vimonses V, Leslie G, Amal R. Degradation of 1,4-dioxane in water using TiO2 based photocatalytic and H2O2/UV processes. *J Hazard Mater*. 2007;146(3):496-501. doi:10.1016/j.jhazmat.2007.04.049

144. Klečka GM, Gonsior SJ. Removal of 1,4-dioxane from wastewater. *J Hazard Mater*. 1986;13(2):161-168. doi:10.1016/0304-3894(86)80016-4

145. Chitra S, Paramasivan K, Cheralathan M, Sinha PK. Degradation of 1,4-dioxane using advanced oxidation processes. *Environ Sci Pollut Res*. 2012;19(3):871-878. doi:10.1007/s11356-011-0619-9

146. Schoonenberg Kegel F, Rietman BM, Verliefde ARD. Reverse osmosis followed by activated carbon filtration for efficient removal of organic micropollutants from river bank filtrate. *Water Sci Technol*. 2010;61(10):2603-2610. doi:10.2166/wst.2010.166

147. Lee IS, Sim WJ, Kim CW, Chang YS, Oh JE. Characteristic occurrence patterns of micropollutants and their removal efficiencies in industrial wastewater treatment plants. *J Environ Monit*. 2011;13(2):391-397. doi:10.1039/c0em00130a

148. Yamazaki S, Yamabe N, Nagano S, Fukuda A. Adsorption and photocatalytic degradation of 1,4-dioxane on TiO2. *J Photochem Photobiol A Chem*. 2007;185(2-3):150-155. doi:10.1016/j.jphotochem.2006.05.024

149. Wols BA, Hofman-Caris CHM. Review of photochemical reaction constants of organic micropollutants required for UV advanced oxidation processes in water. *Water Res*. 2012;46(9):2815-2827. doi:10.1016/j.watres.2012.03.036

150. De Laat J, Truong Le G, Legube B. A comparative study of the effects of chloride, sulfate and nitrate ions on the rates of decomposition of H2O2 and organic compounds by Fe(II)/H2O2 and Fe(III)/H2O 2. *Chemosphere*. 2004;55(5):715-723. doi:10.1016/j.chemosphere.2003.11.021

151. Esplugas S, Bila DM, Krause LGT, Dezotti M. Ozonation and advanced oxidation technologies to remove endocrine disrupting chemicals (EDCs) and pharmaceuticals and personal care products (PPCPs) in water effluents. *J Hazard Mater*. 2007;149(3):631-642. doi:10.1016/j.jhazmat.2007.07.073

152. Lau TK, Chu W, Graham NJD. The aqueous degradation of butylated hydroxyanisole by UV/S 2O82-: Study of reaction mechanisms via dimerization and mineralization. *Environ Sci Technol*. 2007;41(2):613-619. doi:10.1021/es061395a

153. Watts MJ, Linden KG. Chlorine photolysis and subsequent OH radical production during UV treatment of chlorinated water. *Water Res*. 2007;41(13):2871-2878. doi:10.1016/j.watres.2007.03.032

154. Byrne C, Dervin S, Hermosilla D, et al. Solar light assisted photocatalytic degradation of 1,4-dioxane using high temperature stable anatase W-TiO2 nanocomposites. *Catal Today*. 2021;(February):1-10. doi:10.1016/j.cattod.2021.02.001

155. Park IS, Chung KH, Kim SC, Kim SJ, Park YK, Jung SC. Photocatalytic degradation of 1,4-dioxane and hydrogen production using liquid phase plasma on N- and Ni- codoped TiO2 photocatalyst. *Mater Lett*. 2021;283:128751. doi:10.1016/j.matlet.2020.128751

156. Barndõk H, Hermosilla D, Han C, Dionysiou DD, Negro C, Blanco Á. Degradation of 1,4-dioxane from industrial wastewater by solar photocatalysis using immobilized NF-TiO2 composite with monodisperse TiO2 nanoparticles. *Appl Catal B Environ*. 2016;180:44-52. doi:10.1016/j.apcatb.2015.06.015

157. Byrne C, Dervin S, Hermosilla D, et al. Solar light assisted photocatalytic degradation of 1,4-dioxane using high temperature stable anatase W-TiO2 nanocomposites. *Catal Today*. 2021;380(June 2020):199-208. doi:10.1016/j.cattod.2021.02.001

158. Rao G, Brastad KS, Zhang Q, Robinson R, He Z, Li Y. Enhanced disinfection of Escherichia coli and bacteriophage MS2 in water using a copper and silver loaded titanium dioxide nanowire membrane. *Front Environ Sci Eng*. 2016;10(4). doi:10.1007/s11783-016-0854-x

159. Jayamohan H, Smith YR, Gale BK, Mohanty SK, Misra M. Photocatalytic microfluidic reactors utilizing titania nanotubes on titanium mesh for degradation of organic and biological contaminants. *J Environ Chem Eng*. 2016;4(1):657-663. doi:10.1016/j.jece.2015.12.018

160. Zheng X, Shen Z peng, Cheng C, Shi L, Cheng R, Yuan D hai. Photocatalytic disinfection performance in virus and virus/bacteria system by Cu-TiO2 nanofibers under visible light. *Environ Pollut*. 2018;237:452-459. doi:10.1016/j.envpol.2018.02.074

161. Cormier J, Janes M. A double layer plaque assay using spread plate technique for enumeration of bacteriophage MS2. *J Virol Methods*. 2014;196:86-92. doi:10.1016/j.jviromet.2013.10.034

162. Horovitz I, Avisar D, Luster E, Lozzi L, Luxbacher T, Mamane H. MS2 bacteriophage inactivation using a N-doped TiO2-coated photocatalytic membrane reactor: Influence of water-quality parameters. *Chem Eng J*. 2018;354(August):995-1006. doi:10.1016/j.cej.2018.08.083

163. Mamane H, Shemer H, Linden KG. Inactivation of E. coli, B. subtilis spores, and MS2, T4, and T7 phage using UV/H2O2 advanced oxidation. *J Hazard Mater*. 2007;146(3):479-486. doi:10.1016/j.jhazmat.2007.04.050

Appendices

Appendix A – PMFR Fabrication

Preparation of Titanium Chips:

The Grade 1 commercially pure titanium wafers (100 mm) were cleaned using Acetone, Isopropanol, and DI water and placed into the Plasma Enhanced Chemical Vapor Deposition (PECVD) system (Plasmatherm 790) to deposit 4.2 μm of SiO_2 as a hard mask. The Ti wafers were then mounted onto 100 mm polycrystalline Si wafers using 3M double-sided thermally conductive tape. The wafers were cleaned with solvents and photoresist was spun onto the Ti wafers using a spin bench to protect the surface during the next step. Each wafer was then diced into two rectangular chips 60 mm × 40 mm using a dicing saw (Disco DAD 321 Automatic Dicing) with Disco Diamond blades. Each chip was then ultrasonically cleaned in solvents and DI water to remove the residual photoresist.

Fabrication of Micropillar and Planar Reactors:

Both reactors were fabricated using an identical process. Following preparation of titanium chips, these chips were subjected to photolithographic patterning using the photomasks. Two photomasks for both planar and micropillar reactors were made using the IC Layout Editor L-Edit. For the lithographic patterning process, first, HMDS was spun onto the Ti chips to promote photoresist adhesion. Then, SPR-220-7.0 was spun onto the chips to a thickness of 5.5 μm and exposed using a Karl SUSS MA-6 Mask Aligner. Samples were then developed in AZ 300 MIF developer and pattern quality was evaluated

via optical microscopy. Then, the samples were subjected to SiO_2 plasma etching using an ICP Oxford Cobra Plasmalab System 100 with a plasma chemistry of C_4F_8 until the lithographic pattern had been transferred to the hard mask. The residual photoresist was then removed through brief ultrasonic agitation in acetone, rinsed in isopropanol, and DI water, and finally, dried on a hotplate at 115˚C. An Oxford Cobra Plasmalab System 100 Metal Trench Etcher was used with a Cl_2/O chemistry to define the planar reactors, and a Panasonic E626I ICP System was used with a Cl_2/Ar chemistry to etch the micropillar reactors. After Ti etching, the samples were submerged in acetone for 72 hours to dissolve the tape and remove the Si backing from the Ti chip. A Dremel tool was used to drill inlet and outlet holes in the Ti chip, 1 mm in diameter, at the origin of each flow distributor. In the end, the passivation layer formed during Ti deep etching was removed to expose the pure Ti underneath. It was done by subjecting the samples to dilute HF (2.3%) for 40 seconds followed by sonication in a DI water bath for 5 minutes.

Production of NPT:

All reactors were oxidized in 10% H2O2 at 80 ˚C for 5 hours. Upon removal from the H2O2, samples were rinsed with DI water and placed into a Lindberg Blue M Box Oven and annealed in air at 300˚C for 8 hours.

Basic Characterizations:

The micropillar structure and NPT morphology were observed with the Leo Supra 55 Scanning Electron Microscope operated at 5 kV.

Appendix B – Degradation Experiments

Photocatalytic Testing of Micropillar and Planar Reactors on MB:

20 µM (7.478 mg/L) of MB was selected as the target concentration to make the experiment comparable to those reported in the literature. A fixture was used to produce a water-tight seal on the reactor as mentioned previously. To compare the performance of all six devices, 5 fixed residence times were selected (40, 30, 20, 10, 5 seconds) and flow rates were adjusted according to the chamber volume and desired residence time. First, 2 mL of 200 proof ethanol was passed through the device at the longest residence time to purge the system. Then 2 mL of DI water was sent through the device at the same flow rate to clean ethanol out of the system. Afterwards, the MB solution flowed through the reactor at a residence time of 40 seconds for a total of 1 hour while the glass window was covered to allow dark adsorption to occur. After 60 minutes, 1.5 mL of MB was collected for a post-adsorption measurement. A UV-Vis Thermo Scientific Evolution 60 spectrometer was used to take MB absorption measurements at a wavelength of 665 nm. After the adsorption measurement the cover was removed, and the UV lamp was positioned above the sample. To purge the system of unexposed MB, 1 mL was passed through the device before the photocatalytically degraded MB was collected. This procedure was repeated for each of

the five flow rates, after collecting 1.5 mL of degraded MB the flow rate would be increased and 1 mL was passed through before collection at the new flow rate began. This experiment was repeated three times for each device to measure an average. Reactors were reused due to the complexity of device fabrication. To ensure there was minimal contamination between experiments, 5 mL of ethanol was sent through the device at the fastest flow rate followed by 5 mL of DI water. This process helped to remove adsorbed contaminants within the device through shear forces. A new 250 μm PDMS sheet and glass slide were used for each experiment because MB fouling did occur on the PDMS as it was exposed to MB flow. Reactors were also visually inspected with SEM to ensure there was no damage to the NPT or excessive adsorbed MB. In addition, a MP100 and a P100 without NPT were subjected to the same process as above to establish a baseline and ensure that MB degradation was not a result of UV photolysis.

Photocatalytic Testing of MP50 on Nitrobenzene:

The experiment setup was identical to the MB test setup, and only MP50 was used for this study. An 8 μM nitrobenzene solution was prepared and four residence times (5, 10, 20, 30 seconds) were used. DI water was flowed through the system for 30 minutes at 288 μL/min in the beginning of each experiment to eliminate air within the system. Then the nitrobenzene solution was run through the system at the same flow rate for 3 hours under a dark environment to let the physical adsorption by the system reach its saturation. Then the UV lamp was turned on and the nitrobenzene was sent through the system under

different residence times starting from the longest to the shortest. Before collecting the effluents, 1 mL of solution was allowed to pass through the system to purge the remaining nitrobenzene exposed under the previous condition. Then 1.8 mL of effluents for different residence times were collected for analysis. This experiment were repeated three times, and 1 hour flowing of DI water was used to remove the adsorbed nitrobenzene after each run.

Measurements of Nitrobenzene Concentrations:

Concentrations of nitrobenzene was analyzed with an Agilent 1200 Series high performance liquid chromatograph equipped with a diode array detector. For this process, an isocratic elution of 50% 10 mM Formic acid and 50% HPLC-grade acetonitrile were used. The operational conditions consisted of the following: An Agilent ZORBAX Eclipse XDB-C18 column, injection volume of 100 μL, flow rate of 1.0 mL min-1, and a detection wavelength of 270 nm. The retention time for nitrobenzene using the isocratic method was 5.6 minutes under the aforementioned conditions at room temperature. The calibration curve of nitrobenzene was obtained using the procedures described above and its concentrations in actual samples were quantified according to this calibration curve.

Photocatalytic Testing of MP50 on Ethanol and Measurements of TOC Level:

The experiment setup was identical to the MB test setup. A 5 min residence time was used this study. The 25.4 mg L^{-1} ethanol solution was prepared by diluting 13 µL 200 proof pure ethanol purchased from Fisher Scientific into 400 mL Millipore water. All effluent solutions were collected by some 20 mL glass vials. A vial of ethanol was collected directly from the gas tight glass syringe for the purpose of measuring the initial concentration of ethanol solution. At the beginning of tests, 1 hour of Millipore water flowing at 5 seconds residence time was used to purge the reaction chamber followed by 1 hour of 25.4 mg L^{-1} ethanol solution in a dark environment to ensure the chamber being filled by the experiment ethanol. Then, a glass vial was used to collect the effluent ethanol solution after 70 min being flowed in the reactor with a 288 µL min^{-1} flow rate. This solution was used for evaluating the effect of adsorption of the reactor. After that, the UV light source was turned on, and the syringe pump kept the ethanol solution flowing at 4.8 µL min^{-1} for 70 hours under UV irradiation. 20.16 mL effluent solution was collected for the evaluation of the reduction of TOC level at a 5 min residence time. Before doing each run, an ethanol solution was arranged to flow for 30 min at the required flow rates to eliminate the effects of the leftover ethanol from the previous run. For the control studies, the process was identical to the above-mentioned process except the absence of UV irradiation. The experiment groups and control groups were both performed three times. All the collected samples were sent to the Shimadzu TOC-VCPH/CPN TOC analyzer for the TOC level measurements. For the TOC analyzing, after acidifying the sample to pH 2-3, sparging gas was bubbled through the sample to eliminate the inorganic carbon (IC)

component. The remaining total carbon (TC) was measured to determine total organic carbon, and the result is generally referred to as TOC.

Photocatalytic Testing of MP50 on 1,4-Dioxane:

The experiment setup was identical to the MB test setup. The 1,4-dioxane was diluted to a concentration of 100 µM. Five residence times (40, 60, 80, 100, 120 seconds) were used for the study. Each test run began with 30 minutes of DI water flowing through the system to purge the air. Then the 1,4-dioxane solution was sent through the device at 288 µL/min for 1 hour let the system's physical adsorption reach saturation. The UV irradiation was then initiated, 1 mL of 1,4-dioxane solution was passed through the system at the proposed residence time to purge unexposed 1,4-dioxane. The collection of exposed 1,4-dioxane effluent started right after the previous step. This experiment was repeated three times for each residence time. After each experiment, DI water was flowed through the system at 288 µL/min for 1 hour to remove the contaminants adsorbed by the geometry within MP50. Effluents with a volume of 1.8 mL were collected right after the dark adsorption step as well as the experiment step for the calculation of relative concentration.

Measurements of 1,4-Dioxane Concentrations:

Concentrations of 1,4-dioxane was analyzed with an Agilent 1200 Series high performance liquid chromatograph equipped with a diode array detector. An isocratic elution of 95% MilliQ water and 5% HPLC-grade acetonitrile were used for the analysis.

The operational conditions consisted of the following: An Agilent ZORBAX Eclipse XDB-C18 column, injection volume of 100 μL, flow rate of 1.0 mL min-1, and a detection wavelength of 191 nm. The retention time for 1,4-Dioxane using the isocratic method was 3.2 minutes under the aforementioned conditions at room temperature. The calibration curve of 1,4-Dioxane was obtained using the procedures described above and its concentrations in actual samples were determined according to this calibration curve.

Appendix C – Calculation of Steady-State ·OH Concentration in MP50

Knowing

Slope of the best-fit linear regression model of the Napierian logarithm of relative nitrobenzene percentages at different residence times = - 0.0627 s^{-1}

2nd-order-reaction rate constant of reaction between nitrobenzene and ·OH:

$k_{(NB + \cdot OH)}$ = 4.0 × 10 M^{-1} s^{-1}

The steady-state ·OH concentration in MP50 was calculated through

$$[\cdot OH]_{SS} = -\frac{slope}{k(NB + \cdot OH)} = -\frac{-0.0627\ s^{-1}}{4.0 \times 10^{9}\ M^{-1}s^{-1}} = 1.57 \times 10^{-11}\ M$$